NEUTRONICS ANALYSIS OF PEBBLE-BED CORES WITH TRANSURANICS

A Thesis

by

MEGAN LEIGH PRITCHARD

Submitted to the Office of Graduate Studies of
Texas A&M University
in partial fulfillment of the requirements for the degree of

MASTER OF SCIENCE

December 2007

Major Subject: Nuclear Engineering

NEUTRONICS ANALYSIS OF PEBBLE-BED CORES WITH TRANSURANICS

A Thesis

by

MEGAN LEIGH PRITCHARD

Submitted to the Office of Graduate Studies of
Texas A&M University
in partial fulfillment of the requirements for the degree of

MASTER OF SCIENCE

Approved by:

Chair of Committee,	Pavel V. Tsvetkov
Committee Members,	Donald Allen
	Vladimir Horvat
	Sean McDeavitt
Head of Department,	Raymond Juzaitis

December 2007

Major Subject: Nuclear Engineering

ABSTRACT

Neutronic Analysis of Pebble-Bed Cores with Transuranics.

(December 2007)

Megan Leigh Pritchard, B.S., Texas A&M University

Chair of Advisory Committee: Dr. Pavel V. Tsvetkov

At the brink of nuclear waste repository crises, viable alternatives for the long term radiotoxic wastes are seriously being considered worldwide. Minor actinides serve as one of these targeted wastes. Partitioning and transmutation in fission reactors is one possible incineration option and could potentially serve as a source of nuclear fuel required for sustainability of energy resources.

The objective of this research was to evaluate the neutronic performance of the pebble-bed Very High Temperature Reactor (VHTR) configurations with various fuel loadings. The configuration adjustments and design sensitivity studies specifically targeted the achievability of spectral variations. The development of several realistic full-core 3D models and validation of all modeling techniques used was a major part of this research effort. In addition, investigating design sensitivities helped identify the parameters of primary interest.

The full-core 3D models representing the prototype and large scale cores were created for use with SCALE 5.0 and SCALE 5.1 code systems. Initially the models required the external calculation of a Dancoff correction factor; however, the recent

release of SCALE 5.1 encompassed inherent double heterogeneity modeling capabilities. The full core 3D models with multi-heterogeneity treatments are in agreement with available pebble-bed High Temperature Test Reactor data and were validated through benchmark studies. Analyses of configurations with various fuel loadings have indicated promising performance and safety characteristics. It was found that through small configuration adjustments, the pebble-bed design can be tweaked to produce desirable spectral shifts. The future operation of Generation IV nuclear energy systems would be greatly facilitated by the utilization of minor actinides as a fuel component. This would offer development of new fuel cycles, and support sustainability of a fuel source.

ACKNOWLEDGEMENTS

I extend magnificent gratitude toward my advisor Dr. Pavel Tsvetkov, and committee members Dr. Donald Allen, Dr. Sean McDeavitt, and Dr. Vladimir Horvat. Extra thanks go to Dr. Tsvetkov for his extra special caring, incredible teaching, late night emails and constant availability for several years. He's been nothing less than spectacular. I hand picked him as my advisor for a reason, after all.

A special acknowledgement is due for Dr. Vladimir Horvat who has served as a professional mentor and friend since being my professor as a freshman in college. He inspired me to look into research, especially particle physics and accelerator research as a freshman. He is in no way obligated to serve on any committee yet does anyway. I hope he continues to inspire young students in the same way he did me.

Dr. McDeavitt committed to serving on my committee and jumped right in with barely knowing me (or Texas) at all and I greatly appreciate it. The same gratitude goes to Dr. Allen, who hardly knows me at all, but has been nothing less than helpful with his signatures and availability when the times come.

Without my family and their constant distractions, calls, stories and emails I would never have made it anywhere, especially without that car. Thanks to them and my husband for being supportive, 98% of the time. That kick in the rear every so often is enlightening.

Lastly, a very personal thanks to Mark DeHart at Oak Ridge National Lab for his unwavering advice, correction, inspiration, and humor. I have always looked up to Mark

and was finally able to be one of his students for some time. He has done nothing but give when it was absolutely unnecessary.

In addition, this work and degree were made possible through financial support from the Roy G. Post Waste Management Foundation Scholarship.

This thesis is based upon work supported by the U.S. DOE under Award Number DE-FC07-05ID14655 (05-094).

TABLE OF CONTENTS

CHAPTER Page

Page

LIST OF FIGURES

FIGURE Page

FIGURE Page

LIST OF TABLES

CHAPTER I

INTRODUCTION

I.A. BACKGROUND

This chapter discusses the current status and purpose of the research efforts underway in the United States for the future of nuclear energy. The work herein was performed as part of the United States Department of Energy (DOE) Nuclear Energy Research Initiative (NERI) Project, "Utilization of Minor Actinides as a Fuel Component for Ultra-Long Life VHTR Configurations: Designs, Advantages, and Limitations." The overall objectives of the NERI project and the specific objectives of this research effort are stated in Chapter I.B.

I.A.1 GENERATION IV PROGRAM AND THE VHTR CONCEPT

The Next Generation Nuclear Plant (NGNP) concept envisions an advanced, efficient, next-generation nuclear reactor coupled to modern electricity generation and hydrogen producing technologies. The Generation IV nuclear energy systems are an ensemble of nuclear reactor technologies that could be deployed by 2030 and present significant improvements in economics, safety, reliability and sustainability over currently operating reactor technologies. The Generation-IV International Forum (GIF) was established in 2000, comprised of an international membership base of constituents that are interested in nuclear energy technologies. The forum is chartered to investigate

---

This thesis follows the style of *Nuclear Science and Engineering.*

new and existing technologies that could be applied to satisfy current and future energy needs.

One of the six candidates selected by the group of collaborators is the Very High Temperature Reactor (VHTR) design. This concept has promise to address the goals set forth by GIF, including: nonproliferation and personal protection issues, maximizing nuclear safety and conserving natural resources, minimizing repository-bound waste, and maintaining a high economic gain and operational efficiency. [1]

The interest of the United States Department of Energy (U.S. DOE) in the VHTR concept stems from specific safety features including low power density, high heat capacity, and a passive method of heat removal from the reactor vessel without need for active safety systems.

The VHTR design consists of inert helium-gas coolant and graphite moderator to operate in a thermal spectrum with the high outlet temperatures necessary for hydrogen production, sea water desalination, or process heat for the petrochemical industry and other co-applications. High Temperature Gas Cooled Reactors (HTGRs) have successfully demonstrated the feasibility of the technology. The VHTR offers an extension of the conventional HTGRs with added enhancements including higher thermal efficiency and high temperature applications [1].

The VHTR concept has been proposed in two design configurations: (1) a prismatic core consisting of fuel and graphite blocks and (2) a pebble-bed core composed of thousands of fuel and graphite spheres. Prototypes of each of these configurations exist as the High Temperature Test Reactor (HTTR) in Japan and the Chinese High Temperature Test Module (HTR-10) in China [1,2].

The pebble bed concept consists of thousands of graphite spheres containing about 8300 TRISO (TRIstructural ISOtropic) coated fuel particles embedded within the fuel region of each graphite sphere [2]. The 6-centimeter diameter sphere has a 5 centimeter inner graphite matrix containing the micro-particles and an outer layer of only graphite. The ceramic coated fuel particles offer many benefits, including serving as a containment vessel for gaseous fission products at high temperatures [3]. Safety control features of the pebble bed such as control rods are located in the reflector surrounding the cylindrically packed core [4]. A noticeable feature of the pebble-bed configuration is its ability to achieve high fuel burn-up. This feature is possible because the pebbles migrate through the core slowly and can be returned back into the top for another cycle and longer lifetime. The prismatic design core utilizes the same ceramic coated fuel particles as used in the pebble-bed design; however, the particles are embedded in a static matrix. Rather than being located within graphite spheres in the pebble bed design, the TRISO microparticles are embedded within the fuel region of cylindrical compacts to form fuel rods; these rods are in turn inserted within prismatic graphite blocks. The prismatic core is designed to keep all specific safety features such as control rods within graphite blocks [4].

The work of this thesis is focused on the pebble bed cores for the VHTR concept. This concept presents inherent challenges, including some not covered in this work, such as significant heterogeneity encompassing the pebble and microparticle, constant movement and random distribution of pebbles within the core, complex coolant flow paths through the bed, and a pebble discharge and reload system.

I.A.2 NUCLEAR WASTE MANAGEMENT AND THE ADVANCED FUEL CYCLE PROGRAM

By the end of the licensed period of operation (about 20-30 years) of current nuclear reactors in U.S., the quantity of spent fuel will reach close to 87,000 tons. The constituents of the spent fuel include about 95 wt. % of uranium (with a U-235 enrichment comparable to that of natural uranium), about 1-2% of transuranic elements (primarily plutonium), and 3% of fission products and trace quantities of activation elements.

Two classes of nuclides will contribute to the radiotoxicity and heat load in a spent fuel repository, consisting of short and long lived isotopes. Fission products comprise the bulk of short-term nuclides, and will be vastly reduced by decay within 500-1000 years after discharge, after which the longer-lived transuranic elements (TRUs) and fission products will dominate radiotoxicity and decay heat. Today approximately 600 tons of plutonium exist within discharged fuel assemblies from commercial reactors; by the end of the licensing period the plutonium inventory will increase to approximately 870 tons.

The U.S. DOE Advanced Fuel Cycle (AFC) Program is focused on finding efficient technologies to enhance spent fuel treatment. This includes reduction of the raw volume of spent fuel, diminution of decay heat sources to expand repository thermal capacity, separation of elements, and recycling useful materials from spent fuel for transmutation purposes [5]. The program is intended to develop advanced fuel systems for Generation IV reactors and foster fuel cycle technologies that will considerably

reduce the disposal of long-lived, highly radiotoxic transuranic elements while reclaiming the valuable energy remaining in spent fuel. The strategy anticipates a transition from the current once-through fuel cycle to one that is progressively more sustainable over the next several decades. Successful use of partitioning and transmutation of minor actinides could lead to a decrease in waste inventory and recovery of additional fuel materials. The objective of the combined AFC and Generation IV programs is to define and implement a sustainable nuclear energy supply in the U.S. This will make better use of natural resources and generate significantly less waste than the current open fuel cycle [5,6].

I.B RESEARCH OBJECTIVES

One of the objectives of the U.S. DOE Nuclear Energy Research Initiative Project (NERI) is to assess the possibility, advantages, and limitations of VHTRs with advanced fuels containing minor actinides. This research considers and compares capabilities of pebble-bed and prismatic core designs with advanced actinide fuels to approach continuous reactor lifetime operation without intermediate refueling [7]. The combination of VHTR designs with advanced fuels could potentially result in the reduction of long-term radiotoxicity and net heat load of high-level waste sent to a geologic repository by enabling the recovery of energy contained in spent fuel. The principal mechanism to achieve ultra-long life VHTR configurations is an enhanced involvement of self-generated fissile compositions based on spent LWR fuel. The objective of the research in this thesis is to:

- Validate several models and various modeling techniques and capabilities

- Analyze configuration variation capabilities to achieve prolonged operation without intermediate refueling,
- Investigate configuration adjustments to produce spectral shifts,
- Notice the effect of design sensitivities with transuranic fuel.

The study is focused on the impact of design sensitivities on pebble-bed cores with advanced materials and their applications.

The research is focused on the pebble bed core designs with advanced fuels. Utilization of minor actinides (obtained from light water reactor (LWR) spent fuel) as a fuel component would facilitate development of new fuel cycles and support sustainability of a fuel source for nuclear energy, assuring future operation of Generation IV nuclear energy systems. Minor actinides include neptunium, americium, and curium. These elements will be responsible for the bulk of spent fuel long-term radiotoxicity.

The pebble bed design offers many incentives for core configuration flexibility which can lead to improved fissile properties of minor actinides by neutron spectrum shifting. For example, by altering the moderator pebble to fuel pebble ratio, total number of pebbles, or size of the pebbles, various spectral conditions can be achieved within the same core. The uncertainties associated with nuclear data and VHTR design characteristics will become imperative in understanding the reliability of the VHTR modeling. This research analyzes the impact of design uncertainties on pebble-bed cores with advanced materials and their applications. It consists of the following studies:

- Development of full core model for three dimensional pebble-bed configuration
- Reliability analysis of the pebble-bed modeling

- Configuration variations to achieve advanced design targets
- Design sensitivities and their impact on the pebble-bed system applications
- System design envelope of the advanced pebble-bed configurations

I.B.1 PRODCEDURE AND METHODS

A sensitivity analysis can determine the importance of different parameters and components of the model (for example design parameters) on the output parameters of the model (such as multiplication factor and reactivity). In the future, an uncertainty analysis will be conducted after the sensitivity study to describe how the parameter estimate would vary in repeated sampling.

Uncertainties will appear in both nuclear data and VHTR parameters. Discrepancies are obvious among the nuclear data libraries (ENDF/B-6.8, JENDL-3.3, JEF-2.2) [8] and contribute to further uncertainties thereby limiting the validity of analysis results. An analysis of existing uncertainty effects on VHTR parameters will then focus on the effects due to nuclear data and design parameters. A reliability evaluation of the VHTR modeling will follow this analysis using the previously validated three dimensional core models.

Even clean critical benchmark experiments have uncertainties in the nominal system characteristics such as fuel composition and enrichment, impurities, densities, critical dimensions, etcetera. These small deviations are propagated to contribute to an overall discrepancy in the calculated responses of the system. The critical system will have an overall k_{eff} of unity with some associated uncertainty. There may exist little doubt about the value of k_{eff} but there still exist doubt for system parameter

measurements. This may be done by varying the system characteristics and observing the effects on the performance characteristics.

Following these studies the question is posed as to how well the modeling approach represents the actual system and actual performance characteristics. As design elements become more and more complex, the attempts to match a previous calculation or experiment become more distant. The model and underlying assumptions must be understood to a degree of reliability for realistic applications. This includes looking at the model performance characteristics in some atypical states and analyzing the response.

Using the whole core three dimensional models, a variation analysis methodology was developed and applied to studies of VHTR geometry and material variations. Some examples of adjustment parameters include dimensions of fuel particles, coatings and pebbles, and fuel material loading characteristics such as composition and enrichment.

I.C TECHNICAL STATUS OF THE QUESTION

An important aspect of any reactor design is the fuel type, its utilization and resulting cycle. Until recently the fuel of choice has been uranium based, typically uranium dioxide. Use of low enriched uranium (LEU) and mixed oxide (MOX) fuels (a blend of uranium and plutonium oxides) has become increasingly popular in recent years but still pose the issue of storing high level waste.

Partitioning (chemical separation) and transmutation (transformation via neutron bombardment) aims at making nuclear energy more sustainable from the back end of the

fuel cycle and implies a separation and utilization of the valuable materials as well as minimization of high level waste. In actuality, the actinides cannot be recovered completely from spent fuel and the some actinides will remain in the waste stream. However, those which are transformed will produce non-radioactive isotopes or isotopes with shorter half-lives.

The realistic modeling requires a code-to-experiment benchmark analysis to assure high fidelity of the applied models and nuclear data. Code-to-code validation is also a beneficial comparison in understanding the use of various code systems. Use of three-dimensional whole-core VHTR models was exercised in the following work. The analyses utilized the SCALE (Standardized Computer Analysis for Licensing Evaluation) code system [9].

There is a double heterogeneity present in using this type of fuel. The initial level of heterogeneity (micro-level) is described by the fuel kernel and surrounding layers randomly distributed within an inner graphite matrix of a pebble. The final level of heterogeneity (macro-level) is described by the large number of pebble spheres randomly packed into a bed to form the core. The effects of double heterogeneity on resonance self-shielding of cross sections can be a difficult phenomena to account for in analysis of VHTRs [10]. These effects significantly affect VHTR designs and their performance characteristics. In addition, the ability of shifting the neutron spectrum is of importance in promising the use of minor actinides as a fuel component. Since the pebble bed design permits flexibility in component configuration, fuel utilization and

management, it is possible to improve fissile properties of minor actinides by neutron spectrum shifting through configuration adjustments [7].

CHAPTER II

APPLIED CODE SYSTEMS

This chapter will discuss the applied code systems used in modeling, benchmarking, and evaluating the VHTR pebble-bed designs. The 3D whole core computational models were developed using SCALE (Standardized Computer Analysis for Licensing Evaluation) versions 5.0 and 5.1 [9,11], and DANCOFF-MC: A Computer Program for Monte Carlo Calculation of Dancoff Factors in Irregular Geometries [12]. These, among other code systems, are available from the Radiation Safety Information Computational Center (RSICC) at Oak Ridge National Laboratory (ORNL). This Department of Energy sponsored center is authorized to collect, maintain, analyze, and distribute computer software and data sets in the area of radiation transport and safety.

The full-core VHTR pebble-bed model was developed in accordance with the described benchmark problems in order to validate the model design before further performance characteristics studies. Of primary interest in the benchmark problems was the experimental data provided by the IAEA-TECDOC-1382, "Evaluation of High Temperature Gas Cooled Reactor Performance: Benchmark Analysis Related to Initial Testing of the HTTR and HTR-10" [2]. The 3D full-core computational model of the existing HTR-10 was created for the benchmarking purposes.

II.A SCALE 5.0

The 3D full-core pebble-bed VHTR model was initially built using SCALE version 5.0. The modular code system is developed and maintained by ORNL and is readily validated and accepted for use in thermal reactor analysis around the world.

The SCALE system initially begins with calling upon the Criticality Safety Analysis Sequence (CSAS25, CSAS6) control module [13,14]. CSAS was developed within the SCALE code system to provide automated, problem-dependent cross section processing followed by calculation of the neutron multiplication factor for the systems being modeled using KENO. The two available versions of KENO were utilized including KENO-V.a. and KENO-VI corresponding to CSAS25 and CSAS26, respectively [15,16]. The code system has several available problem-independent multigroup cross section libraries. For calculations done in SCALE 5.0, the 238 group ENDF/B-V cross section library was used [17].

In both sequences, the default execution path follows BONAMI, NITAWL-III, XSDRNPM, and KENO [18-20]. BONAMI performs Bondarenko calculations for resonance self-shielding, with the cross sections to perform resonance correction for the unresolved energy range and create a new master cross section library. WORKER then follows to convert the master multigroup library into a working multigroup library.

NITAWL-III applies the Nordheim Integral Treatment to perform neutron cross section processing in the resonance energy range. This module performs a fine group calculation of the slowing down flux across each resonance with subsequent flux weighting of the resonance cross sections. NITAWL also contains a built in Dancoff

factor calculation tool utilizing the SUPERDAN algorithm, however, this factor can also be externally supplied. The resulting output of NITAWL is a converted cross section library from problem-independent to problem-dependent form. The Nordheim integral treatment has built in assumptions which prove to be an excellent method for processing resonance cross sections for use in the analysis of light water reactor (LWR) fuel pin cells, and large homogeneous media, but should be exercised with caution in other applications.

CENTRM/PMC is an optional module as an alternative to NITAWL-III and is discussed in Chapter II.C.

The XSDRNPM module uses a one-dimensional discrete ordinates transport code to perform neutron calculations in creating a homogenized cell-weighted mixture cross-section based on the unique unit cell. These cell-weighted cross sections are then passed to KENO for full system analysis.

KENO-V.a and KENO-VI are multigroup Monte Carlo criticality safety codes applied to calculate the effective multiplication factor for a 3D system. Geometry capabilities in KENO allow modeling of any shape that can be described with quadratic equations. KENO-VI has enhanced capabilities such as geometrically intersecting regions, but at the expense of computational time when compared to KENO-V.a.

A schematic flow chart of the CSAS6 control module path is shown in Fig. 1.

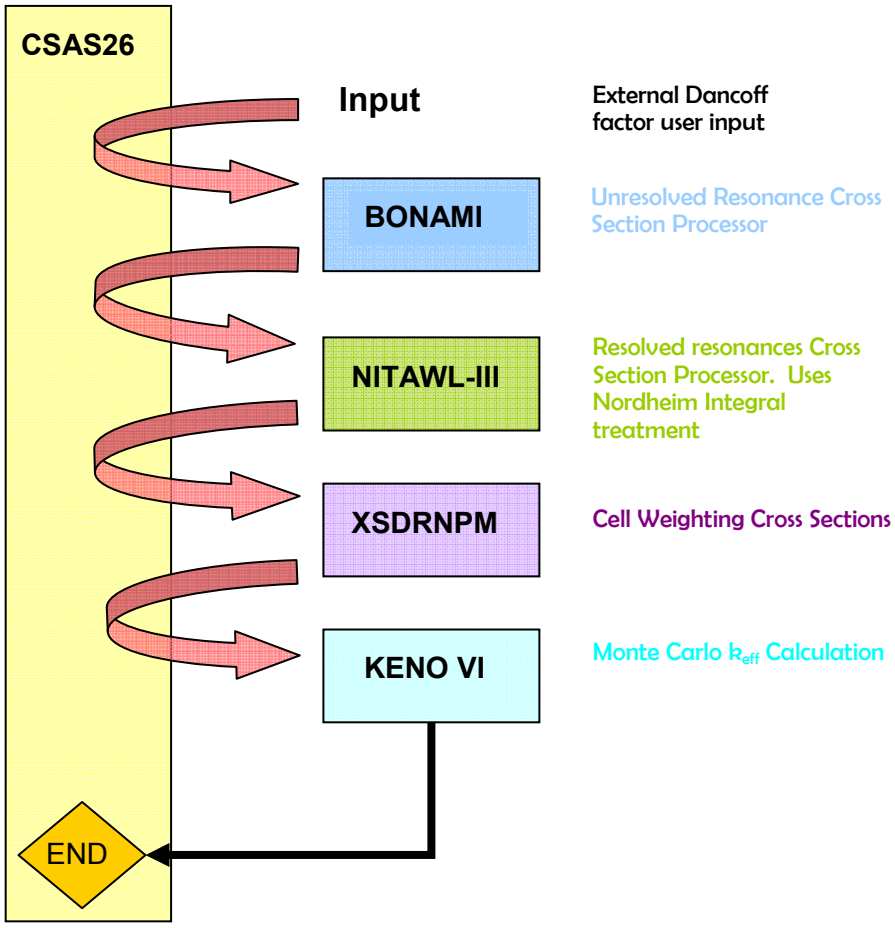

Fig. 1. Flow Chart of the CSAS6 Control Module in SCALE 5.0

There are several limitations associated with CSAS6, some of which come as a result of using preprocessed multigroup cross sections. Other limitations are derived from assumptions in the Nordheim integral treatment and can be eliminated by using CENTRM/PMC as the resolved resonance processor. The limitation of CSAS6 using CENTRM/PMC is as follows [13,14]:

- 2D effects such as fuel rods in assemblies where some positions are filled with control rod guide tubes, burnable poison rods and/or fuel rods of different

enrichments. The cross sections are processed as if the rods are in an infinite lattice of rods.

And those associated with using NITAWL-III are as follows [19]:

- The treatment assumes no resonance overlap from other resonances or other material regions.
- The treatment of an external moderator assumes an asymptotic flux present at the absorber-moderator interface.
- The treatment of spatial transport uses the first-flight escape probability for the absorber, the two-region reciprocity theorem, and Dancoff factors. For correct multi-heterogeneity treatment, a Dancoff factor must be calculated externally and supplied as input.
- The treatment assumes no flux profile interference from resonance material in adjacent zones.

II.B. DANCOFF-MC

A Monte Carlo method is implemented in the computer code DANCOFF-MC in order to calculate the Dancoff correction factor which is then input into SCALE 5.0 to determine the flux reduction in the resonance integral calculations [12].

The initial, historical definition of the Dancoff correction factor was proposed by Dancoff and Ginsburg and stated that in a closely packed lattice, the flow of resonance neutrons into the fuel is reduced as compared to the flow of resonance neutrons into a single fuel lump with an infinite moderator because of the shadowing effects of surrounding fuel lumps. The Dancoff factor is then the relative reduction of the flow

[21]. A more common definition found today is that derived from the method of collision probabilities. This states that the Dancoff factor is the probability that an isotropically emitted neutron from the surface of a fuel element will have a collision in the fuel region of a surrounding fuel element without colliding with a moderator nucleus on the way. Through Monte Carlo methods, DANCOFF-MC calculates the factor based on the latter definition [22].

The DANCOFF-MC code can accommodate an array of geometries including spherical fuel elements and account for those surrounding a single pellet. The input values for DANCOFF-MC allow for varying fuel region, clad, and gap radii, annular configurations, and macroscopic fuel and clad cross sections.

Neutrons are emitted from the surface of the fuel lump and tracked via histories until an intersection with another fuel region. The Monte Carlo method uses random numbers to establish an arbitrary starting position and direction for travel. Analytical methods are used to calculate the neutron path length and the transport probabilities in the given material.

The SCALE 5.0 code system has a built in method for calculating the Dancoff factor based on the SUPERDAN algorithm [23]. This algorithm is not directly applicable to VHTR configurations. Many reactor physics code systems do an automatic calculation of the Dancoff factor based on certain assumptions and approximations that may not be valid [24].

There are limitations associated with the DANCOFF-MC program. The complexity of the problem restricts the ability of rods and pellets to be mixed in the

same arrangement. The central cylindrical axis must be parallel to rod arrangements, and calculation of the "grey-effect" is not available for annular geometries.

An option for external entry of a Dancoff factor is available in the SCALE package and this option is utilized taking the factor from the DANCOFF-MC result. The externally calculated result is inserted into the input file for the VHTR pebble-bed SCALE model as shown in Fig. 1 and is expected to improve the accuracy of the neutronic results.

II.C SCALE 5.1

November of 2006 marked the anticipated release of the newest version of the SCALE code package. Version 5.1 has numerous enhancements to the code to allow more general and easier modeling and analysis. Growth in nuclear systems designs requires this growth in code systems to accommodate current and future research.

Some of the major renovations to version 5.1 are in the following areas:

- New ORIGEN-ARP libraries
- New covariance libraries in TSUNAMI
- KENO-VI array and hole enhancements
- GeeWiz/KENO3D calculates KENO-VI volumes
- ENDF/B-VI data and HTML output
- Double heterogeneity capabilities in CENTRM
- Three dimensional depletion calculation in TRITON

Of primary interest for this work is the enhancement of continuous energy CENTRM transport code to accommodate double heterogeneous unit cells. This capability in

SCALE 5.1 can eliminate the need for external Dancoff factor calculation in DANCOFF-MC [25].

The DOUBLEHET cell treatment is essentially a combination of MULTIREGION and LATTICECELL treatments. Specifications in the cell declaration include number of grain types, and number of particles, pitch, or volume fraction. The grains are homogenized into a new mixture to be used in the fuel element (macro-cell) cell calculation. These grains and fuel elements are treated as 1-D cells.

The primary weakness in CENTRM/PMC is that it assumes only 1-D spatial variations. This is acceptable for most cases but can break down in systems with 2-D or 3-D behavior, except for doubly-heterogeneous fuels such as those in HTGRs. These are handled with the DOUBLEHET treatment [25,26].

When the DOUBLEHET unit cell type is selected, first the point-wise flux disadvantage factors (the flux depression in the fuel due to absorption of neutrons) in the first level of heterogeneity (TRISO particle) are calculated with the 1-D point-wise S_N code CENTRM. The point-wise flux disadvantage factors are then used to generate the cell-weighted point-wise cross sections for the homogenized fuel region in the fuel element. In the second CENTRM run, these spatially-averaged point-wise cross sections are used to calculate the flux distribution in the fuel element. PMC, a coupled code to CENTRM, will then generate the multi-group, problem-dependent cross sections.

When double heterogeneity treatment is used in SCALE 5.1, the default cross-section processor is the CENTRM/PMC/CHOPS sequence. CENTRM and PMC work together to produce a set of problem-dependent group cross sections using a pointwise

continuous energy cross section library and a cell description. The CHOPS module is called to compute cell-homogenized point data for a CENTRM nuclear data library [25].

A schematic, similar to Fig. 1 is shown in Fig. 2 for the SCALE sequence following a DOUBLEHET unit cell declaration. The primary functions of each module are mentioned.

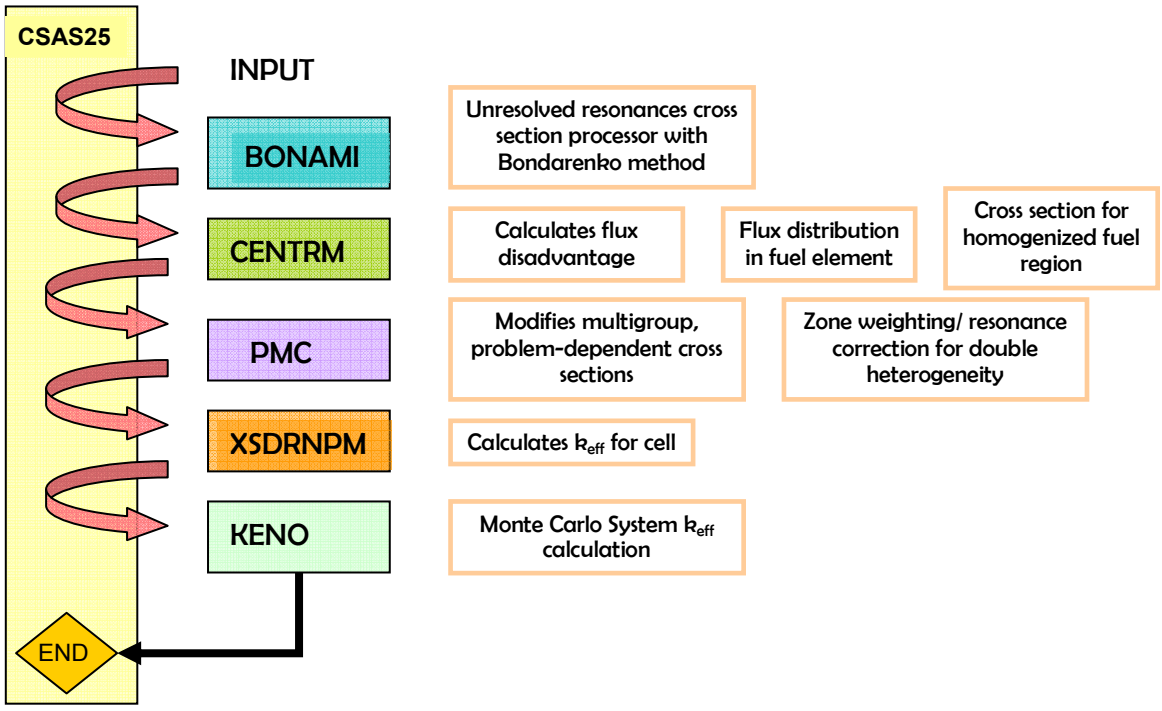

Fig. 2. Flow Chart of the CSAS6 Control Module in SCALE 5.1

CHAPTER III

VHTR PEBBLE-BED MODEL

III.A. VHTR PEBBLE-BED CORE

Described in the preceeding sections is a detailed synopsis of the development of the three dimensional full-core pebble-bed VHTR configurations. The model description as well as the validation and verification aspects of the initial design is based on China's 10 MW High Temperature Gas cooled reactor test module (HTR-10). The first section (III.A.1) provides general information about the HTR-10 and its experimental program. The next section (III.A.2) describes the computational model and its purpose.

III.A.1 HTR-10

The HTR-10 is a graphite moderated, helium cooled, modular reactor which includes spherical fuel elements with fuel regions containing fuel particles. The HTR-10 design program began in the late 1980s with an effort to incorporate original German pebble-bed technology and China's plans to move forward with a modular HTGR [1].

The primary objectives of the HTR-10 program are (1) to acquire knowledge in the design, construction and operation of HTGRs, (2) to demonstrate inherent safety features of the modular HTGR, and (3) to establish a facility to produce experimental results. The design specifications of the HTR-10 are shown in Table I.

Table I. HTR-10 Design Specifications

Reactor thermal power	10 MW
Primary helium pressure	3.0 Mpa
Active core volume	5 m^3
Reactor core diameter	180 cm
Average core height	197 cm
Average helium temperature at reactor outlet	700 ˚C
Average helium temperature at reactor inlet	250 ˚C
Helium mass flow rate at full power	4.3 kg/s
Main steam pressure at steam generator outlet	4.0 Mpa
Main steam temperature at steam generator	440 ˚C
Feed water temperature	104 ˚C
Fuel-to-graphite ball ratio	0.57/0.43
Number of control rods in side reflector	10
Number of absorber ball units in side reflector	7
Nuclear fuel	UO_2
Heavy metal loading per fuel element	5
Enrichment of fresh fuel element	17%
Number of fuel elements in equilibrium core	27 000
Fuel loading mode	multi-pass

In selecting a reference pebble-bed design to model, several factors were considered including the availability of design parameters and experimental and computational results. The HTR-10 program had the most available reference material for core specifications, material characteristics, and other relevant information to develop the computational model. Experimental test results were also available for experiment-to-code benchmark studies as well as analytical computation results for code-to-code benchmarks [2].

III.A.2 VHTR MODEL WITH PEBBLE-BED CONFIGURATION

The core of the initial pebble-bed model based on the HTR-10 consists of a 5 m^3 graphite cavity which is 180 cm in diameter and 197 cm in total height. The "active core" region has an active height filled with fuel while the remainder is a helium cavity. The fuel region is surrounded by axial and radial graphite reflectors. A vertical cross section of the HTR-10 model is shown in Fig. 3 (not to scale).

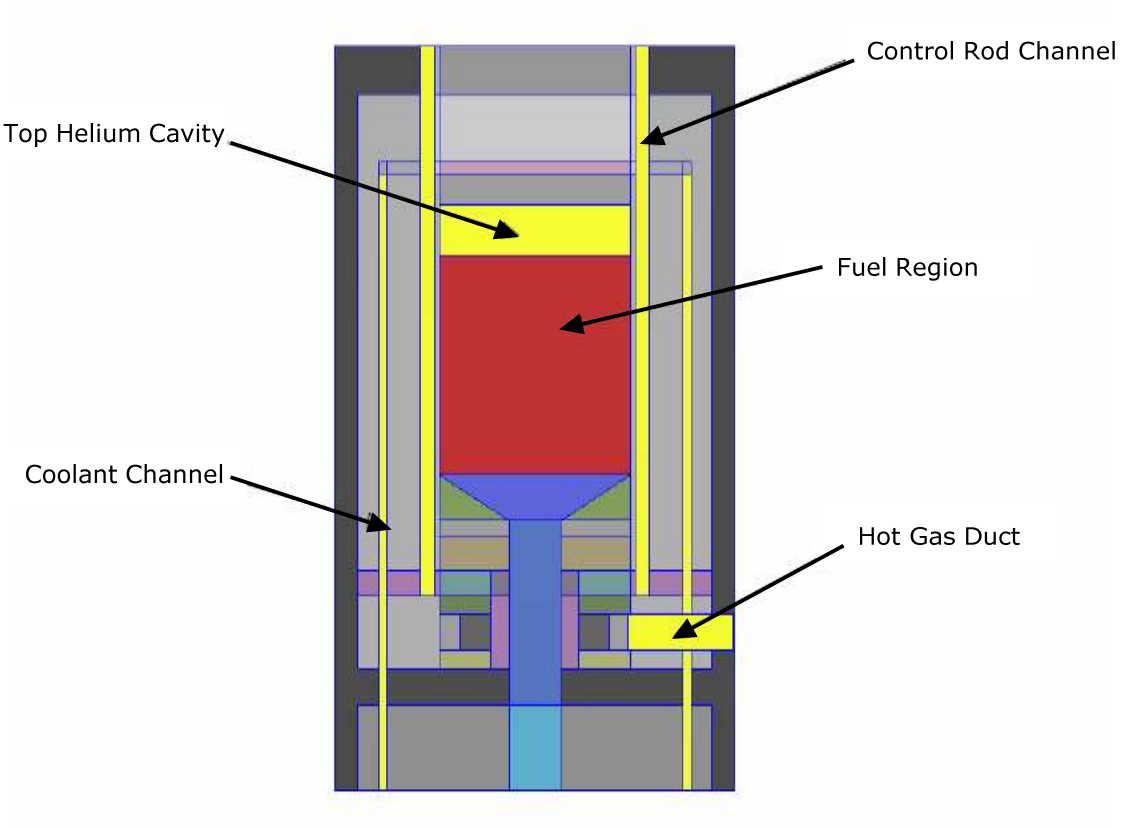

Fig. 3. Vertical Cross Sectional View of the HTR-10 Model (KENO 3D)

The radial graphite reflector consists of two concentric rings of borings. The inner ring of borings contains ten control rod channels and three irradiation channels all with a diameter of 13 cm. The remaining seven of the 20 borings are absorber ball channels with a rectangular cross section through the middle and semi circle cross sections at each end. Helium flow channels, 8 cm in diameter, make up the outer ring of borings. These regions can be seen in the horizontal cross sectional view shown in Fig. 4.

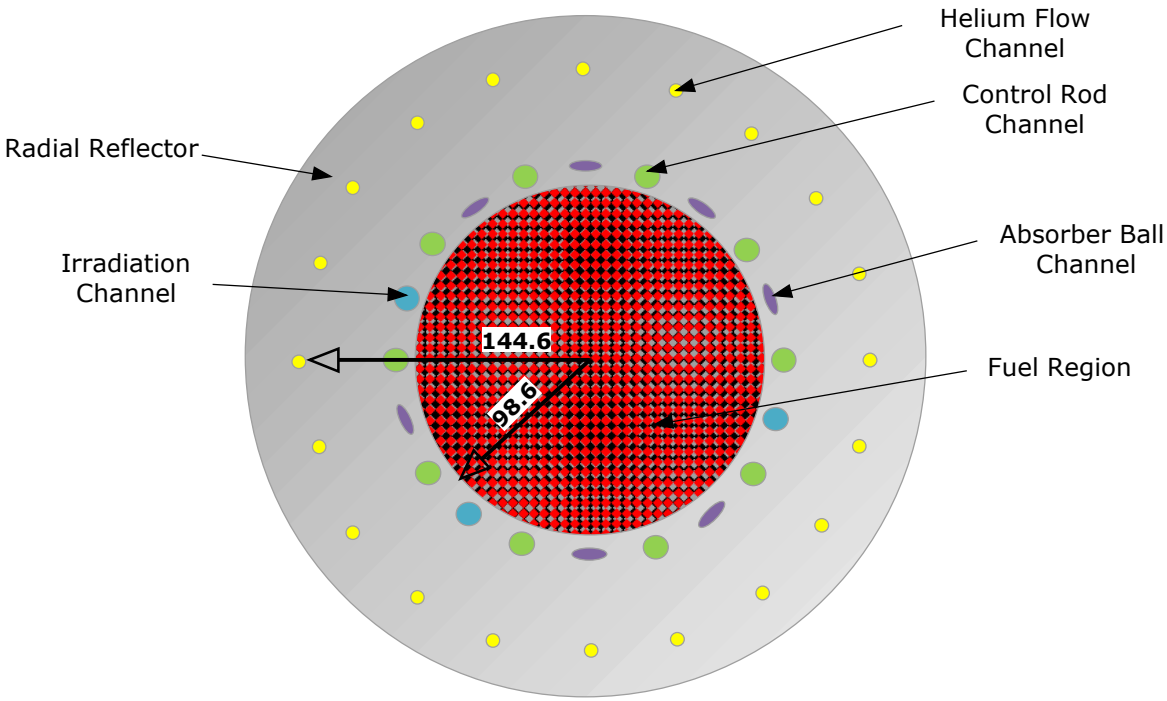

Fig. 4. Horizontal Cross Sectional View of the HTR-10 Model

A reactor physics model is shown in Fig. 5. A configuration for benchmark study purposes is constructed following this representation.

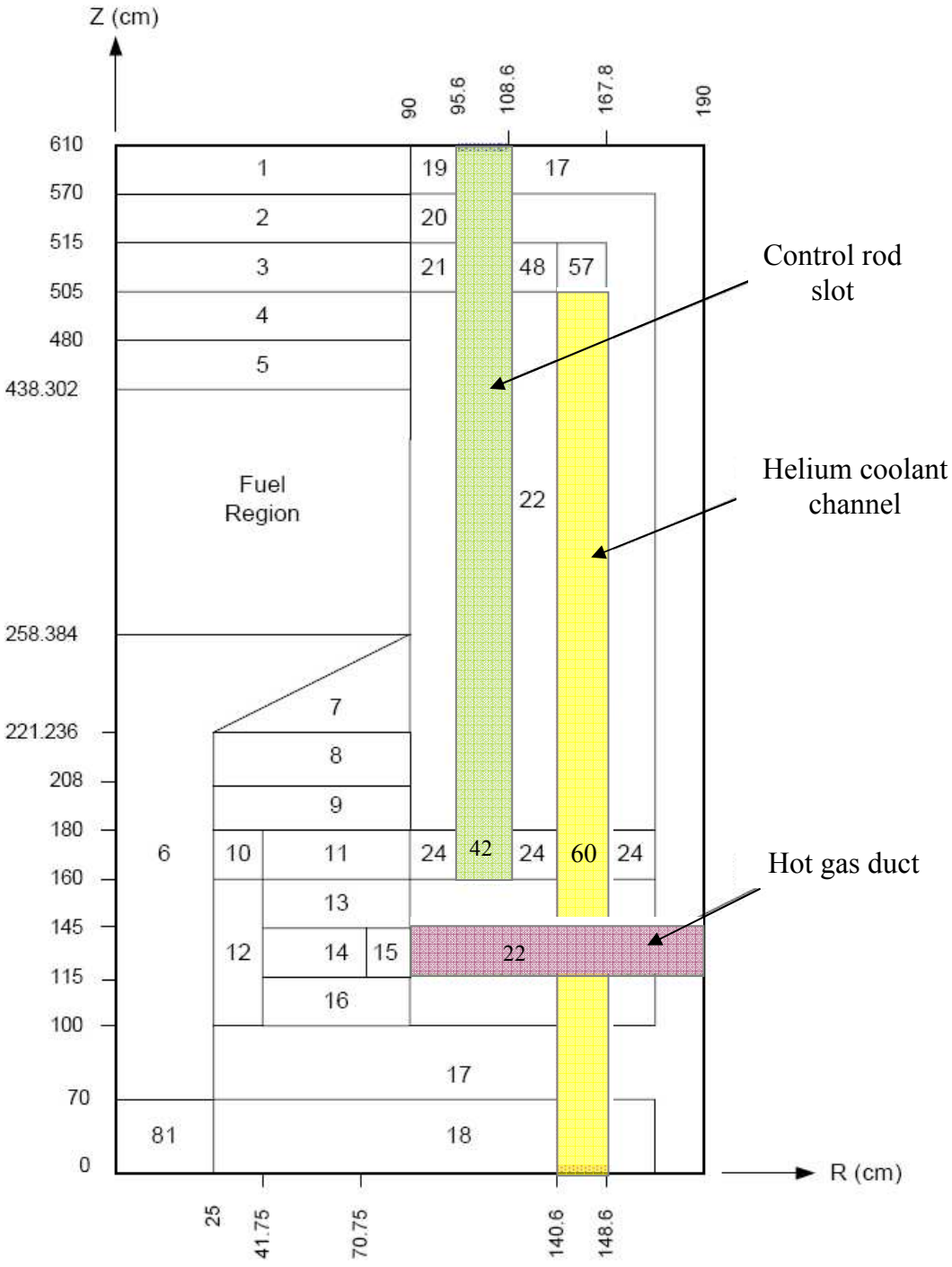

Fig. 5. Vertical Cross Section with Zone Material Identification Numbers

The numbers shown each indicate a zone with a material of specific properties, including density, nuclides included, and temperature. The schematic diagram has radial and axial axes to illustrate the size and layout of each zone. These dimensions are shown in centimeters. The zone identification numbers correspond to material properties as described in Table II.

Table II. Homogenized Atom Density of Nuclide in Reflector Zones (*1/ barn-cm*)

Zone Number	Carbon	Natural boron	Remarks
1	7.29410E-02	3.29811E-03	Boronated carbon bricks
2	8.51462E-02	4.57148E-07	Top graphite reflector
3	1.45350E-2	7.80384E-08	Cold helium chamber
4	8.02916E-02	4.31084E-07	Top reflector
5			Top core cavity
6	5.38275E-02	2.88999E-07	Dummy balls, simplified as graphite of lower density
7	8.51047E-02	4.56926E-07	Bottom reflector with hot helium borings
8	7.81408E-02	4.19537E-07	Bottom reflector structures
9	8.23751E-02	4.42271E-07	Bottom reflector structures
10	8.43647E-02	2.98504E-04	Bottom reflector structures
11	8.17101E-02	1.56416E-04	Bottom reflector structures
12	8.50790E-02	2.09092E-04	Bottom reflector structures
13	8.19167E-02	3.58529E-05	Bottom reflector structures
14	5.41118E-02	5.77456E-05	Bottom reflector structures
15	3.32110E-02	1.78309E-07	Bottom reflector structures
16	8.81811E-02	3.58866E-05	Bottom reflector structures
17	7.65984E-02	3.46349E-03	Boronated carbon bricks
18	7.97184E-02	0.00000E+00	Carbon bricks
19	7.61157E-02	3.44166E-01	Boronated carbon bricks
20	8.78374E-02	4.71597E-07	Graphite reflector structure
21	5.79696E-02	3.11238E-07	Graphite reflector structure
22	8.82418E-02	4.73769E-07	Graphite reflector structure
24	8.79541E-02	1.68369E-04	Graphite reflector structure
29	5.24843E-02	1.81969E-07	Graphite reflector structure
42	8.79637E-02	1.62903E-04	Graphite reflector structure
48	5.82699E-02	3.12850E-07	Graphite reflector structure
57	7.28262E-02	3.91003E-07	Graphite reflector structure
60	8.79538E-02	1.68369E-04	Graphite reflector, cold helium flow region
81	7.97184E-02	0.00000E+00	Dummy balls, but artificially taken as carbon bricks

III.A.3 FUEL REGION

The models constructed for the HTR-10 are explicit in modeling all structural features, nuclide compositions, and regions independently, with the exception of the fuel region. A pebble fuel element consists of TRISO fuel particles embedded within a graphite matrix in the shape of a sphere (fuel element properties listed in Table V). Each of the approximately 27,000 pebbles contains about 8,300 coated fuel particles which contain a small, spherical fuel kernel of 17% enriched (low enriched in ^{235}U) uranium dioxide (UO_2) with TRISO coatings. The TRISO coating is made up of four layers: a low density, porous, pyrolitic carbon (PyC) buffer layer closest to the fuel kernel, a high density isotropic PyC layer, a silicon carbide barrier layer, and final outer PyC layer. These coatings have the principal purpose to contain fission products. The coating characteristics are individually listed in Table III.

Table III. TRISO Particle Material Specifications

Layer	Composition	density (g/cm^3)	radius (mm)
fuel kernel	UO2	10.41	0.300
coating 1	PyC	1.14	0.359
coating 2	PyC	1.89	0.390
coating 3	SiC	3.20	0.419
coating 4	PyC	1.87	0.465

The spherical fuel element has a total diameter of 6 cm: 5 cm diameter inner region is composed of the graphite matrix containing the TRISO particles, the outer 0.5 cm thick covering is solely graphite to serve as a moderator material around the fuel and

to protect the fuel region during pebble motion. Fig. 6 shows a schematic of the TRISO particle and how it is contained in the pebble.

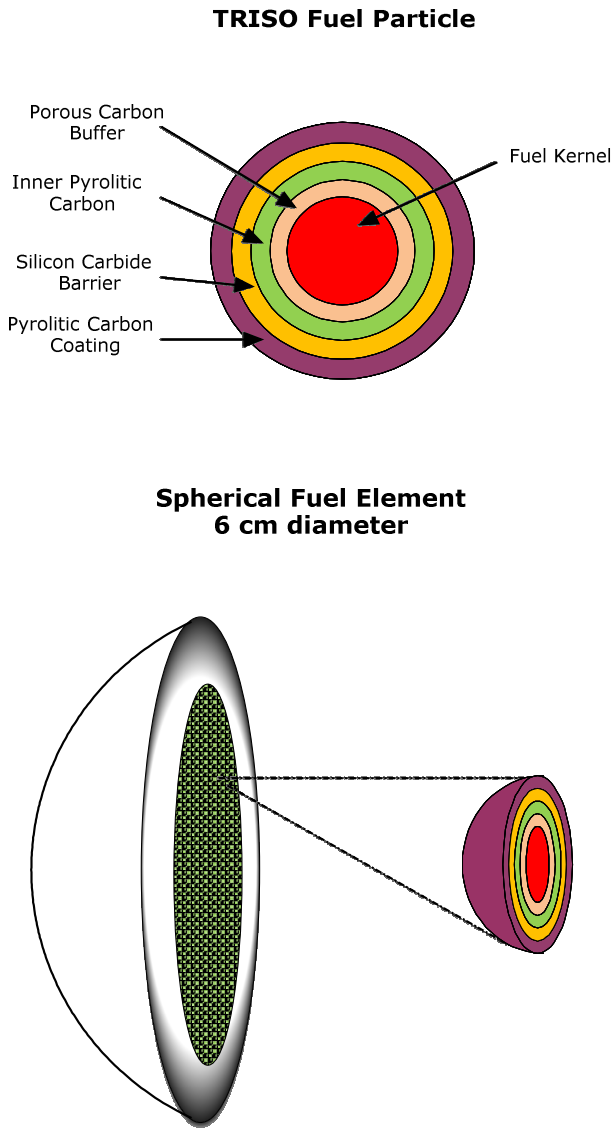

Fig. 6. Fuel Element Schematic

There were two modeling techniques used for the pebble bed core. The first method involved homogenizing only the fuel regions in the fuel pebbles, while the second homogenized the entire pebble bed including fuel pebbles and dummy graphite pebbles. The identifiers used for these models are as follows: the explicit pebble model, and the homogenized model. Both models properly account for the double heterogeneity features as it is described later in this thesis. Aside from the fuel region of each of the models, the remainder of design stayed the same.

III.A.3.1 EXPLICIT PEBBLE MODEL

The explicitly modeled pebble core is one of the most detailed representations possible to implement within the SCALE code system. As opposed to homogenizing the entire bed of pebbles in the fuel region, only the TRISO particles are homogenized within the central graphite matrix of the pebble. An example of this scheme is shown in Figure 7. A half sphere slice made up of TRISO particles in a graphite matrix, is shown homogenized into a central region.

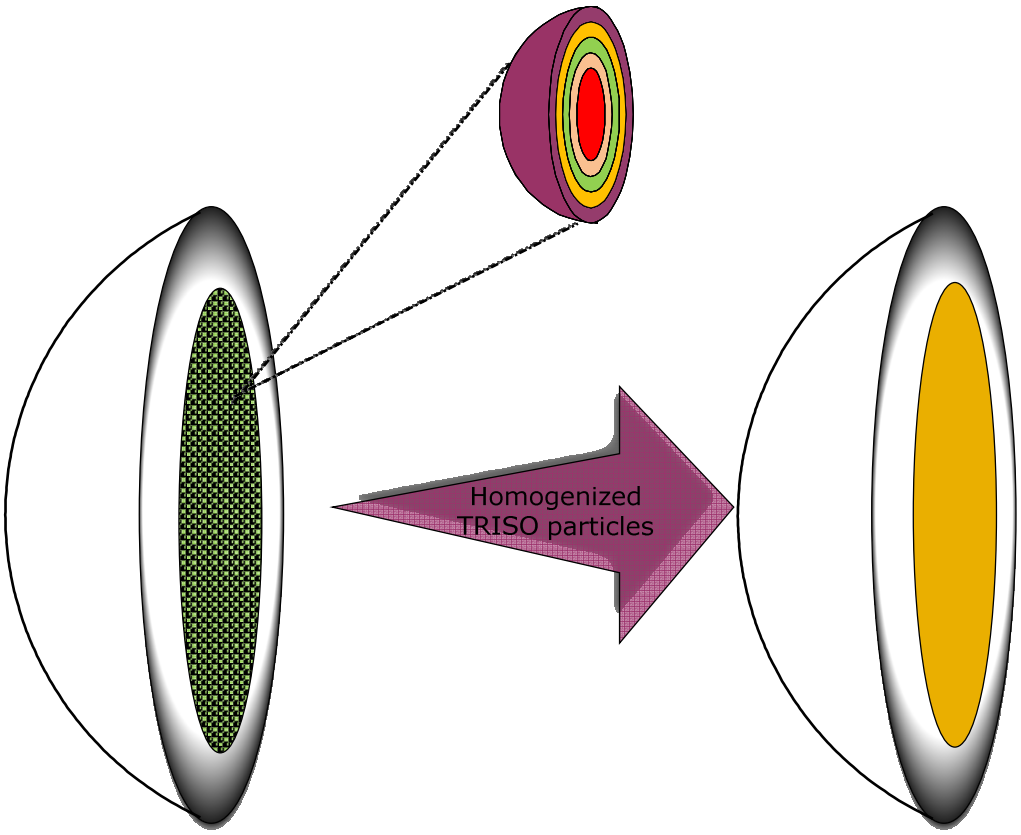

Fig. 7. Fuel Pebble Homogenization Scheme

The modeling ability is well represented in SCALE by creating an array of spheres arranged in a triangular-pitch (dodecahedral) lattice. The cross sectional view of the unit cell for this lattice is shown in Fig. 8 and contains three regions: 1) fuel kernel, 2) all coating layers, 3) outer graphite matrix. Given the number of fuel particles per fuel compact and the geometric construction of each, the unit cell dimensions were calculated and are listed in Table IV.

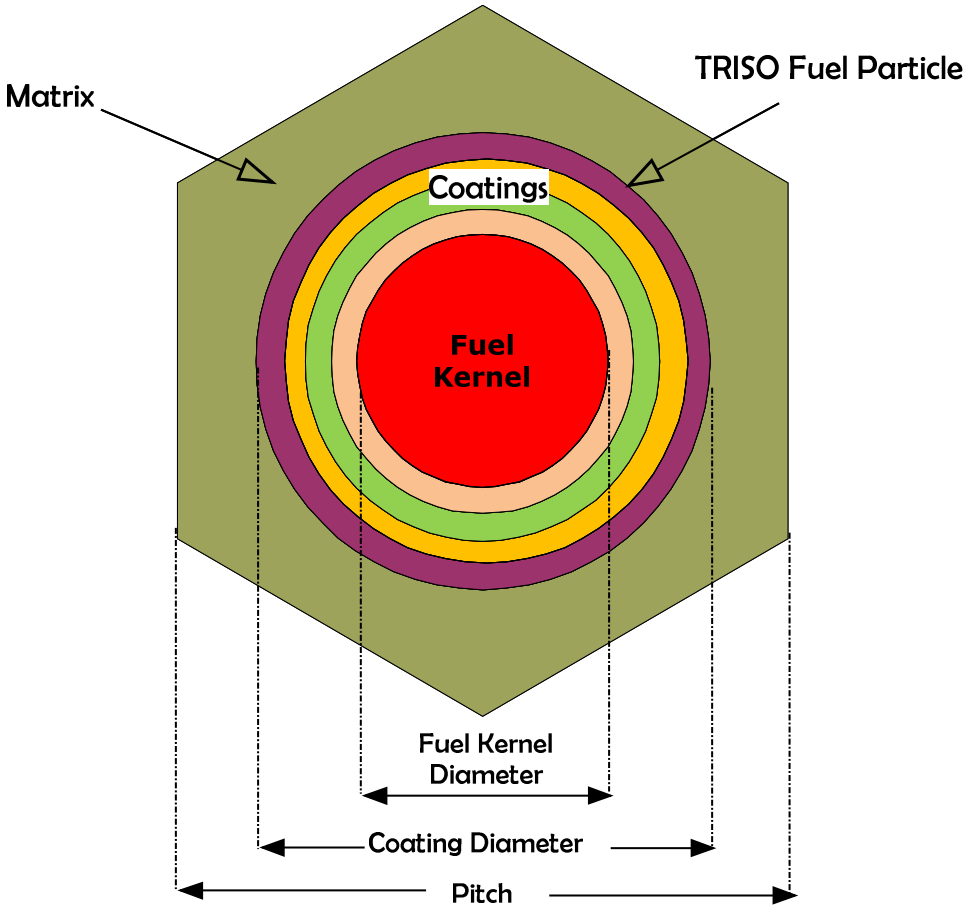

Fig. 8. Vertical Cross Section of Triangular Pitch Unit Cell (Explicit Pebble Model)

Table IV gives the dimensions of each region in the unit cell. These values were calculated based on the number of particles per pebble, pebble geometry specifications, and specified void fractions.

Table IV. Unit Cell Dimensions (Explicit Pebble Model)

Fuel Kernel Diameter	0.050 cm
Fuel Coating Diameter	0.091 cm
Pitch	0.2085 cm

A random packing fraction of pebbles is considered in the range of 0.61-0.62 (or void fraction of 0.38-0.39). This random packing cannot directly be simulated in SCALE, thus a body-centered cubic (BCC) lattice structure was implemented. This unit cell contains a fuel pebble at the center and fractions of moderator pebbles at each corner for a total of two spheres in a unit cell. This design facilitates altering the moderator-to-fuel pebble ratio. By simply changing the diameter of the moderator pebble, the desired ratio is achieved. Figure 9 gives an idea how this unit cell was constructed and stacked into an array to form the core. The final array size of a fully loaded cylindrical core is 27 by 27 by 21 unit cells.

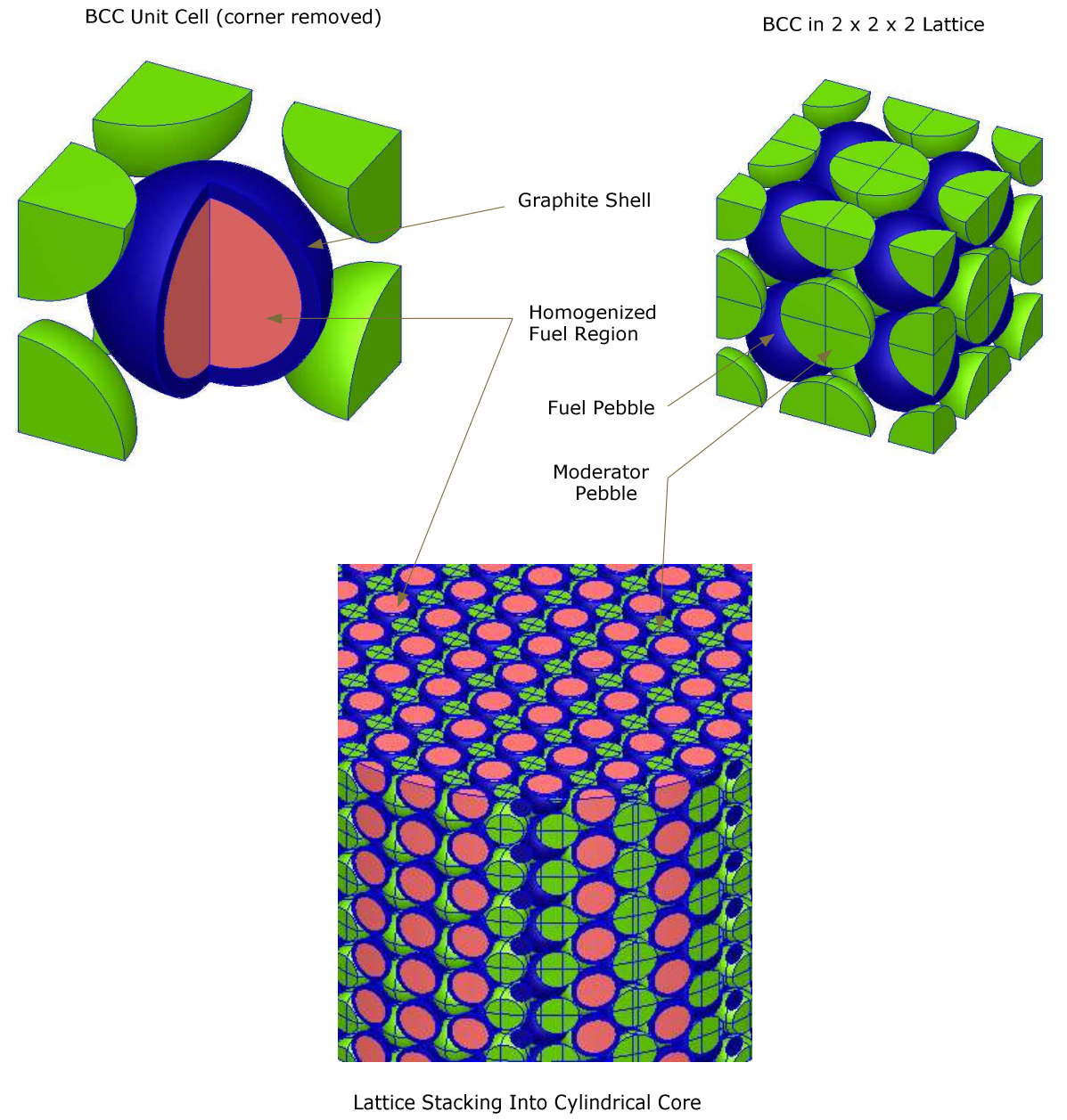

Fig. 9. BCC Unit Cell Schematic (KENO 3D)

Geometry specifications for the pebble-bed model were kept the same in both model configurations. These included moderator to fuel pebble ratio, radii, packing fraction, and unit cell dimension. They are summarized in Table V.

Table V. Pebble-Bed Geometry Specifications

Fuel to Moderator Pebble Ratio	57:30
Fuel Pebble Radius	3.0 cm
Fuel Region Radius	2.5 cm
Graphite Shell Thickness	0.5 cm
Packing Fraction	0.61
Moderator Pebble Radius	2.731 cm
Unit Cell Size	6.8873 cm

The input file created for this model contained 347 lines of code with 124 geometry regions. The computations were run on three machines: 1) 2005 Dell Precision 670 Elite Workstation with 4 GB of RAM and a 3.80 GHz processor, 2) 2006 Dell Precision Workstation with two dual core processors and 4 GB of RAM, and 3) the Oak Ridge National Laboratory NUC Cluster. This cluster is composed of 30 machines which are four processor Compaq Alphas. The processors are the Alpha AXP (667 MHz), a 64 bit RISC microprocessor. The memory on most machines is 2 GB, 4-6 GB on some, 18 GB on one and 31 GB on another. Most of the calculations were run with 200 generations and 1,000 histories per generation, resulting in a sample size of 200,000 and a four hour runtime for machine 1 and 2, and about a two to three hour runtime for machine 3.

III.A.3.2 HOMOGENIZED MODEL

In the fully homogenized model, the entire pebble bed core is lumped into one homogeneous region. This virtually smears the fuel particles with the graphite matrix, moderator pebbles, and void space (occupied by helium coolant). The SCALE module CSAS6 was used in a similar fashion to the explicit pebble model with the triangular-pitch (dodecahedral) lattice. The cell contains three regions: 1) UO_2 fuel kernel, 2) homogenized TRISO coatings, and 3) mixture containing a fraction of the graphite matrix from the fuel pebble, moderator pebbles, and void space between pebbles in the core. This unit cell setup is shown as a cross section in Fig. 10.

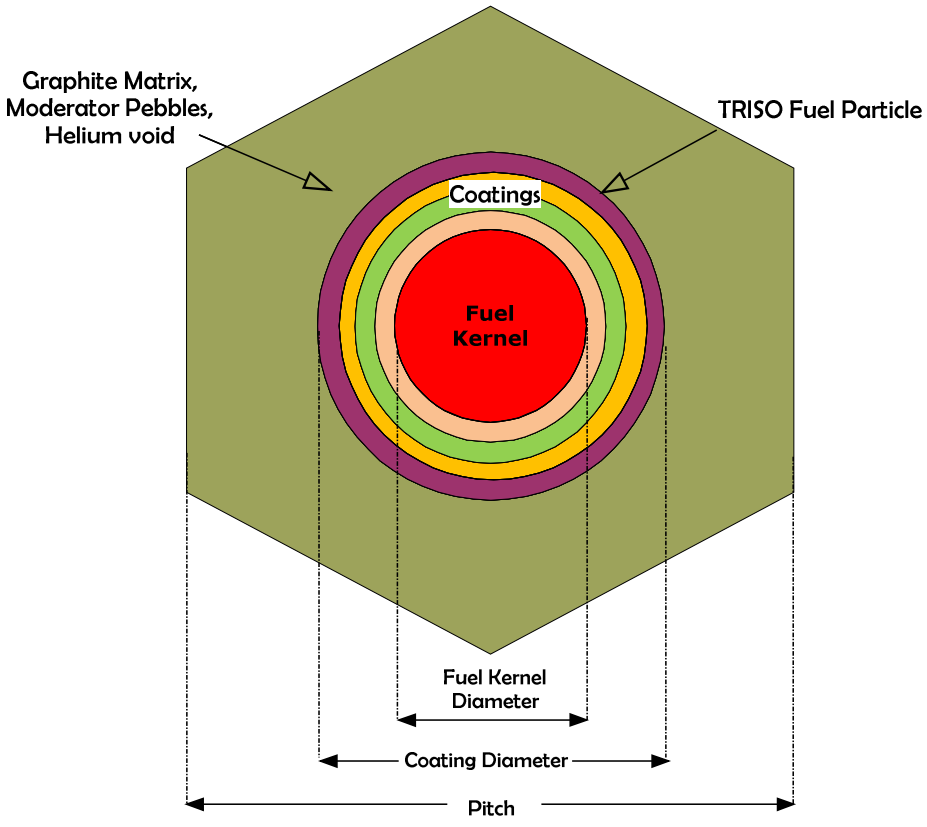

Fig. 10. Vertical Cross Section for Triangular Pitch Unit Cell (Homogenized Model)

The unit cell dimensions for this model are shown in Table VI. These are based on knowing the number of particles per fuel element, the number of fuel elements, and the geometry of the fuel region.

Table VI. Unit Cell Measurements for Homogenized Model

Fuel Kernel Diameter	0.05 cm
Fuel Coating Diameter	0.091 cm
Pitch	0.3562 cm

III.B. DOUBLE HETEROGENEITY TREATMENT

The two VHTR designs both encounter modeling complications with double heterogeneity. The first level of heterogeneity is seen with the microparticle fuel. Each fuel kernel is surrounded first by the coating layers of the TRISO particle, and then by the central graphite matrix of the pebble. Within each pebble, the central fuel region (containing the randomly distributed microparticles) is surrounded first by the graphite shell of the pebble and in addition, by the helium coolant and dummy graphite pebbles. This produces two level of heterogeneity.

There are various neutron streaming passages formed by the pebble-bed voids, coolant channels, instrumentation and handling channels, plenums, etc. The proximity to outer and central reflector regions is also an important factor that influences the VHTR physics.

The resonance self-shielding effects are determined by the microscopic flux behavior in the fuel, which strongly depends on the geometry of the fuel configuration.

As a result, the resonance absorption should be calculated on the basis of the microscopic lattice of the coated fuel microparticles. The neutron mean free path in this lattice is so large compared to the dimensions of a pebble that the lattice cannot be considered infinite. Therefore, other pebbles as well as additional core features cannot be neglected [27-29].

III.B.1. SCALE 5.0 AND DANCOFF FACTOR

As part of the unit cell declaration in creating the SCALE version 5.0 input file, CSAS6 allows for an externally entered Dancoff correction factor. This factor can greatly improve the accuracy of the model (Chapter II.B) and was calculated using DANCOFF-MC. The program input values are: the type of lattice, radius of the environment (the number of pitches within the radius of the fuel pebble), fuel radius, outer coating radius, pitch, total macroscopic cross section for the coating, and total macroscopic cross section of the graphite matrix containing the TRISO particles. The cross sections were taken from the materials at 0.0253 eV (2200 m/sec, room temperature). This modeling also uses an array of spheres in a triangular-pitch (dodecahedral) lattice. The input values are listed in Table VII.

Table VII. DANCOFF-MC Input Parameters

Environment	$\Sigma_{coating}$	$\Sigma_{moderator}$	Fuel Radius	Coating Radius	Pitch
8.4 pitches	0.37 cm^{-1}	0.402 cm^{-1}	0.02985 cm	0.04645 cm	0.3562 cm

Fig. 11 is an illustration of the cross section of a fuel pebble with the central graphite matrix containing TRISO particles. The environment dimension is shown in this picture.

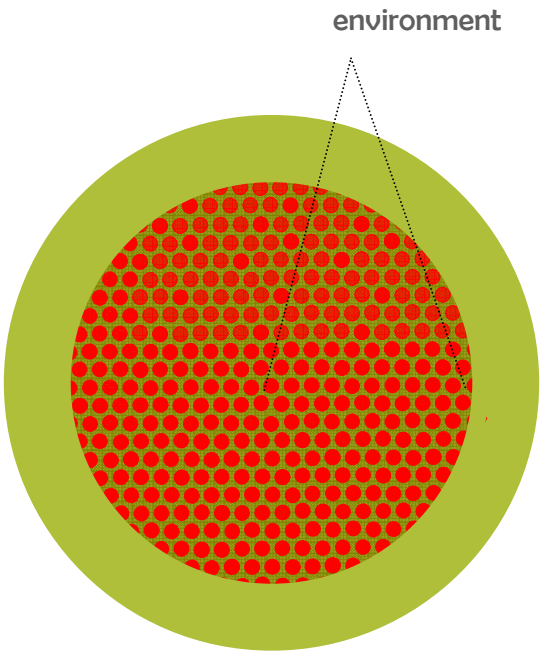

Fig. 11. Pebble Representation for DANCOFF-MC Input Parameters

The homogenized model had calculations initially run using the SCALE 5.0 code package. Since this version of the SCALE system requires an externally entered Dancoff factor for proper double heterogeneity treatment, DANCOFF-MC was used to produce it. The value produced for the homogeneous model was 0.24564. This number corresponds to the probability that a neutron isotropically emitted from the surface of a fuel element will enter another fuel element without colliding with a moderator nucleus

along the way. This Dancoff factor is specific for the specified moderator to fuel ratio as listed in Table I. As the ratio is altered, a new factor is produced.

III.B.2 SCALE 5.1 AND DOUBLEHET

With the release of SCALE version 5.1 came the enhanced capabilities of directly modeling a doubly heterogeneous unit cell in the CSAS6 unit cell declaration. The unit cell was recreated for the homogeneous model for comparison, exactness, and consistency using the DOUBLEHET cell declaration option.

This option has two input regions: Layer 1 (microparticle level) and Layer 2 (pebble level). Layer 1 includes the TRISO particle (fuel and all coatings) and an outer matrix. The outer matrix is essentially the inner pebble graphite matrix material. Fig. 12 shows a cross section representation of the unit cell for Layer 1 and each dimension used in the declaration. Table VIII gives the input parameters for the cell with measurements and material makeup.

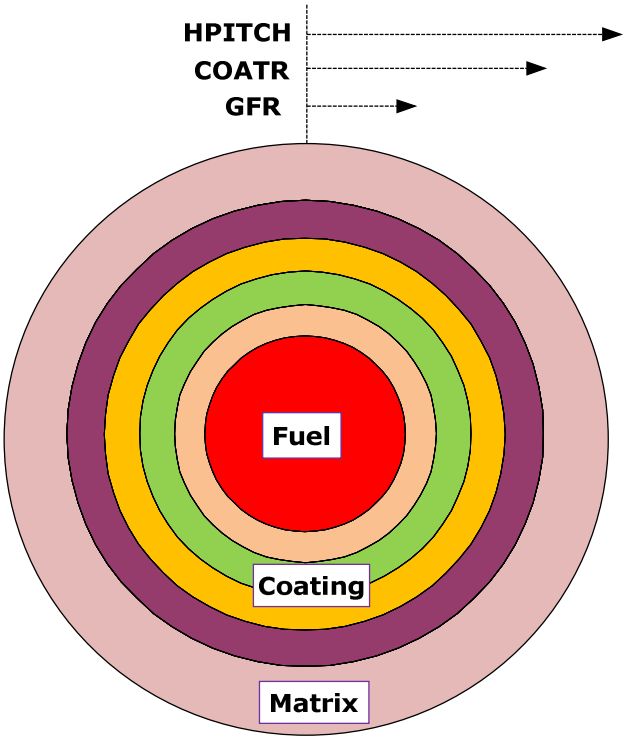

Fig. 12. Cross Sectional Representation of Layer 1 for DOUBLEHET Unit Cell

Table VIII. CSAS Input Parameters for Layer 1 of DOUBLEHET Unit Cell

GFR	fuel radius	UO2	0.02985
COATR	coating radius	SiC, PyC	0.04645
MATRIX	Inner graphite matrix	Graphite	no dimension
NUMPAR	number of particles	TRISO	8300

The second level of heterogeneity (Layer 2) is made up of the pebble and surrounding helium coolant. This level includes three zones which are described by the user's choice. This modeling procedure had two methods, labeled A and B. Both modeling approaches label the inner most zone (Zone 1) as the fuel region. This region

is the inner pebble graphite matrix containing the TRISO particles (taken from layer 1). Approach A puts the outer graphite shell of the pebble plus a fraction of the surrounding moderator pebbles into Zone 2. The helium coolant alone then comprises Zone 3. In Approach B, Zone 2 contains only the outer graphite shell of the pebble, and Zone 3 is made up of the helium coolant and a fraction of the surrounding moderator pebbles. The mathematical relationships for the geometrics can be seen in Appendix X.

Fig. 13 is a general picture of how the cross section of Layer 2 looks and where each zone is located. Tables IX and X give the makeup of those zones for each modeling approach and the dimensions used for CSAS6 input.

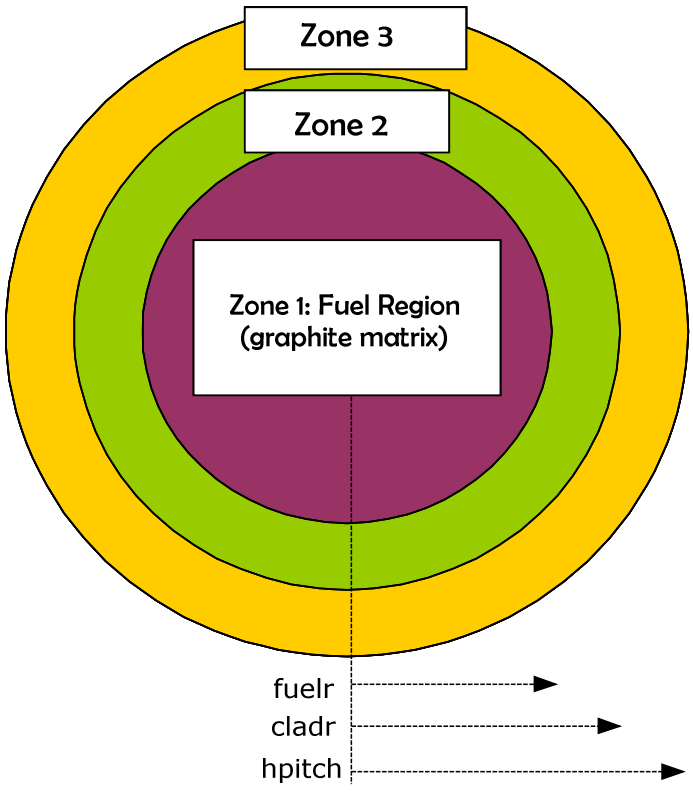

Fig. 13. Cross Sectional Representation of Layer 2 for DOUBLEHET Unit Cell

Table IX. Material Makeup for Two DOUBLEHET Modeling Approaches

	Approach A	**Approach B**
Zone 2	Outer graphite shell of fuel pebble + moderator pebble fraction	Outer graphite shell of fuel pebble
Zone 3	surrounding coolant	Surrounding coolant + moderator pebble fraction

Table X. CSAS Input Parameters for Layer 2 of DOUBLEHET Unit Cell

fuelr	2.5000 cm
cladr	3.4341 cm
hpitch	3.6400 cm

CHAPTER IV

RELIABILITY ANALYSIS OF THE PEBBLE-BED MODELING

IV.A VALIDATION OF THE PEBBLE-BED CORE MODEL (BENCHMARK ANALYSIS)

The benchmark problems are derived from start-up core physics tests and include analysis of the initial criticality (critical height benchmark), control rod worth (for initial and full core), and the isothermal temperature coefficient of reactivity.

Because the sufficiently well-defined HTR-10 experimental benchmark data are very limited, both experiment-to-code and code-to-code model evaluations were performed for the developed 3D VHTR pebble-bed core model. Due to the significant differences between code systems, the experiment-to-code model evaluations were of paramount importance in determining performance of the developed 3D pebble-bed model. The code-to-code model evaluation was performed only to compensate for scarcity of the available experimental information.

All calculations were performed in SCALE version 5.0 at room temperature (300K) with a Dancoff correction factor of 0.2527, as calculated by DANCOFF-MC. The total sample size for all benchmark cases was 200,000: 1,000 histories per generation and 200 generations.

IV.A.1 INITIAL CRITICALITY BENCHMARK

This benchmark involves evaluating the height of the fuel loading in the pebble-bed region at which the core produces an effective multiplication factor (k_{eff}) of 1.0.

This height is measured in centimeters from the upper surface of the conus region. The measurement was taken with the core under a helium atmosphere with all control rods withdrawn. The available height for pebbles to fill is 197 cm. The remainder of the region not filled with pebbles is a space containing helium.

Results from the initial criticality benchmark problem were compared to available experimental data for the same problem. The actual measured critical core height is one of the available experimental values describing the HTR-10 core.

IV.A.2 ISOTHERMAL TEMPERATURE COEFFICIENT BENCHMARK

This analysis included a calculation of the effective multiplication factor of the full (5 m^3) core under helium atmosphere and core temperatures of 300K, 393K, 473K, and 523K also with control rods withdrawn.

The obtained SCALE 5.0, CSAS6/KENO-VI sequence results were compared to the various code-to-code benchmark results for the temperature coefficient benchmark problem produced by researchers worldwide using the following code systems:

- VSOP – diffusion at the whole-core level (China – ENDF/B-V, GAM-THERMOS-CITATION, 4-group whole-core calculations, 3D reactor geometry)
- PANTHER – diffusion at the whole-core level (The Netherlands – JEF 2.2, coupled 2D thermal-hydraulics/3D diffusion, 2-group whole-core calculations, 3D reactor geometry)
- SRAC – diffusion at the whole-core level (Japan – JENDL-3.2, 6-group whole-core calculations)

- MCNP – continuous energy Monte Carlo at the whole-core level (U.S. and China – ENDF/B-V, 3D reactor geometry)

The isothermal temperature coefficient, α_T^n, for the fully-loaded core was evaluated using the effective multiplication factors, k_n and k_{n+1}, according to the following relationship:

$$\alpha_T^{\ n} = \frac{k_{n+1} - k_n}{k_{n+1} \cdot k_n} \cdot \frac{1}{T_{n+1} - T_n}$$

where:

α_T^n: Temperature coefficient between T_n and T_{n+1} ($\Delta k / k / K$)

T_n: Core temperature at n^{th} measurement (K)

T_{n+1}: Core temperature at $n+1^{th}$ measurement *(K)*

k_n: Effective multiplication factor at T_n

k_{n+1}: Effective multiplication factor at T_{n+1}

The critical control rod positions are changed with temperature elevation in the actual reactor operation. However, the control rod position is not changed in the calculation to obtain reactivity difference.

IV.A.3 SUMMARY OF BENCHMARK RESULTS

In the present analysis, a 10% discrepancy between computed values and the available experimental values was considered as the model acceptability threshold [8]. The results of the benchmark analysis showing comparison to experimental and code data are summarized in Table XI.

Table XI. Experiment-to-Code and Code-to-Code Benchmark Analysis

Isothermal Core Temperature	**HTR-10 Benchmark [2]**	**SCALE 5.0 (CSAS6, 238 Group, ENDF/B-V)**		
		3D VHTR Model		**Discrepancy (%)**
Dancoff Correction Factor	-	0.2527		-
Critical Pebble-Bed Height (cm)	123.06	126.10		+2.47
Core Multiplication, k_{eff} (Control Rods Withdrawn, Isothermal Core)				
300K	1.1358	Homo Core	1.153 ± 0.002	+1.5
		Expl Pebble	1.321 ± 0.003	+16.3
393K	1.1262	Homo Core	1.135 ± 0.002	+0.8
		Expl Pebble	1.301 ± 0.002	+15.5
473K	1.1168 (interpolation)	Homo Core	1.125 ± 0.002	+0.3
		Expl Pebble	1.286 ± 0.002	+14.6
523K	1.1111	Homo Core	1.115 ± 0.002	+0.3
		Expl Pebble	1.274 ± 0.002	+14.7
Isothermal Temperature Coefficient, α_T (Δk/k/K)				
Isothermal Core	-9.70E-05	Homo Core	-1.40E-04	+39.8
		Expl Pebble	-1.30E-04	+31.6

The HTR-10 cases with the control rods fully withdrawn resulted in the discrepancies in k_{eff} up to +1.5% in the homogenized core model and +16.4% in the explicit pebble model. The observed over prediction of the homogenized core model is due to the small size of the pebble-bed affecting calculations using SCALE 5.0 and the limited availability of HTR-10 design data.

The explicit pebble model produced larger deviations on the order or 14-16%. This is due to ambiguity of available information regarding modeling techniques and the core configuration. The computational results for the homogenized core are in agreement with the available experimental data. The obtained results from the

experiment-to-code benchmark analysis resulted in successful validation of the VHTR pebble-bed core model with the homogenized fuel region.

There was a larger deviation (40%, 32%) of the temperature coefficient of reactivity from available computational results. There are several possibilities for this large discrepancy. It is expected that increasing the sample size of the model would lead to reducing the discrepancy some. In addition, there are differences due to the reactor physics features and limited design information.

The initial results for critical pebble-bed height at 300K are consistent with published benchmark data to within 3%. A code-to-experiment discrepancy of less than 10% is generally accepted internationally and was the targeted goal in this research in order to proceed with using the model. This data validates the 3D full core model and hybrid calculations using the SCALE code system.

IV.B PROTOTYPE PEBBLE-BED VHTR CONFIGURATION

The pebble-bed configuration with fully withdrawn control rods, and a fully homogenized core at a height of 123.06 cm was chosen as the prototype configuration. This case had the best observed agreement with the experimental benchmark. Table XII summarizes basic reactor physics characteristics obtained for the prototype VHTR configuration.

Table XII. Basic Reactor Physics Characteristics of the Prototype HTR-10 at 300K

k_{eff}	Fission-Inducing Energy (eV)	Mean Free Path (cm)	Fission Neutron Yield	SCALE 5.0 Run Time (min)
1.153 ± 0.002	0.0491 ± 0.0001	3.352 ± 0.002	2.43729 ± 2E-6	273.47733

Through adjusting configurations of the pebble-bed core, it is proposed that spectrum shifting can be achieved. This could provide an end result of improving fissile properties of minor actinides. With this as the final target, the energy-dependent neutron flux of the fuel region is a carefully monitored output throughout every analysis. Fig. 14 is a plot of the average energy-dependent neutron flux obtained for the cylindrical fuel region for the prototype configuration. The flux profile matched expectations of the VHTR system. This includes a large thermal peak, a 1/E dependence in the resonance region and the smaller fast peak.

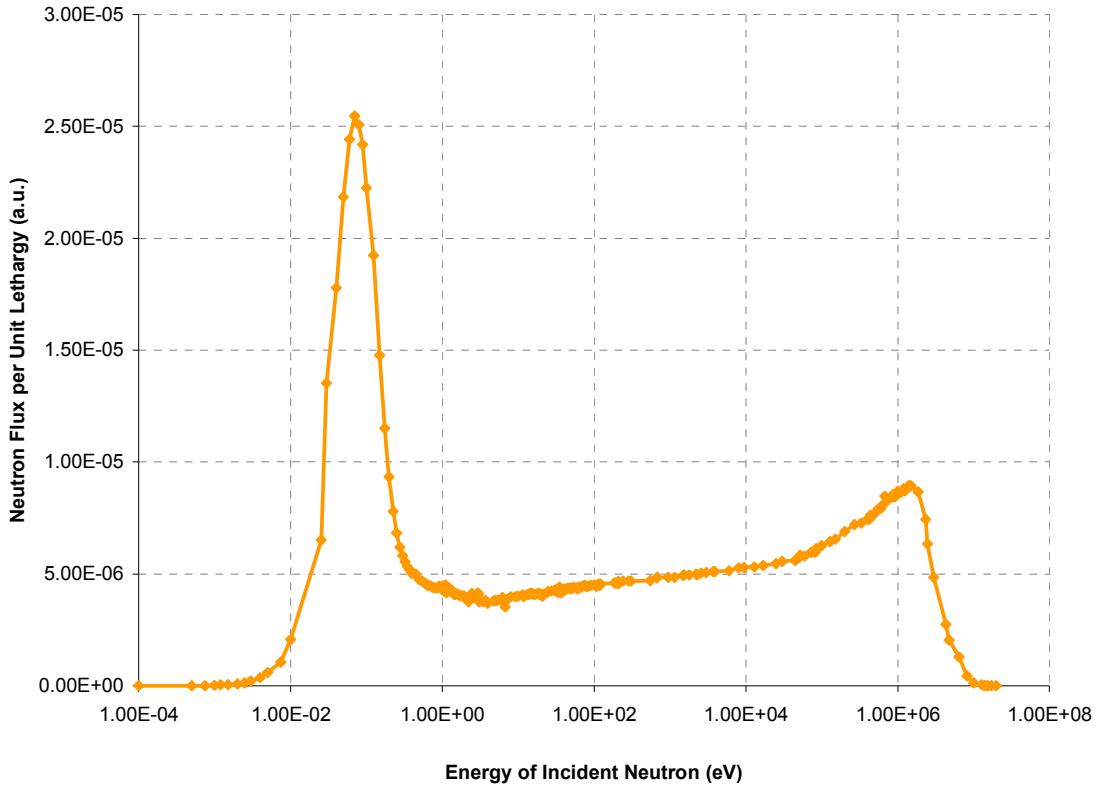

Fig. 14. Energy-Dependent Neutron Flux in the Fuel Region

Fig. 15 shows the average energy dependent neutron flux in each layer of the TRISO microparticle. These flux values are taken from the output of the XSDRN module of SCALE which is responsible for the double heterogeneity cell treatment. Zone 1 corresponds to the inner most region, or the fuel kernel, and zone 6 corresponds to the outer most region, or the graphite matrix that the TRISO particles are embedded within.

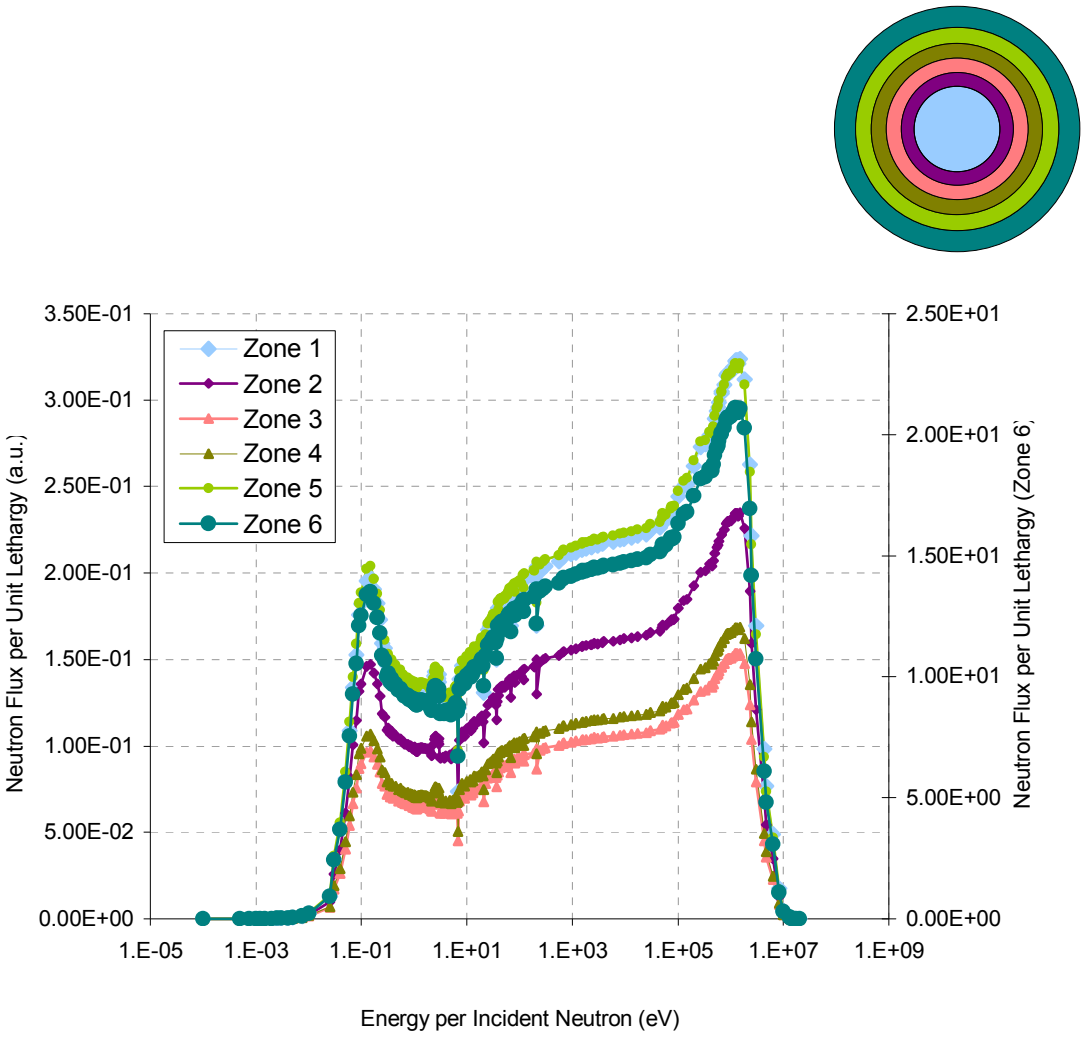

Fig. 15. Energy Dependent Neutron Flux in Microparticle Zones

The flux spectrum within the microparticle resembles that from a fast system. The small peak in the thermal region and large peak in the fast region are due to the lack of moderating graphite in the TRISO particle. It is composed of a fuel kernel, SiC, and PyC, none of which provide sufficient moderating power to cause the thermal energy

region to peak significantly. Many neutrons are born in the fuel which produces the large peak in the fast region.

The average neutron flux through the various zones of the pebble is shown in Fig. 16 which is a closer representation to the system spectrum. Zone 1 corresponds to the central fuel region, Zone 2 to the outer graphite shell, and Zone 3 to the matrix.

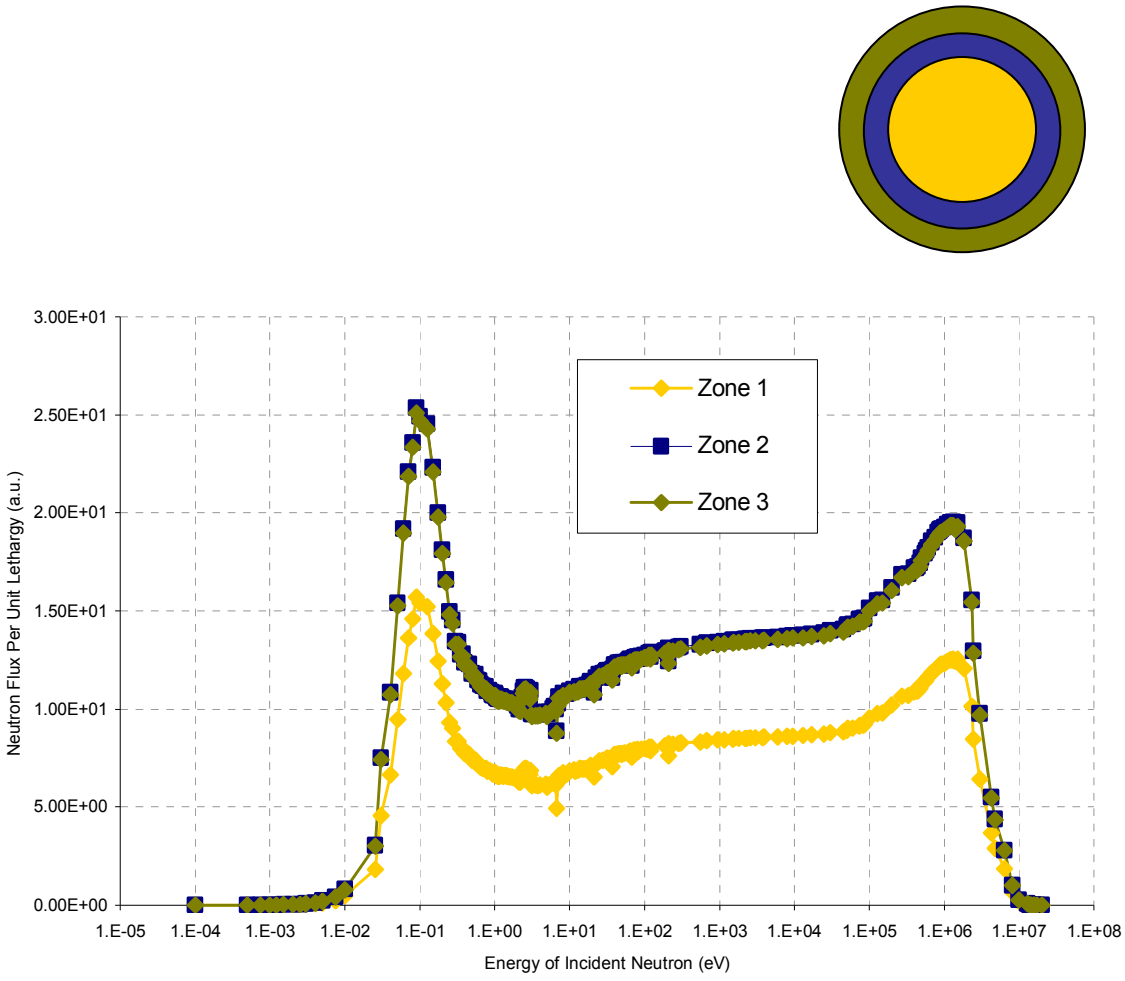

Fig. 16. Energy Dependent Neutron Flux in Pebble Zones

With the presence of more graphite in the pebble compared to that in the microparticle, there is much more moderation of fast neutrons. This additional graphite is responsible for the more pronounced thermal peak.

IV.C NEUTRON SPECTRUM SHIFTING CAPABILITIES

Specific spectral characteristics can be varied in the pebble-bed VHTR by mixing dummy graphite pebbles and fuel pebbles at a desired ratio. The degree of heterogeneity and the moderator to fuel ratio (M/F ratio) can be adjusted to achieve the desirable spectrum shift. Therefore, there is a possibility to enhance fissile properties of minor actinides by configuration adjustments.

An easy adjustment of the moderator to fuel ratio is found in the model's unit cell. Fig. 17 is a simple diagram showing how a cell could look with a different moderator to fuel ratio. The new cell has both a new pitch, and new Dancoff correction factor but the same central fuel region. Table XIII gives these values for the five ratios used.

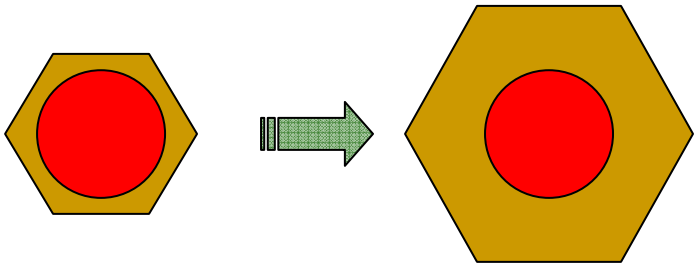

Fig. 17. Unit Cell Geometric Modifications for M/F Ratio Adjustments

Table XIII. Geometric Specifications for Pebble Ratio Adjustments

M/F Ratio	Carbon-to-Fuel Atom Ratio	Pitch (cm)	Dancoff Factor
0/1	735.9	0.31396	0.24676
1/3	976.3	0.34554	0.24612
1/1	1277.4	0.39558	0.24577
2/1	2179.9	0.45282	0.24536
4/1	3623.9	0.53688	0.24523

Table XIV gives a complete summary of the effect of altering the moderator to fuel ratio on reactivity, average energy inducing fission, and the system mean free path. This table also shows that variations to the moderator to fuel pebble ratio are equivalent to the variations of the carbon to fuel atom ratio for the particular core configuration.

Table XIV. Moderator to Fuel Pebble Adjustments for the HTR-10 Core

Moderator-to-Fuel Pebble Ratio	Carbon-to-Fuel Atom Ratio	Dancoff Factor	Reactivity (%)	Average Energy Inducing Fission (eV)	Mean Free Path (cm)
Isothermal whole core criticality calculations at 300 K					
0/1 (0.000)	735.9	0.24676	5.7404	0.07224 ± 4.955E-04	3.497 ± 9.24E-03
1/3 (0.333)	976.3	0.24612	2.42	0.06190 ± 3.557E-04	3.480 ± 9.95E-03
1/1.3 (0.750)	1277.4	0.24577	-3.1999	0.05444 ± 3.482E-04	3.481 ± 7.13E-03
2/1 (2.000)	2179.9	0.24536	-19.6745	0.04499 ± 3.108E-04	3.488 ± 5.23E-03
4/1 (4.000)	3623.9	0.24523	-47.645	0.03952 ± 1.845E-04	3.488 ± 6.48E-03
Isothermal whole core criticality calculations at 393 K					
0/1 (0.000)	735.9	0.24676	5.321	0.08365 ± 1.895E-04	3.458 ± 2.53E-03
1/3 (0.333)	976.3	0.24612	0.5371	0.07170 ± 1.905E-04	3.460 ± 2.90E-03
1/1.3 (0.750)	1277.4	0.24577	-4.5587	0.06364 ± 1.097E-04	3.462 ± 2.31E-03
2/1 (2.000)	2179.9	0.24536	-22.43	0.05351 ± 1.164E-04	3.462 ± 2.81E-03
4/1 (4.000)	3623.9	0.24523	-51.676	0.04821 ± 6.741E-05	3.460 ± 2.00E-03
Isothermal whole core criticality calculations at 523 K					
0/1 (0.000)	735.9	0.24676	4.3062	0.10002 ± 1.986E-04	3.428 ± 2.33E-03
1/3 (0.333)	976.3	0.24612	-0.4016	0.08712 ± 1.927E-04	3.434 ± 3.12E-03
1/1.3 (0.750)	1277.4	0.24577	-6.5871	0.07818 ± 1.373E-04	3.435 ± 2.32E-03
2/1 (2.000)	2179.9	0.24536	-25.6913	0.06701 ± 1.157E-04	3.442 ± 2.73E-03
4/1 (4.000)	3623.9	0.24523	-56.2744	0.06104 ± 7.862E-05	3.436 ± 1.96E-03
Isothermal whole core criticality calculations at 1000 K					
0/1 (0.000)	735.9	0.24676	0.299	0.16297 ± 2.721E-04	3.376 ± 2.18E-03
1/3 (0.333)	976.3	0.24612	-5.2742	0.14606 ± 2.601E-04	3.387 ± 2.97E-03
1/1.3 (0.750)	1277.4	0.24577	-12.9944	0.13387 ± 2.087E-04	3.385 ± 2.16E-03
2/1 (2.000)	2179.9	0.24536	-37.0614	0.11899 ± 1.729E-04	3.386 ± 2.23E-03
4/1 (4.000)	3623.9	0.24523	-77.3993	0.11106 ± 1.143E-04	3.380 ± 1.73E-03

Fig. 18 displays the spectra for various moderator to fuel ratios in the fuel element at 1000K. The shift is relatively small compared to what it may look like in a large pebble-bed core (300,000 pebbles).

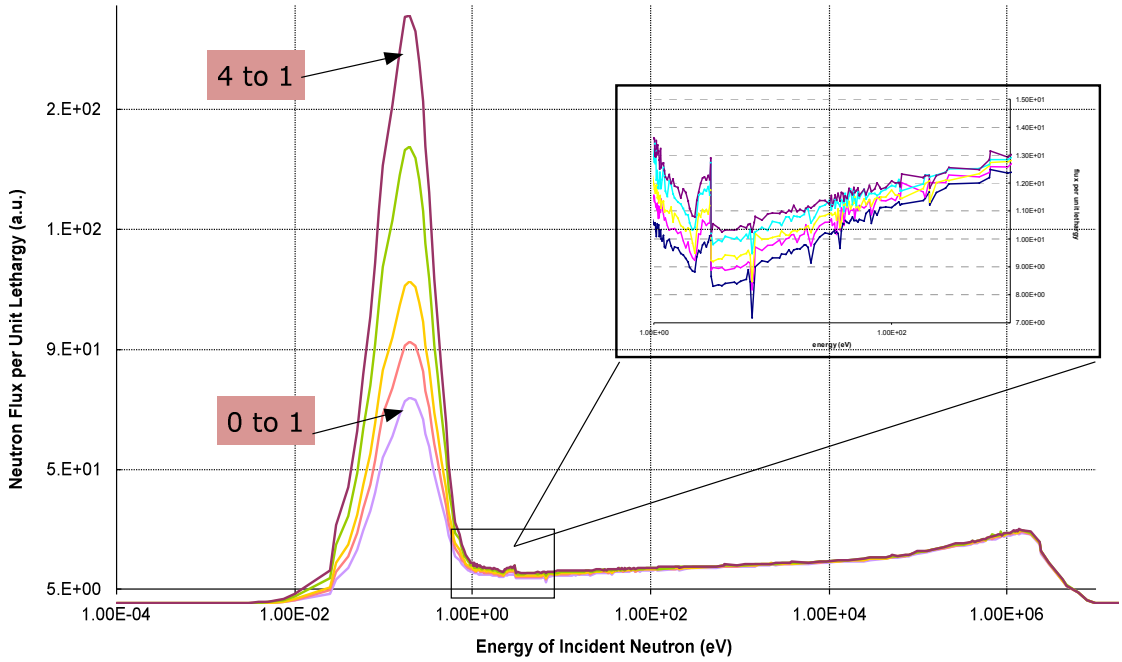

Fig. 18. Spectral Variations in the Prototype Pebble-Bed Core

At least in principle, promising core features and performance characteristics have been demonstrated. The spectral variations, although slight, give rise to the possibility of enhancing fissile properties of minor actinides by configuration adjustments. Under certain spectral conditions, minor actinides should be able to contribute to the core neutron balance by compensating for fuel depletion effects through their chain transformations.

CHAPTER V

CONFIGURATION VARIATIONS TO ACHIEVE ADVANCED DESIGN TARGETS

The work presented in this chapter is part of the analysis of large scale configuration adjustments in pebble-bed cores, including the power and cylindrical core designs, and advanced actinide fuel loadings.

V.A LARGE SCALE POWER REACTOR CONFIGURATION

The HTR-10 is the operating pebble-bed VHTR design and categorized as a small-scale VHTR. The core is about half of that of a full power VHTR [30]. The future reactors will most likely have annular core designs, whereas the HTR-10 has a cylindrical core design.

The annular core design is one of the more promising core designs for future industry VHTRs because of its high inherent safety characteristics following a loss of coolant accident. The decay heat removal is enhanced by introduction of the central graphite column. The heat transfer path is shortened since the active core region is relatively thin. As a result, the fuel temperature in a loss of coolant accident can be maintained at less than the fuel temperature limit of 1600˚C [29].

In the effort to integrate this research into a more practical setting, the HTR-10 research reactor model was transformed into a larger scale, pebble-bed reactor with dimensions on the order of a VHTR power reactor. The reactor was proportionately increased in size from the HTR-10 based on documented recommended dimensions of the large scale VHTR [31]. In addition to increasing the reactor's dimensions radially and axially, the large graphite column was added down the center of the entire model. Since this model was considered in a static environment, the pebble discharge system originally modeled in the HTR-10 was eliminated for this design for ease of modeling.

The large scale model has an available pebble bed fill height of 379 cm. The remainder of the pebble bed that isn't filled with pebbles contains helium gas. Fig. 19 gives a diagram of the large scale power reactor with the universal dimensions used for both the prismatic core and pebble bed core.

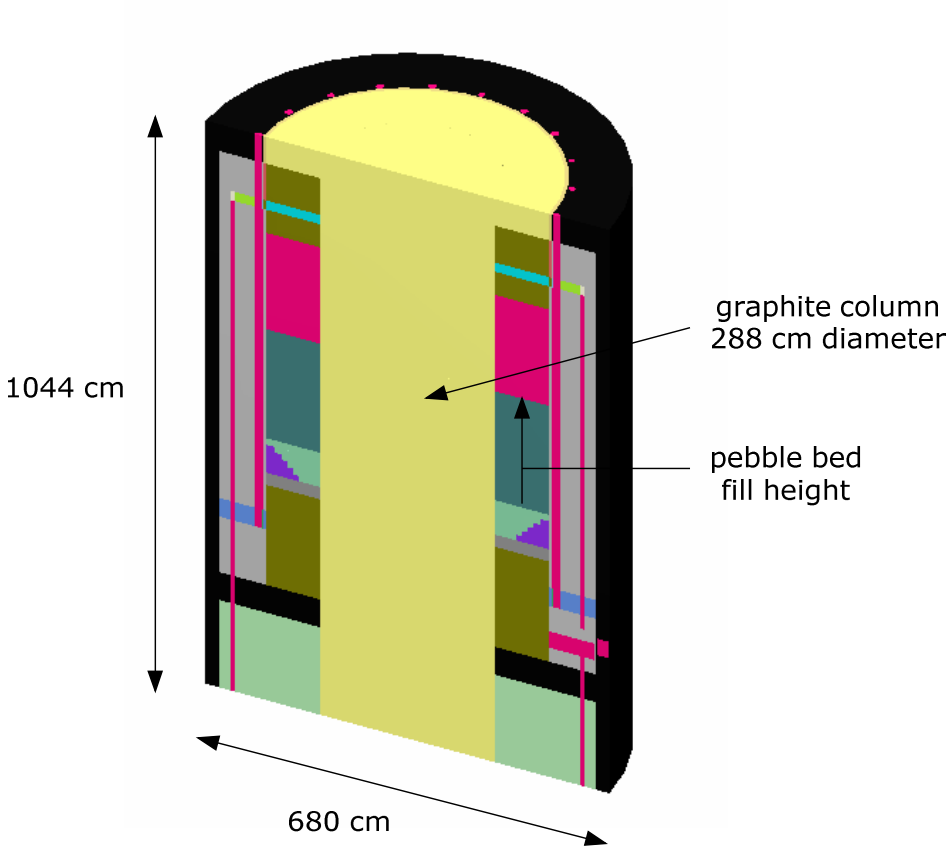

Fig. 19. Vertical Cross Section of Large Scale Power Reactor

The central graphite column has a primary purpose of heat removal, supplying a conducting medium for heat dissipation in accidents involving loss of primary coolant circulation. In a large power reactor, safety features such as the central graphite column are imperative.

V.A.1 LARGE SCALE MODEL NEUTRON ENERGY DISTRIBUTIONS

The annular core, like the cylindrical core, contains one fuel region filled to a desired height with pebbles. The neutron energy spectrum for this fuel region was

similar in shape to that for the small-scale prototype reactor (HTR-10). The two spectra are shown together in Fig. 20 for a fully homogenized fuel region modeled in KENO-V.a and run in SCALE version 5.0 using the Dancoff correction factor for double heterogeneity treatment.

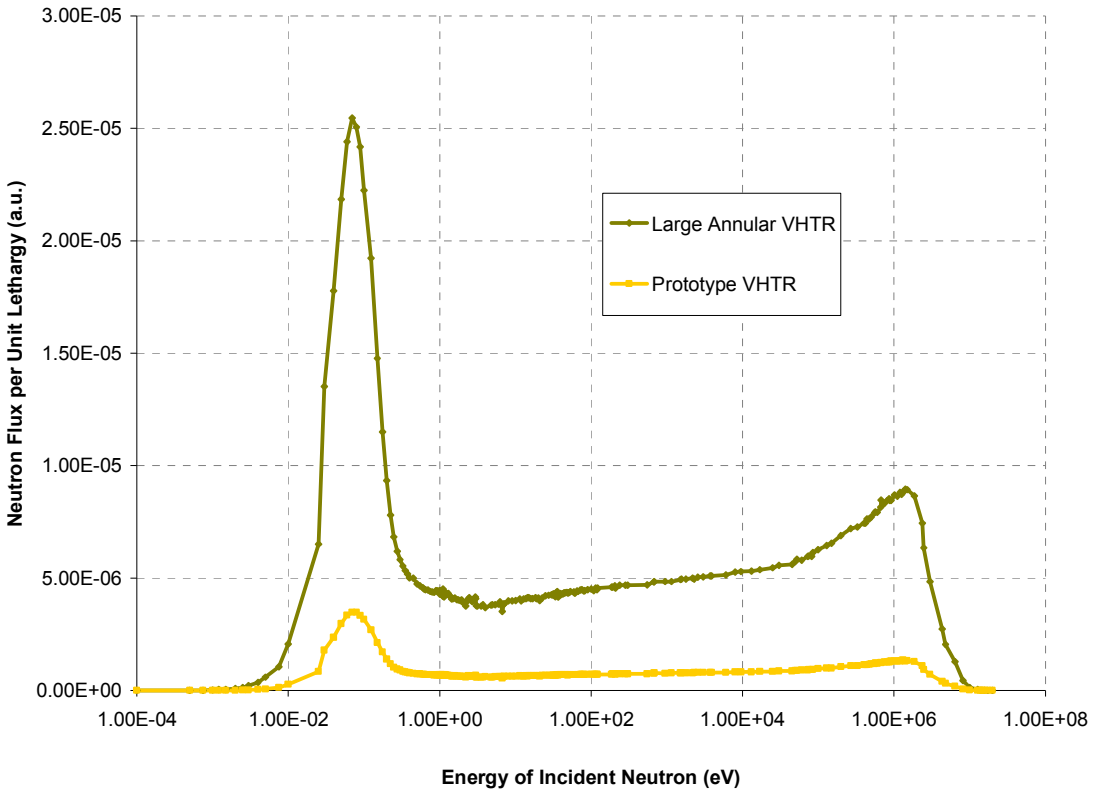

Fig. 20. Energy Dependent Neutron Flux for Small and Large Scale UO_2 Fueled Cores

As expected, the magnitude of the neutron flux in the large scale pebble-bed core is much larger than that in the small scale core. The large power reactor is more than

double the size of the prototype HTR-10 design but for this purpose was filled to a height of only 137 cm which resulted in a subcritial core.

It is expected to see a difference in the neutron flux spectrum as enrichment is increased. An example of this is seen in Fig. 21 with two enrichments (8% and 17%) of UO_2 fuel in ^{235}U. The higher enrichment of UO_2 simply increases the magnitude of the thermal peak and leaves the fast region unchanged since ^{235}U is a thermal fission material.

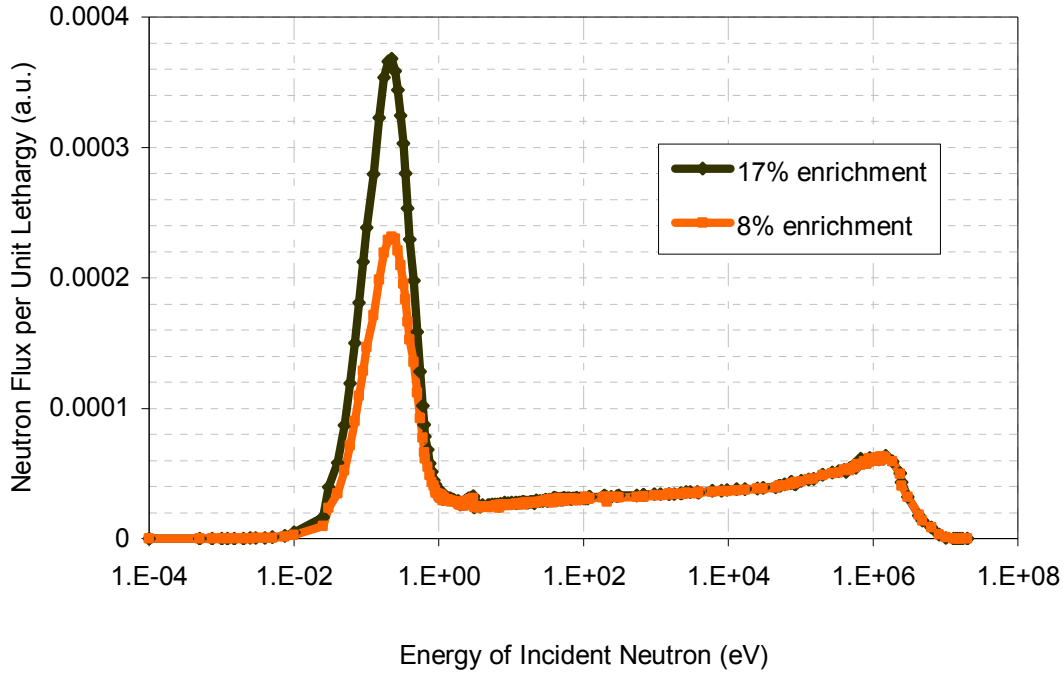

Fig.21. Energy Dependent Neutron Flux in the Fuel Region of the Large Scale Configuration: Different Fuel Enrichments

There is also a small effect in the thermal peak with increasing temperature. Fig. 22 shows an example of how an increase in temperature shifts the spectrum toward higher energies. The location of the peak is a function of the thermal motion of a neutron in the system. As the temperature of the surroundings increases, the thermal energy will also increase.

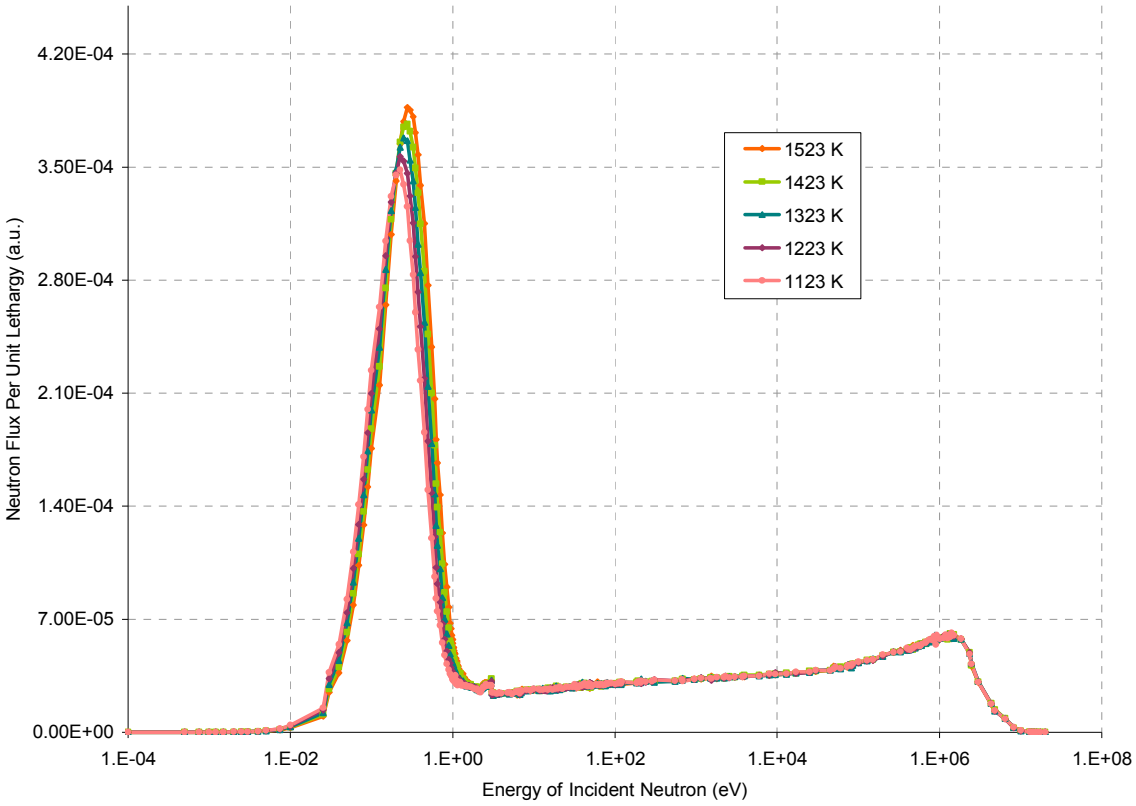

Fig. 22. Energy Dependent Neutron Flux in the Fuel Region of the Large Scale Configuration: Different Temperatures

In addition, by utilizing capabilities in SCALE version 5.1, a plot of the average energy dependent neutron flux in all regions of the large scale power reactor was produced. Fig. 23 shows how the flux within the fuel kernel compares to that in the microparticle system, fuel region of the pebble, entire pebble, and full system.

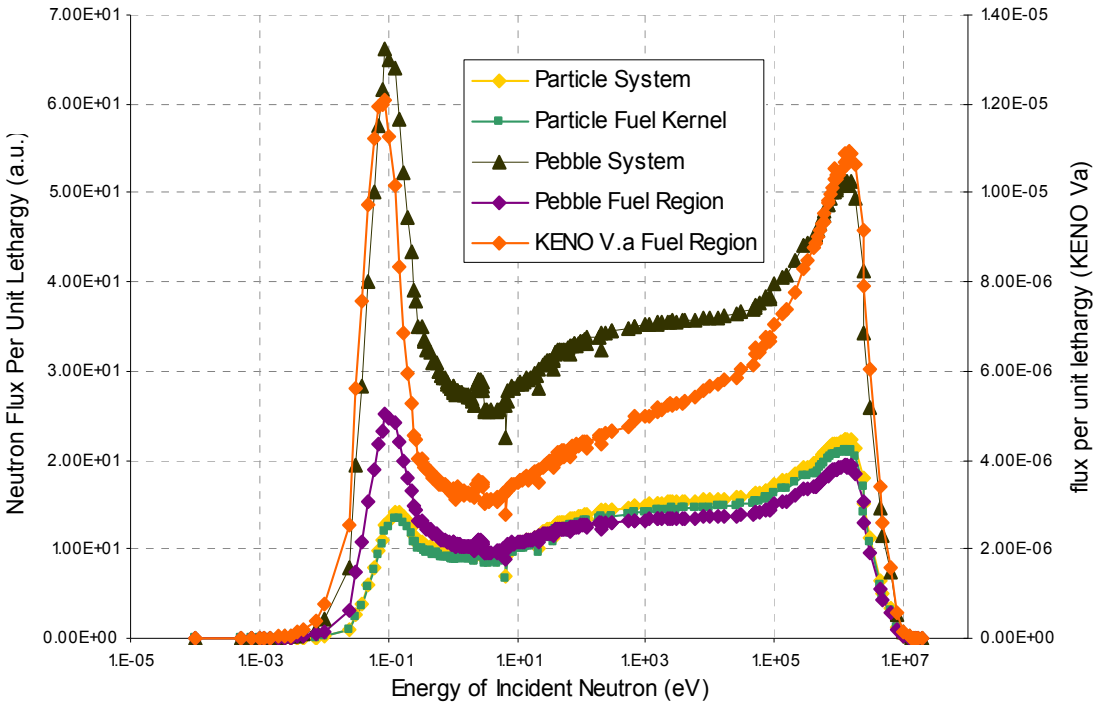

Fig. 23. Energy Dependent Neutron Flux for All Regions in the Large Scale Core

V.B FUEL LOADINGS CONTAINING ADVANCED ACTINIDES

The fuel pebbles within the cylindrical small scale and annular large scale core configurations were assumed to be loaded with the following fuels in order to perform an introductory analysis of the system's behavior:

- Uranium Dioxide (UO_2)
- Uranium Carbide (UC)
- Transuranics (TRU)
- Minor Actinides (MA)
- Reactor Grade Plutonium (RGPu)

V.B.1 VALIDATION OF MODELING TECHNIQUES WITH VARIOUS FUELS

The new version of SCALE (version 5.1) was released with direct double heterogeneity modeling capabilities. In order to reproduce the unit cell in the newer version and authorize its use for continued studies, a small analysis was performed in order to compare versions 5.0 and 5.1 of SCALE with and without direct double heterogeneity modeling and the two Monte Carlo codes, KENO-V.a and KENO-VI. This analysis was performed for the five fuels to get a detailed comparison.

V.B.1.1 SCALE SYSTEMS AND DOUBLE HETEROGENEITY METHODS

Several previous benchmark studies were selected to be run in the newest publicly available version of SCALE for comparison with the previously utilized version. This would not only show discrepancies and shortcomings with the benchmark studies but also provide a level ground for future work using the newer version, SCALE 5.1.

Table XV gives some reactor physics parameters associated with the performance of the model in each code system. The deviation between the two systems

is generally within the error bar. The fuel loading height was being held constant for other purposes and resulted in a subcritical core. This was not important for this validation and was left alone.

Table XV. Reactor Physics Results of the Large Scale Pebble Bed Core in KENO-V.a.

	Fuel	k_{eff}	Fission Inducing Energy (eV)	Mean Free Path (cm)
SCALE 5.0	Minor Actinides	0.0530 ± 0.00012	5.716 ± 6.722E-02	3.052 ± 2.646E-03
	Transuranics	0.8182 ± 0.0015	5.751E-01 ± 2.839E-03	3.060 ± 2.349E-03
	Uranium Carbide	0.7785 ± 0.0017	4.846E-02 ± 7.256E-05	3.119 ± 1.731E-03
	Reactor Grade Plutonium	0.9448 ± 0.0019	6.076E-01 ± 3.424E-03	3.069 ± 2.612E-03
	Uranium Dioxide	0.9757 ± 0.0022	6.377E-02 ± 1.099E-04	3.120 ± 1.845E-03
SCALE 5.1	Minor Actinides	0.0531 ± 0.0001	5.851 ± 6.673E-02	3.286 ± 1.432E-04
	Transuranics	0.8206 ± 0.0013	5.720E-01 ± 2.813E-03	2.897 ± 1.568E-05
	Uranium Carbide	0.7798 ± 0.0016	4.855E-02 ± 8.124E-05	2.437 ± 3.530E-06
	Reactor Grade Plutonium	0.9418 ± 0.0015	6.049E-01 ± 2.842E-03	2.894 ± 1.567E-05
	Uranium Dioxide	0.9750 ± 0.0022	6.370E-02 ± 1.080E-04	2.437 ± 2.673E-06

Fig. 24 displays two energy dependent neutron flux plots for the large scale power reactor model using KENO-V.a. The two spectra are taken from identical input files run in SCALE version 5.0 and version 5.1. It is clear from the diagram that the results are basically identical in energy spectra.

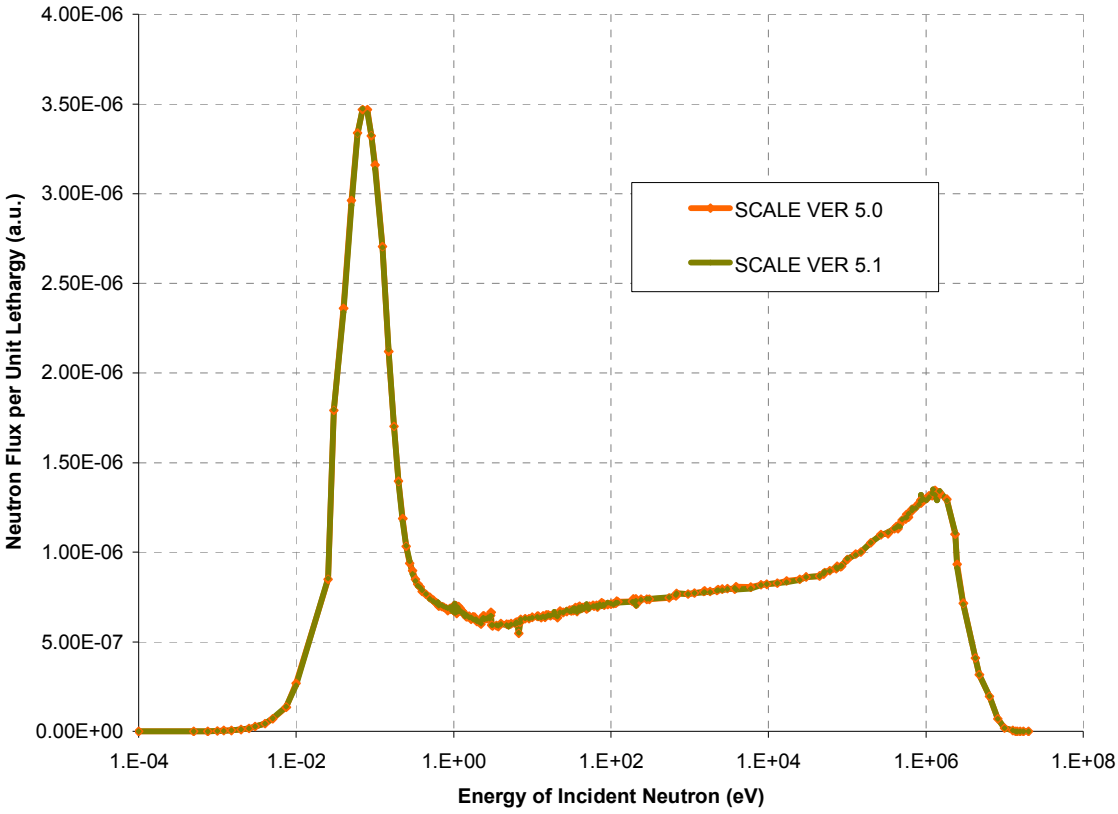

Fig. 24. Energy Dependent Neutron Flux for the Large Scale Reactor in KENO-V.a

A similar study was performed for the small scale prototype reactor with identical results.

Validating the use of various double heterogeneity modeling techniques is more complex than looking at the two version of SCALE. An entirely new unit cell declaration was implemented as explained in Chapter III.B.2. Since studies would continue with the DOUBLEHET unit cell option in SCALE 5.1, it was necessary to make sure that for these purposes it was performing as expected and to evaluate how the externally entered Dancoff correction factor from DANCOFF-MC had performed.

This small study was carried out for the small scale cylindrical core using SCALE 5.0 with an external Dancoff factor and SCALE 5.1 with DOUBLEHET unit cell treatment for five fuels. All of the cases chosen for this comparison were modeled in KENO-VI.

Table XVI gives a summary of the results from this study. All cases are subcritical; however, the benchmark was based on the near critical case of UO_2 while keeping the pebble bed fill height, volume fraction, and other variable parameters at a constant value with previous analyses.

Table XVI. Comparison of Double Heterogeneity Modeling Procedures for All Fuel Loadings

	DOUBLEHET		**DANCOFF FACTOR**		
	k_{eff}	±	k_{eff}	±	*% deviation*
MA	0.0573	0.00013	0.0532	0.0001	7.81
TRU	0.8179	0.0016	0.8206	0.0013	0.33
UO_2	0.9847	0.0019	0.9750	0.0022	0.99
UC	0.8335	0.002	0.7798	0.0016	6.44
RGPu	0.9429	0.0017	0.9418	0.0015	0.12

These results build confidence in the DANCOFF-MC calculations and previous modeling methods while indirectly validating the DOUBLHET unit cell treatment in SCALE 5.1. One possible explanation for the high discrepancy in minor actinides is that SCALE is not intended to be used for multiplication factors so extremely low thus the associated error is high. In addition, the two versions utilize different nuclear data files (ENDF-B/V and ENDF-B/VI, respectively) which could contribute to the difference.

V.B.1.2 SCALE SYSTEMS AND MONTE CARLO KENO CODES

In addition to the versions of SCALE and their associated modeling capabilities, the Monte Carlo criticality module, KENO, has two possible geometry packages. The differences between the two were explained in Chapter II.A and the results they produced are compared here.

Fig. 25 shows the neutron specra for the small scale, uranium dioxide fueled configuration in KENO-V.a and KENO-VI. Both cases were calculated in SCALE 5.0.

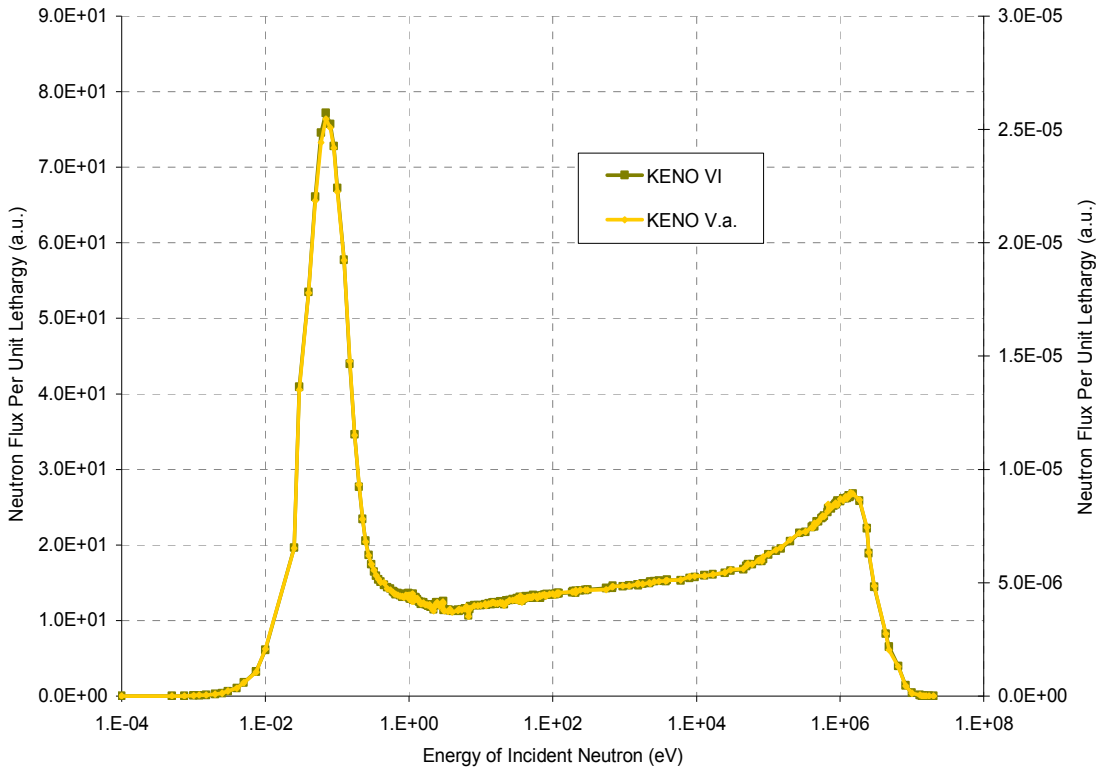

Fig. 25. Energy Dependent Neutron Flux for the Large Scale Reactor in KENO

From this plot it is clear that the two versions of KENO produce virtually identical results and there are no significant discrepancies between them. The models created in each version should be comparable and interchangeable. This is important because the large power configuration was made only in KENO-V.a.

V.B.2 SPECTRA ADJUSTMENTS WITH ADVANCED FUELS

Among the five fuels investigated, each produces a slightly different shape flux profile based on the individual nuclides involved and their associated cross sections as a function of energy.

The average energy dependent flux in the homogenized fuel region (for each loading: UO_2, UC, TRU, MA, and RGPu) of the large scale power reactor model at 1123K are shown in Fig. 26. Fig. 27 is a zoomed in plot from 10 keV to 10 MeV for the same fuels at 1523K which has slightly more exaggerated peak differences between fuels.

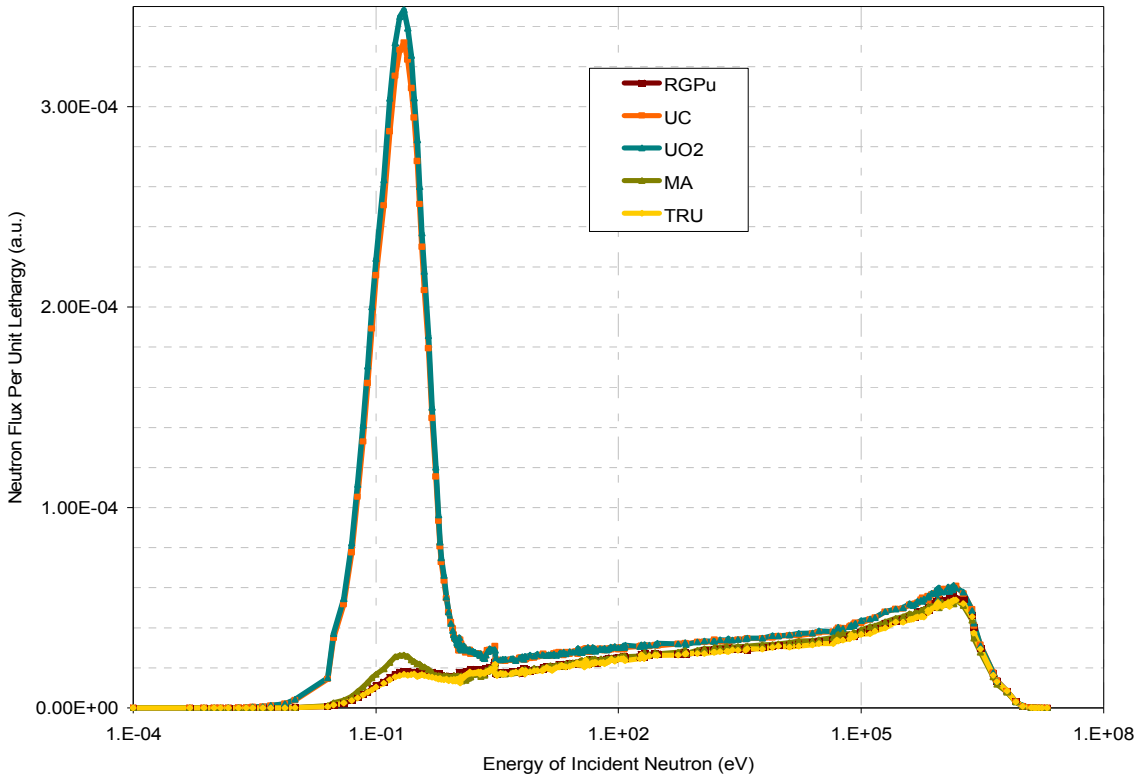

Fig. 26. Energy Dependent Neutron Flux in the Fuel Region for the Large Scale Configuration with Advanced Actinides at 1123K

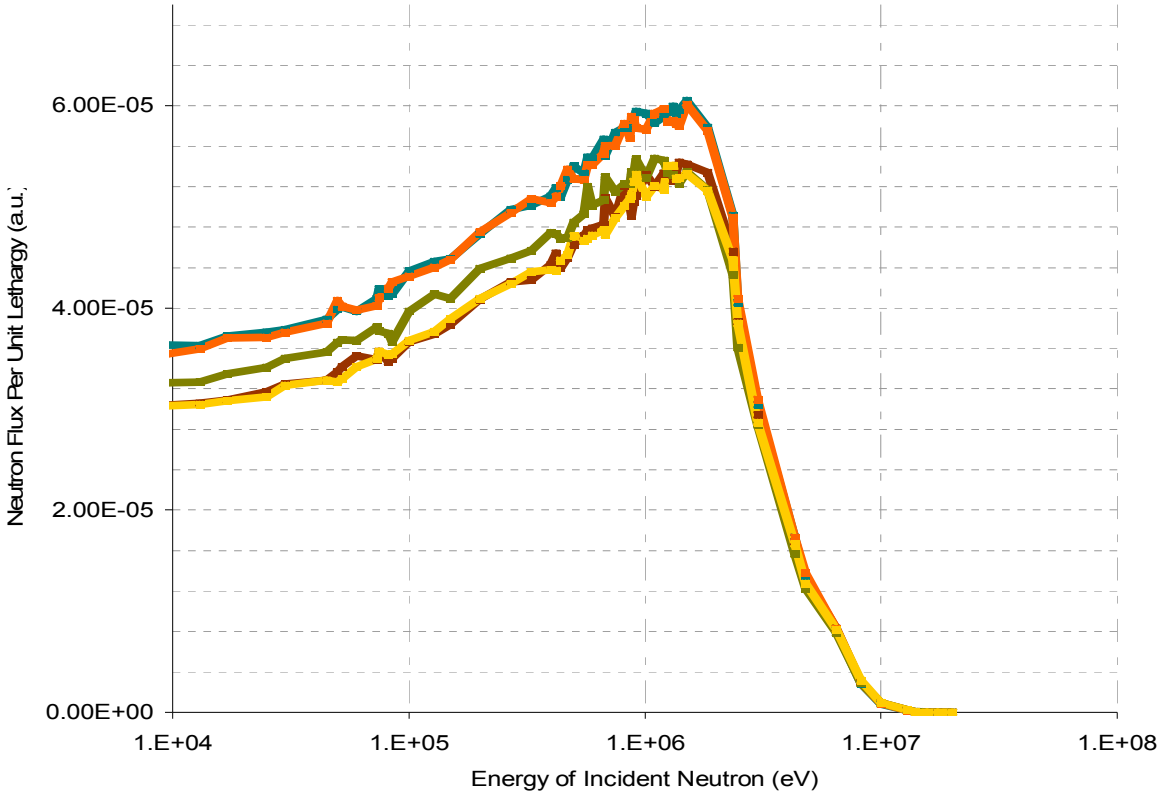

Fig. 27. Energy Dependent Neutron Flux in the Fuel Region for the Large Scale Configuration with Advanced Actinides at High Energies and 1523K

Figs. 26 and 27 show that it's difficult to distinguish between the various fuels at some points but it is clear that the uranium based fuels (UO_2 and UC) display the same general profile, marked by a peak in the thermal region. A slightly larger thermal peak is seen in UO_2 but is mostly consistent with the UC profile in all other energies. This effect could be contributed to the slightly higher absorption rate of carbide (in UC) at thermal energies compared to that of dioxide in UO_2.

The remaining fuels, TRU, RGPu, and MA, produce a relatively similar flux profile, marked by a peak in the fast region and the absence of a thermal peak. To see

this more clearly, the average energy dependent neutron flux for these fuel loadings at 1123K is provided in Fig. 28. It is clear that the absence of the thermal neutron peak for TRUs, RGPu, and MAs is due to dominant thermal neutron capture in those configurations.

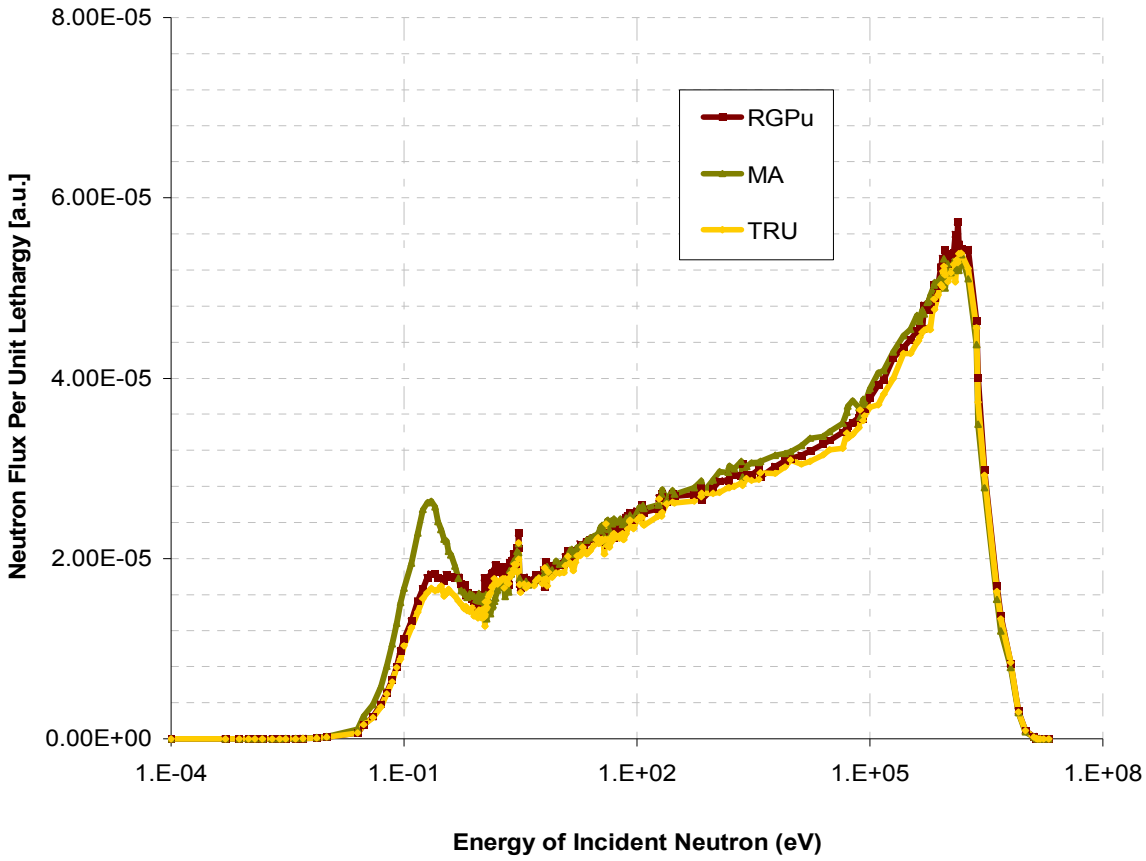

Fig. 28. Energy Dependent Neutron Flux in the Fuel Region of the Large Scale Configuration with TRU, RGPu, and MA fuel loadings at 1123K

As displayed, a definite fast spectrum is evident. There is a more pronounced peak in the MAs at lower energies and while this profile is higher throughout, the RGPu

peaks a little above MA in the fast region. However, according to Fig. 26 at 1523K, the RGPu does not have this slightly larger amplitude profile in the fast peak.

Table XVII summarizes basic reactor physics characteristics obtain for each of the fuel loadings in the large scale power configuration. A critical system is not reached in any of the cases. In order for the system to become critical, the volume fraction, fuel enrichment, or loading height must be increased. This was addressed in subsequent analyses, but for comparison between spectra, criticality was not necessary.

Table XVII. Basic Reactor Physics of the Large Scale Power Configuration at 1123K

Fuel	k_{eff}	Fission Inducing Energy (eV)	Mean Free Path (cm)
Minor Actinides	0.0531 ± 0.0001	5.851 ± 6.673E-02	3.286 ± 1.432E-04
Transuranics	0.8206 ± 0.0013	5.720E-01 ± 2.813E-03	2.897 ± 1.568E-05
Uranium Carbide	0.7798 ± 0.0016	4.855E-02 ± 8.124E-05	2.437 ± 3.530E-06
Reactor Grade Plutonium	0.9418 ± 0.0015	6.049E-01 ± 2.842E-03	2.894 ± 1.567E-05
Uranium Dioxide	0.9750 ± 0.0022	6.370E-02 ± 1.080E-04	2.437 ± 2.673E-06

For comparison purposes, the core configurations with different fuel loadings are presented relative to the reference UO_2 cores. Only fuel compositions are varied. However, in all cases there was not enough fissile content to achieve criticality but the geometry needed to remain fixed. The minor actinide fuel loading was unable to sustain anything near criticality in that arrangement. Evidence is provided to support the proposition that MAs could be blended with uranium based fuels to create a fuel loading that would produce a critical system. The UO_2 portion of the fuel would provide the

thermal energy peak needed for criticality. Fig. 29 shows the energy dependent neutron fluxes for the large scale pebble-bed core with UO_2 and MA fuel loadings at 1523K.

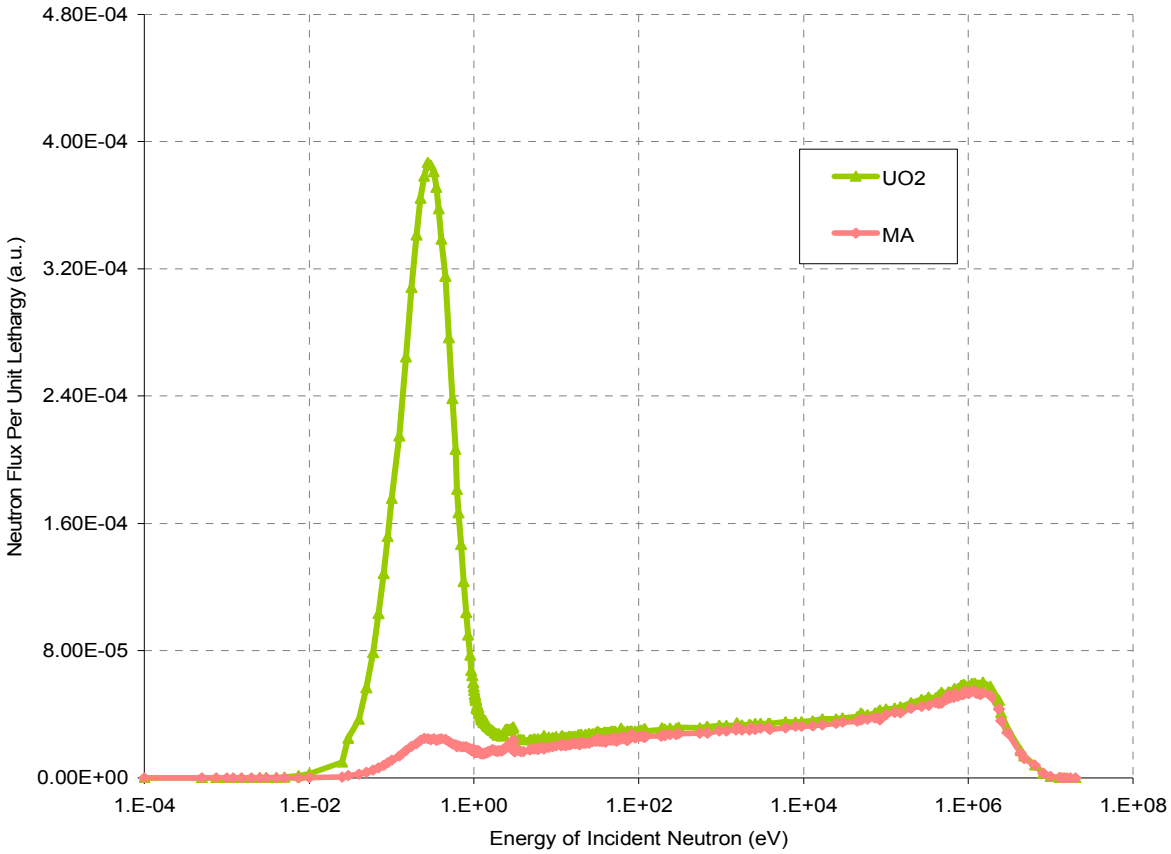

Fig. 29 Large Scale Pebble-Bed Core With MAs and UO_2 at 1523K

In Chapter V.A.1 a plot was shown (Fig. 20, p.58) with the spectra for the UO_2 fueled large and small scale pebble-bed VHTR configurations. There was clear increase in magnitude and shape in the large scale annular core. In addition, Fig. 30 shows this same relationship for the MA fueled core.

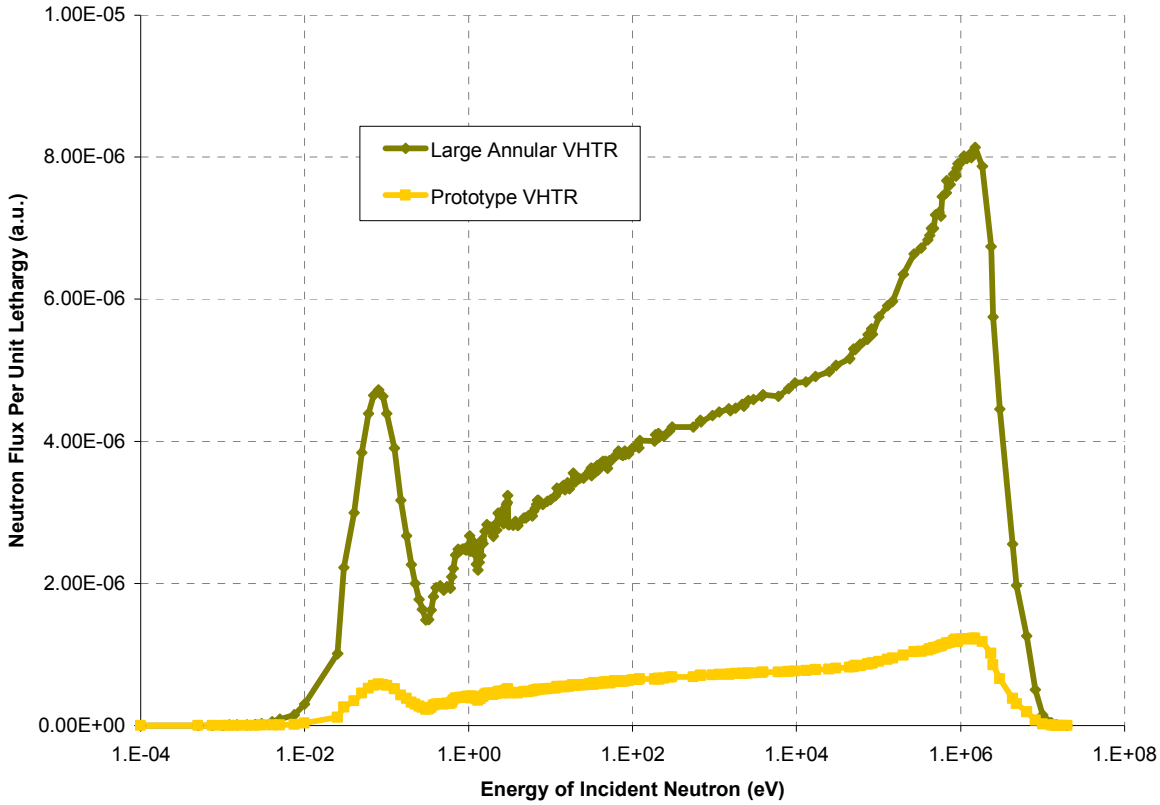

Fig. 30. Energy Dependent Neutron Flux for Small and Large Scale MA Fueled Cores

As a preliminary safety analysis, the isothermal temperature coefficient for each fuel loading was evaluated. The temperature range was 100K and the effective multiplication factor was determined starting at 1123K until 1523K which produced four coefficients per fuel loading. These were averaged to get a single temperature coefficient for each. Table XVIII shows the calculated values obtained for the temperature coefficients for specified fuel loadings for the large scale annular configuration. As noted, the coefficients in all cases are negative.

Table XVIII. Isothermal Temperature Coefficient for Various Fuel Loadings

Fuel	***Isothermal Temperature Coefficient (Δk/k/˚C)***
RGPu	-6.107E-05
UC, 8% LEU	-1.909E-04
UO_2	-2.145E-04
MA	-5.541E-03
TRU	-8.513E-05

V.C SAFETY ANALYSIS

The VHTR systems achieve their safety through their design approach, the materials used, and the fuel form. The key safety features of the VHTRs, in addition to the radionuclide retention capability of the TRISO particle, is a small operational excess reactivity, a large negative temperature coefficient, and a passive heat removal capability of the reactor design.

The combination of the small excess reactivity and large negative temperature coefficient stops the nuclear fission process with only a conservative temperature rise in the core in the event the control and shutdown systems fail. The introduction of an annular core allows fuel decay heat to be conducted through the reactor structures to the vessel cavity and further to the atmosphere without intervention.

The benchmark study included calculating the isothermal temperature coefficient for the critical HTR-10 core; the procedure is described in Chapter IV.A.2. The calculation was extended to the large-scale, annular core for the various fuels as described in Chapter V.B.2. Table XIX shows the calculated values obtained for the isothermal temperature coefficient for low enriched Uranium (LEU) fuel in the two configurations.

Table XIX. Isothermal Temperature Coefficients

Core Configuration	**Isothermal Temperature Coefficient** ***(Δk/k/˚C)***
HTR-10	-1.40E-04
Large Scale Annular	-2.15E-04

CHAPTER VI

DESIGN SENSITIVITIES AND THEIR IMPACT ON PEBBLE-BED SYSTEMS

The work presented in this chapter is part of the analysis of small scale configuration adjustments and sensitivities to design parameters on the large scale, annular pebble-bed core. Using the system 3D model, a variation analysis method was applied to VHTR geometry and material characteristics.

The studies included variations in:

- enrichment in reactor grade plutonium (RGPu), uranium dioxide (UO_2, LEU), and transuranics (TRU),
- the dimension of the central graphite column,
- pebble-bed fuel loading height
- number of coated particles per pebble (volume fraction)

VI.A SENSITIVITY OF THE PEBBLE-BED PERFORMANCE TO LOADING HEIGHT

The variations in all the listed parameters proved interdependent: a slight manipulation in one parameter produced an ill desired result in another and vice versa. Altering enrichment, dimensions of the column, the pebble bed loading height, and the volume fraction was done by holding all but one parameter constant, and by getting an entire data set with all options investigated. This essentially allowed an optimization: the ability to choose the most desirable configuration with regards to all variables.

Beginning with investigating the effect of loading height, based on the critical respective case, three fuel loadings were examined at room temperature. The configurations looked at in this study included: 1) 20% enriched LEU with a 144 cm radius central graphite column, 2) 35% enriched RGPu with a 104 cm radius central graphite column, and 3) 60% enriched TRU with a 124 cm radius central graphite column. Fig. 31 displays effective multiplication factor as a function of loadings height spanning from 20 cm to 360 cm.

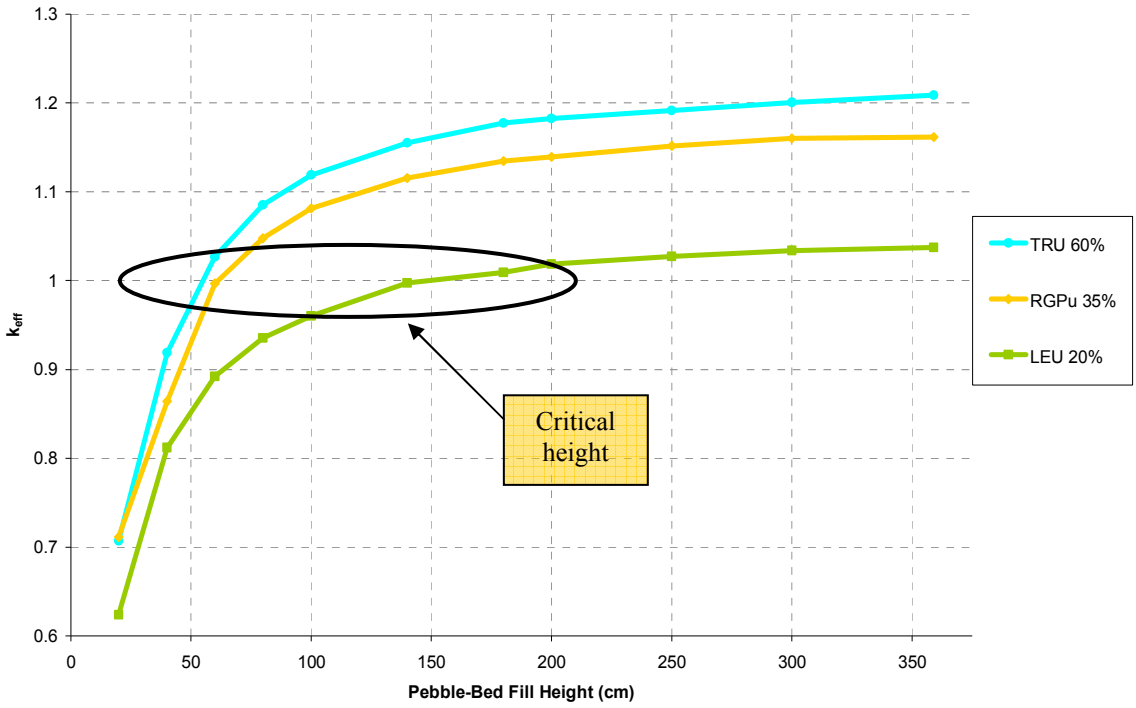

Fig. 31. Effect of Core Loading Height on Multiplication Factor for Three Fuel Loadings

There is a similar functional dependence of the three fuel's behaviors. Beginning with a steep climb there is a drastic change in effective multiplication factor for every additional cm of fill height. The curve levels off into a plateau for all fuels; but sooner for the TRU and RGPu loadings and slightly later for the LEU loading. The critical height for the TRU and RGPu occurs just past 50 cm and at 150 cm for the LEU fuel. The three loadings are not quantitatively comparable because they differ in the central graphite column size and fissile content, but the three reasonable combinations are comparable.

VI.B SENSITIVITY OF THE PEBBLE-BED PERFORMANCE TO THE CENTRAL GRAPHITE COLUMN

The effect of the size of the central graphite column can be seen by selecting one critical combination of a fuel loading, volume fraction, pebble-bed fill height, and enrichment. The radius of the full core was altered slightly while increasing the height of the central column to keep the fuel region volume consistent. The original model was created with an inner graphite reflector radius of 144 cm. The effect of changing this to 124 cm and 104 cm was examined.

Fig. 32 shows the effect on the average energy dependent neutron flux from altering the radius of the inner reflector. The plot was taken from the model with 20% enriched LEU, a 30% volume fraction, at 300K, and a fill height of 359 cm. As expected, the thermal peak increased in amplitude but all cases retained the same general shape through the fast region. This was most likely due to the increase in the amount of

moderating material near the core. There was a slight shift in the spectrum through the resonance and fast regions with increasing dimensions.

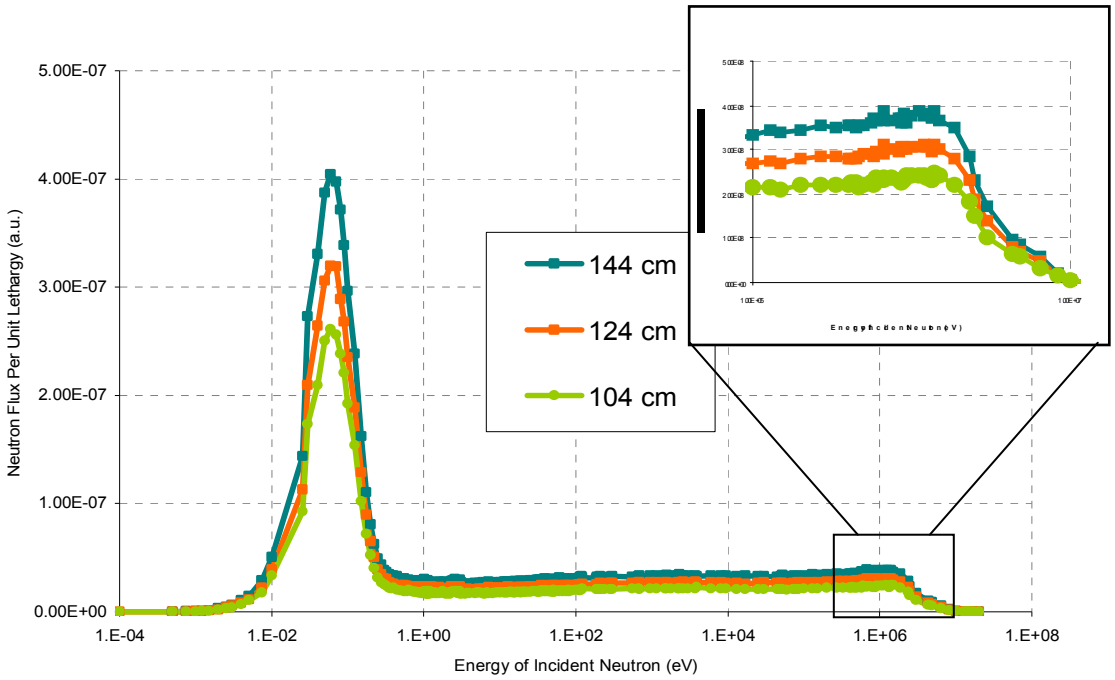

Fig. 32. Energy Dependent Neutron Flux for 20% LEU at 359 cm Height

A detailed look at how the smaller graphite column affects the multiplication factor is shown in Table XX for the same fuel loadings that are displayed in Fig. 32.

Table XX. Effect of Central Graphite Column Size on Multiplication Factor

			k_{eff}		
	Fuel Enrichment	**Fissile Content**	*104 cm*	*124 cm*	*144 cm*
TRU	60	24	1.1831	1.2046	1.2201
RGPu	35	21	1.1294	1.1507	1.1619
LEU	20	20	1.037	1.0494	1.0564

There is a decent increase in the multiplication factor for each fuel loading as the radius of the inner reflector is decreased. The largest jump was seen in the increase from 104 cm to 124 cm radius, followed by a smaller increase at 144 cm. The largest changes were seen in the 60% enriched TRU because it contains the most fissile material of the three.

VI.C SENSITIVITY OF THE PEBBLE-BED PERFORMANCE TO FUEL ENRICHMENT

The effect of enrichment on the multiplication factor and flux spectrum is a well predicted event. However, the degree to which these are affected in a pebble-bed core is analyzed. Table XXI displays results for the three types of fuel loadings at various enrichments for the three sizes of an inside reflector. The fissile content is also listed for a more consistent comparison between the three. All cases were calculated with a pebble-bed fill height of 359 cm at room temperature and a volume fraction of 30%.

Fig. 33 is the corresponding plot associated with Table XXI shown only for the two extreme central column sizes.

Table XXI. Summary of Design Sensitivity Effects

			k_{eff}		
Fuel	**Fuel Enrichment**	**Fissile Content**	*104 cm*	*124 cm*	*144 cm*
LEU	10	10	0.8529	0.8591	0.8635
	15	15	0.9543	0.9618	0.9684
	20	20	1.037	1.0494	1.0564
	25	25	1.1089	1.1237	1.1339
	30	30	1.1776	1.1892	1.1985
	35	35	1.2317	1.2515	1.2607
RGPu	10	6	0.7086	0.7142	0.7155
	15	9	0.8139	0.8251	0.8296
	20	12	0.9087	0.9221	0.92933
	25	15	0.9915	1.0082	1.01736
	30	18	1.064	1.0838	1.0937
	35	21	1.1294	1.1507	1.1619
TRU	40	16	1.0266	1.04153	1.055
	60	24	1.1831	1.2046	1.2201
	80	32	1.3114	1.3368	1.3539
	100	40	1.4315	1.4577	1.4783

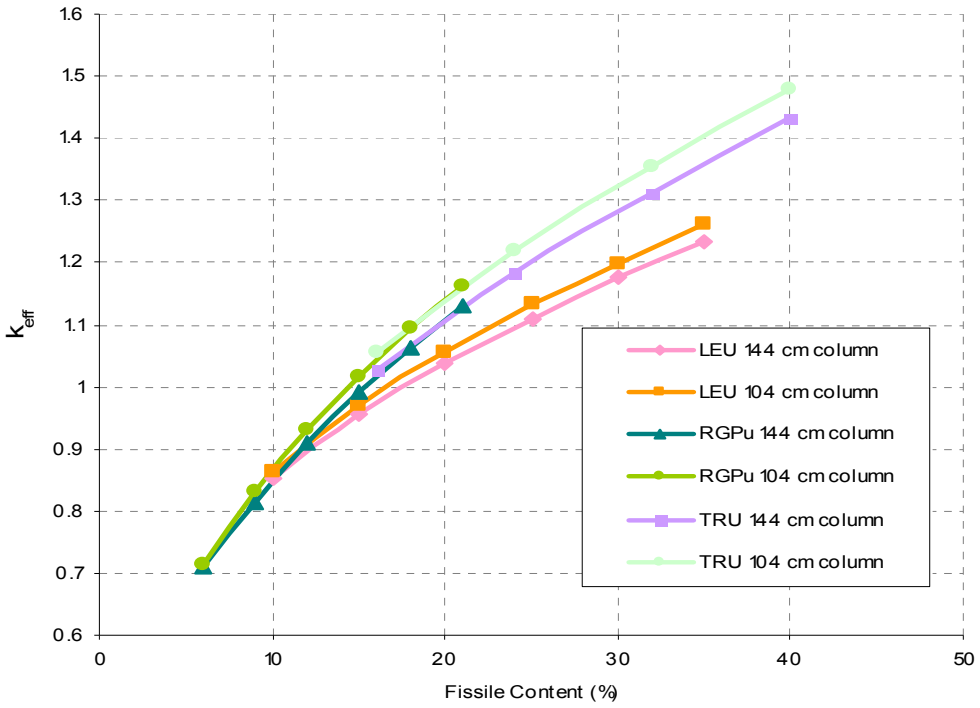

Fig. 33. Effect of Fissile Content on Multiplication Factor for Three Fuel Loadings

The TRU and RGPu fuels increased the multiplication factor at a greater rate than the LEU fuel. This same trend was seen in the effect of pebble loading height on multiplication factor. An increase in fissile material has a lesser effect on LEU than on the other two fuels.

VI.D SENSITIVITY OF THE PEBBLE-BED PERFORMANCE TO THE KERNEL PACKING FRACTION

Altering the loading ratio of fuel to moderator in any pebble has an odd effect. There is a fine line between too much and too little fuel in terms of getting the most multiplication.

The value analyzed in this section relates the amount of fuel (TRISO particles) to the space occupied by the graphite matrix of the central part of the pebble (per pebble). These numbers are often described as a volume fraction percent (VF %), number of particles per pebble (SCALE input NUMPAR), or fuel loading in grams. Table XXII and Fig. 34 show the effect on multiplication factor as the packing fraction was increased from 3% to 80% for four types of fuel loadings.

Table XXII. Effect of Kernel Packing Fraction on Multiplication Factor at 300 K

			k_{eff}			
VF (%)	**NUMPAR**	**Loading (g)**	***RGPu 30%***	***RGPu 35%***	***LEU 20%***	***TRU 60%***
3	4,677	2.8	0.8947	0.9033	1.3495	0.8047
5	7,795	4.7	0.8375	0.8588	1.232	0.8263
8	12,472	7.5	0.8465	0.8854	1.1247	0.8999
10	15,590	9.4	0.8718	0.91575	1.0914	0.95027
12	18,708	11.2	0.8989	0.9501	1.064	0.99212
14	21,827	13.1	0.92691	0.98318	1.0496	1.0208
18	28,063	16.8	0.9791	1.0396	1.0367	1.0848
20	31,180	18.7	1.0022	1.0669	1.036	1.10917
25	38,976	23.4	1.0535	1.11985	1.0408	1.1604
30	46,772	28.1	1.0937	1.1619	1.0564	1.2046
35	54,567	32.7	1.1301	1.1974	1.0692	1.2475
40	62,360	37.4	1.1582	1.2326	1.0857	1.2843
50	77,950	46.8	1.2178	1.289	1.1196	1.3508
60	93,543	56.1	1.2587	1.3377	1.1464	1.4128
70	109,134	65.5	1.3029	1.3832	1.1677	1.4769
80	125,724	75.4	1.3429	1.4263	1.1896	1.533

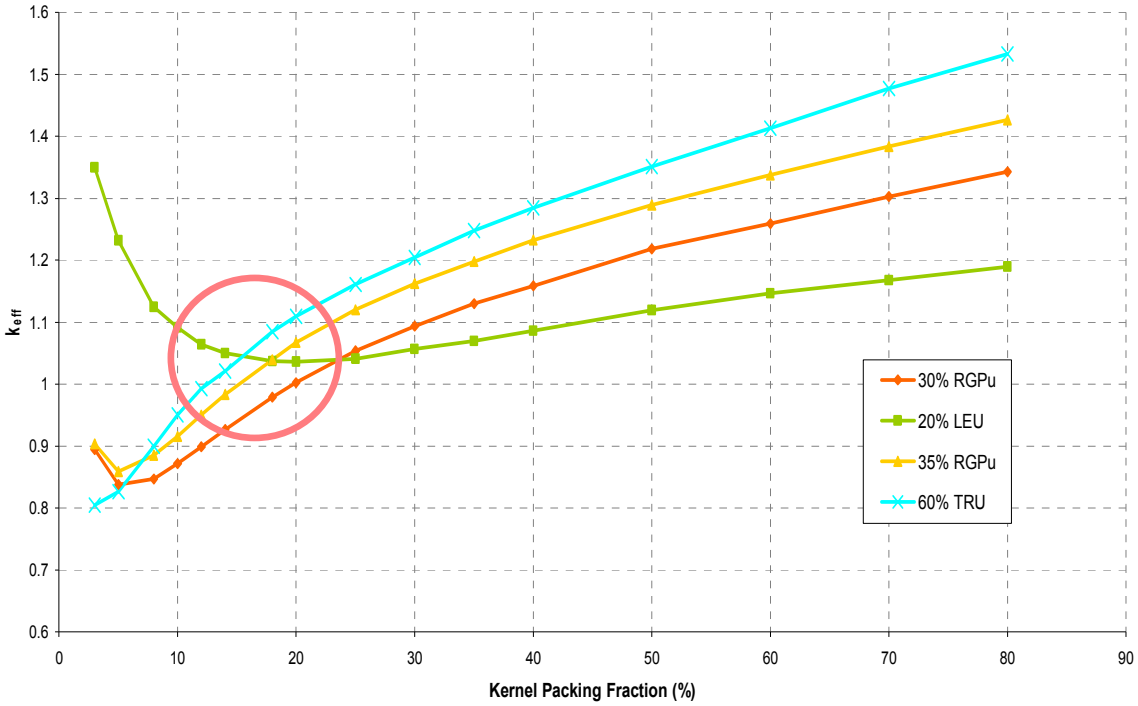

Fig. 34. Effective Multiplication Factor as a Function of Kernel Packing Fraction at 300K

The RGPu and TRU loadings began subcritical at 3% and increased to reach criticality around 18-20% packing fraction. The two RGPu fuels began with a slightly higher k_{eff} at 3% before dipping and rising again slowly. The LEU fuel loading was the only one to have the highest multiplication factor associated with the lowest packing fraction.

The possible reasoning behind this trend is hidden in the amount of moderating material present. At low packing fractions, there is an abundance of graphite in the inner matrix of the pebble. Since the LEU fuel contains the thermal fissile nuclide, ^{235}U, the

larger amount of moderating graphite sustains super criticality. As the amount of graphite is replaced with fueled particles, thermal neutrons are less abundant and therefore k_{eff} is reduced. RGPu and TRU both contain a large amount of ^{239}Pu and other fast fissioning nuclides. These fuels produce a higher k_{eff} when less graphite is present. Thus, at higher packing fractions these loadings are supercritical.

Table XXIII gives the same type of result as Table XXII for a different operating temperature. Fig. 35 shows the results in a graphical form. The trend is similar to that at 300K but, as expected, the multiplication factors are slightly lower.

Table XXIII. Effect of Kernel Packing Fraction on Multiplication Factor at 1223K

			k_{eff}		
VF (%)	**NUMPAR**	**Loading (g)**	*TRU 60%*	*RGPu 35%*	*LEU 20%*
3	4,677	2.8	0.7796	0.8399	1.3404
5	7,795	4.7	0.8064	0.8174	1.2322
8	12,472	7.5	0.88265	0.8501	1.1362
10	15,590	9.4	0.93042	0.882	1.1014
12	18,708	11.2	0.97131	0.91866	1.079
14	21,827	13.1	1.00478	0.9498	1.0617
18	28,063	16.8	1.0622	1.0015	1.052
20	31,180	18.7	1.0869	1.0279	1.0516
25	38,976	23.4	1.1401	1.081	1.058
30	46,772	28.1	1.1853	1.12203	1.0689
35	54,567	32.7	1.2258	1.15751	1.0836
40	62,360	37.4	1.2657	1.1924	1.1008
50	77,950	46.8	1.3378	1.2499	1.1316
60	93,543	56.1	1.3992	1.30631	1.1576
70	109,134	65.5	1.4633	1.34893	1.1803
80	125,724	75.4	1.5215	1.3965	1.2024

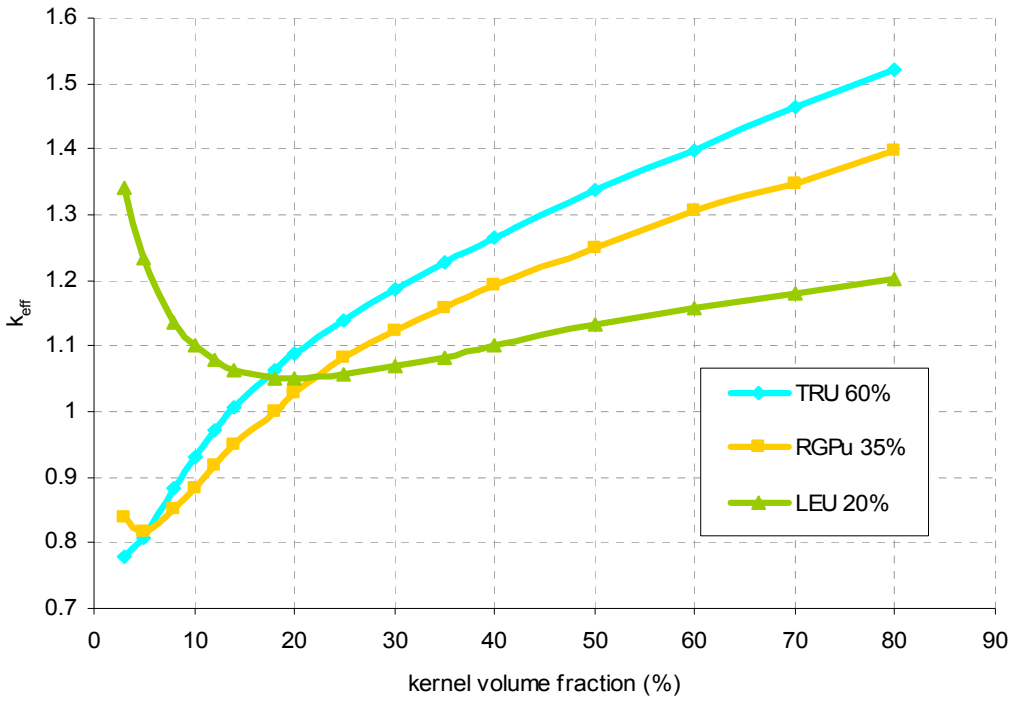

Fig. 35. Effective Multiplication Factor as a Function of Kernel Packing Fraction at 1223K.

CHAPTER VII

CONCLUSIONS

A detailed full core 3D pebble-bed VHTR model was developed. As an imperative part any modeling scheme, the models were verified and validated by performing experiment-to-code and code-to-code benchmarking procedures. In addition, two double heterogeneity modeling techniques were compared. This provided ratification for obtained data and results. Configuration adjustments and design sensitivity studies in VHTR pebble-bed cores were performed and included advanced actinide fuel loadings.

A configuration adjustment was made to the small scale, cylindrical HTR-10 core to create a large scale, annular core design. This core is a more realistic layout for possible use in future VHTR systems due to its inherent safety features. The preliminary safety analysis of the large scale core showed promising performance characteristics.

Fuel loadings consisting of advanced actinide fuels were evaluated for both small and large scale models in flux spectra, multiplication factor, and temperature coefficient. Initial studies indicate a strong potential for the use of minor actinides as one possible fuel component in VHTRs.

This research, in combination with similar studies of the VHTR prismatic core, offers an excellent basis for transitioning into finalizing the objective of the project as a whole: to assess the possibility, advantages and limitations of achieving ultra-long life

VHTRs with minor actinides as a fuel component. This includes a comparison between the many VHTR configurations.

Several challenges lie ahead for successful completion of future research. Some of the challenges include:

- Additional configuration adjustments and heterogeneity treatments,
- Uncertainty effects of nuclear data and design parameters
- Depletion and error propagation
- Final loadings containing minor actinides to assess ultra-long life capabilities

The primary advantage of the ultra-long life VHTR configurations are their inherent capabilities for utilization of minor actinides from spent LWR fuel, reduction of spent fuel flows and handling per unit of produced energy, and potential for autonomous operation with minimized maintenance. Their broad deployment would allow reducing the long-term radiotoxicity and head load of high level waste sent to a geologic repository and most importantly, enable recovery of the energy contained in spent fuel.

The completion of this work has laid a basis for the additional research in areas which aim to aid the energy crisis facing future generations. Creating advanced nuclear energy systems requires a modeling-based design that relies on simulating features of the entire life cycle of the system before actual physical prototyping. With the ground work laid from this research and the modeling-based designs, the Generation IV VHTR can transform into a real technology that can deliver electricity and hydrogen, as well as assist in spent fuel treatment while being inherently safe, environmentally friendly and show proliferation resistance.

Generation IV designs including the VHTR offer seemingly endless possibilities and advances, but the primary goal is not far off: making available to every developing country, and every individual, the common commodity we call electricity.

REFERENCES

1. YUANHUI XU, "High Temperature Gas-Cooled Reactor Programme in China," Institute of Nuclear Energy Technology, Tsinghua University, Beijing, China (1999).
2. "Evaluation of High Temperature Gas-Cooled Reactor Performance: Benchmark Analysis Related to Initial Testing of the HTTR and HTR-10," IAEA-TECDOC-1382, International Atomic Energy Agency, Vienna, Austria (2003).
3. "Materials Behavior in HTGR Environments," NUREG/CR-6824 (ANL-02/37), July 2003, Prepared for Office of Nuclear Regulatory Research, U.S. Nuclear Regulatory Commission (2003).
4. T. IYOKU, S. UETA, J. SUMITA, M. UMEDA, M. ISHIHARA, "Design of Core Components," *Nuc. Sci. and Design* **233**, 71-79 (2004).
5. "Report to Congress on Advanced Fuel Cycle Initiative: The Future Path for Advanced Spent Fuel Treatment and Transmutation Research," 03-GA50439-06, January 2003, Office of Nuclear Energy, Science, and Technology, USDOE (2003).
6. "Generation IV Nuclear Energy Systems Ten Year Program Plan Volume I," March 27, 2005, Office of Nuclear Energy, Science, and Technology, USODE (2005).
7. P.V. TSVETKOV, D.E. AMES II, A.B. ALAJO, M.L. PRITCHARD, "Self-Sustainability of VHTR Configurations with Advanced Actinide Fuels," ANS

Topical Meeting on Reactor Physics (PHYSOR 2006), Vancouver, Canada, September 10-14, 2006, ANS Topical Meeting, paper #D071 (2006).

8. P.V. TSVETKOV, "Utilization of Minor Actinides as a Fuel Component for Ultra-Long Life VHTR Configurations: Designs, Advantages, and Limitations", Year One Activities Report, 2006, DOE NERI Project 2005-094, Texas A&M University (US DOE NERI Research Project) USA (2006).

9. SCALE: A Modular Code System for Performing Standardized Computer Analysis for Licensing Evaluation, NUREG/CR-0200, Rev. 7 (ORNL/NUREG/CR/CSD-2R7), 3 vols., April 2004. Available from the Radiation Safety Information Computational Center at Oak Ridge National Laboratory as CCC-545.

10. J.VALKÓ, P.V. TSVETKOV, J.E. HOOGENBOOM, "Calculation of the Dancoff Factor for Pebble-Bed Reactors", *Nucl. Sci. Eng.,* **135**, 304 (2000).

11. SCALE: A Modular Code System for Performing Standardized Computer Analysis for Licensing Evaluation, ORNL/TM-2005/39, Version 5.1, Vols I-III, November 2006. Available from the Radiation Safety Information Computational Center at Oak Ridge National Laboratory as CCC-732.

12. S. FEHER and P.F.A. DE LEEGE, "DANCOFF-MC: A Computer Program for Monte Carlo Calculation of Dancoff Factors in Irregular Geometries," IRI-131-95-003 (June 1997).

13. S. GOLUOGLU, N.F. LANDERS, L.M. PETRIE, D.F. HOLLENBACH, "CSAS: Control Module for Enhanced Criticality Safety Analysis Sequences",

Vol. I, Sect, C4 of SCALE: A Modular Code System for Performing Standardized Computer Analysis for Licensing Evaluation, NUREG/CR-0200, Rev. 7 (ORNL/NUREG/CR/CSD-2R7), 3 vols., April 2004. Available from the Radiation Safety Information Computational Center at Oak Ridge National Laboratory as CCC-545.

14. D.F. HOLLENBACH and L.M. PETRIE, "CSAS6: Control Module for Enhanced Criticality Safety Analysis with KENO-VI," Vol. I, Sect. C6 of SCALE: A Modular Code System for Performing Standardized Computer Analysis for Licensing Evaluation, NUREG/CR-0200, Rev. 7 (ORNL/NUREG/CR/CSD-2R7), 3 vols., April 2004. Available from the Radiation Safety Information Computational Center at Oak Ridge National Laboratory as CCC-545.

15. L.M. PETRIE, N.F. LANDERS, D.F. HOLLENBACH, B.T. REARDEN, "KENO V.a: An Improved Monte Carlo Criticality Program," Vol II, Sect. F11 of SCALE: A Modular Code System for Performing Standardized Computer Analysis for Licensing Evaluation, NUREG/CR-0200, Rev. 7 (ORNL/NUREG/CR/CSD-2R7), 3 vols., April 2004. Available from the Radiation Safety Information Computational Center at Oak Ridge National Laboratory as CCC-545.

16. D.F. HOLLENBACH, L.M. PETRIE, N.F. LANDERS, "KENO-VI: A General Quadratic Version of the KENO Program," Vol II, Sect F17 of SCALE: A Modular Code System for Performing Standardized Computer Analysis for

Licensing Evaluation, NUREG/CR-0200, Rev. 7 (ORNL/NUREG/CR/CSD-2R7), 3 vols., April 2004. Available from the Radiation Safety Information Computational Center at Oak Ridge National Laboratory as CCC-545.

17. W.C. JORDAN and S.M. BOWMAN, "SCALE Cross-Section Libraries," Vol. III, Sect. M4 of SCALE: A Modular Code System for Performing Standardized Computer Analysis for Licensing Evaluation, NUREG/CR-0200, Rev. 7 (ORNL/NUREG/CR/CSD-2R7), 3 vols., April 2004. Available from the Radiation Safety Information Computational Center at Oak Ridge National Laboratory as CCC-545.

18. N.M. GREENE, "BONAMI: Resonance Self-Shielding by the Bondarenko Method," Vol. II, Sect. F1 of SCALE: A Modular Code System for Performing Standardized Computer Analysis for Licensing Evaluation, NUREG/CR-0200, Rev. 7 (ORNL/NUREG/CR/CSD-2R7), 3 vols., April 2004. Available from the Radiation Safety Information Computational Center at Oak Ridge National Laboratory as CCC-545.

19. N.M. GREENE, L.M. PETRIE, and R.M. WESTFALL, "NITAWL-III: SCALE System Module for Performing Resonance Shielding and Working Library Production," Vol. II, Sect. F2 of SCALE: A Modular Code System for Performing Standardized Computer Analysis for Licensing Evaluation, NUREG/CR-0200, Rev. 7 (ORNL/NUREG/CR/CSD-2R7), 3 vols., April 2004. Available from the Radiation Safety Information Computational Center at Oak Ridge National Laboratory as CCC-545.

20. N.M. GREENE and L.M. PETRIE, "XSDRNPM: A One-Dimensional Discrete-Ordinates Code for Transport Analysis," Vol. II, Sect. F3 of SCALE: A Modular Code System for Performing Standardized Computer Analysis for Licensing Evaluation, NUREG/CR-0200, Rev. 7 (ORNL/NUREG/CR/CSD-2R7), 3 vols., April 2004. Available from the Radiation Safety Information Computational Center at Oak Ridge National Laboratory as CCC-545.

21. S.M. DANCOFF and M. GINSBURG, "Surface Resonance Absorption in a Close-Packed Lattice," CP-2157 (October 1944).

22. G.I. BELL and S. GLASSTONE, *Nuclear Reactor Theory*, Chap. II.5, Van Nostrand Reinhold Company, New York (1970).

23. J.R. KNIGHT, "SUPERDAN: Computer Programs for Calculating the Dancoff Factor of Spheres, Cylinders, and Slabs," ORNL/NUREGCSD/TM-2, RSIC/PSR-282, Oak Ridge National Laboratory (1978).

24. S. FEHÉR, J.E. HOOGENBOOM, P.F.A. DE LEEGE and J. VALKÓ, "Monte Carlo Calculation of Dancoff Factors in Irregular Geometries," *Nucl. Sci. Eng.*, **117**, 227 (1994).

25. M.L. WILLIAMS, M. ASGARI, D.F. HOLLENBACH, "CENTRM: A One-Dimensional Neutron Transport Code for Computing Pointwise Energy Spectra", Vol. II, Book 4, Sect. F18 of SCALE: A Modular Code System for Performing Standardized Computer Analysis for Licensing Evaluation, ORNL/TM-2005/39, Version 5.1, Vols. I-III, November 2006. Available from the Radiation Safety

Information Computational Center at Oak Ridge National Laboratory as CCC-732.

26. D.F. HOLLENBACH, L.M. PETRIE, "CSAS6: Control Module for Enhanced Criticality Safety Analysis with KENO-VI", Vol. I, Book 1, Sect. C6 of SCALE: A Modular Code System for Performing Standardized Computer Analysis for Licensing Evaluation, ORNL/TM-2005/39, Version 5.1, Vols I-III, November 2006. Available from the Radiation Safety Information Computational Center at Oak Ridge National Laboratory as CCC-732.

27. P.V. TSVETKOV, "Basic Reactor Physics Parameter Study of the Pebble-Bed Nuclear Reactor System," IRI-131-97-002, Jan. 1997, TUDelft, the Netherlands (1997).

28. R. PLUKIENE, D. RIDIKAS, "Modeling of HTRs with Monte Carlo: from a Homogeneous to an Exact Heterogeneous Core with Microparticles," *An. Nucl. En.,* **30**, 1573 (2003).

29. T.A. TAIWO, T.K. KIM, W.S. YANG, H.S. KAHLIL, "Evaluation of High Temperature Gas-Cooled Reactor Physics Experiments as VHTR Benchmark Problems," ANL-GenIV-059, Argonne National Laboratory, September 2005 (2005).

30. K. KUNITOMI, "Development of New Type of HTGR," (Proc. 73rd JSME Fall Annual Meeting), JSME, Japan (1995).

31. T.K. KIM, T.A. TAIWO, R.N. HILL, W.S. YANG, "A Feasibility Study of Reactor-Based Deep-Burn Concepts," ANL-AFCI-155, Nuclear Engineering Division, Argonne National Laboratory, August 2005 (2005).

32. Y. XU, "HTGR Program in China," Institute of Nuclear Energy Technology, Beijing, China (1999).

APPENDIX A

EXAMPLE SCALE 5.1 INPUT FILE

SCALE 5.1 Input File (Power Reactor Model in KENO V.a, Control Rods Withdrawn, Part of Sensitivity Study)

```
'leu20%_vf=0.3_219cm
=csas25 parm=(centrm)
PowerReactor(cr removed):LEU 20%=10.41,VF=30%,ModelA
v6-238
read comp
'upper reflector:
 c-graphite  1 0 0.072941 300 end
 b           1 0 0.00329811 300 end
 c-graphite  2 0 0.0851462 300 end
 b           2 0 4.57148e-07 300 end
 c-graphite  3 0 0.014535 300 end
 b           3 0 7.80384e-08 300 end
 c-graphite  4 0 0.0802916 300 end
 b           4 0 4.31084e-07 300 end
'helium coolant:
 he          5  den=0.0001604 1 300 end
'dummy balls, simplified as graphite of lower density:
 c-graphite  6 0 0.0538275 300 end
 b           6 0 2.88999e-07 300 end
 c-graphite  7 0 0.0851047 300 end
 b           7 0 4.56926e-07 300 end
'bottom reflector:
 c-graphite  8 0 0.0781408 300 end
 b           8 0 4.19537e-07 300 end
 c-graphite  9 0 0.0823751 300 end
 b           9 0 4.42271e-07 300 end
 c-graphite  10 0 0.0843647 300 end
 b           10 0 0.000298504 300 end
 c-graphite  11 0 0.0817101 300 end
 b           11 0 0.000156416 300 end
 c-graphite  12 0 0.085079 300 end
 b           12 0 0.000209092 300 end
 c-graphite  13 0 0.0819167 300 end
 b           13 0 3.58529e-05 300 end
 c-graphite  14 0 0.0541118 300 end
 b           14 0 5.77456e-05 300 end
 c-graphite  15 0 0.033211 300 end
 b           15 0 1.78309e-07 300 end
 c-graphite  16 0 0.0881811 300 end
 b           16 0 3.58866e-05 300 end
 c-graphite  17 0 0.0765984 300 end
 b           17 0 0.00346349 300 end
'carbon bricks on bottom:
 c-graphite  18 0 0.0797184 300 end
'radial reflector:
 c-graphite  19 0 0.0761157 300 end
 b           19 0 0.344166 300 end
 c-graphite  20 0 0.0878374 300 end
 b           20 0 4.71597e-07 300 end
 c-graphite  21 0 0.0579696 300 end
```

```
 b           21 0 3.11238e-07 300 end
 c-graphite  22 0 0.0882418 300 end
 b           22 0 4.73769e-07 300 end
 c-graphite  24 0 0.0879541 300 end
 b           24 0 0.000168369 300 end
 c-graphite  29 0 0.0524843 300 end
 b           29 0 1.81969e-05 300 end
 c-graphite  42 0 0.0879637 300 end
 b           42 0 0.000162903 300 end
 c-graphite  48 0 0.0582699 300 end
 b           48 0 3.1285e-07 300 end
 c-graphite  57 0 0.0728262 300 end
 b           57 0 3.91003e-07 300 end
 c-graphite  60 0 0.0879538 300 end
 b           60 0 0.000168369 300 end
'dummy balls, taken as carbon bricks:
 c-graphite  81 den=1.59 1 300 end
'dummy balls, simplified as graphite of lower density:
 c-graphite  83 0 0.0538275 300 end
 b           83 0 2.88999e-07 300 end
'fuel kernel, 20% 235:
 uo2         91 den=10.41 1 1223 92234 0.005407837 92235 20 92238
79.99459 end
'fuel coating:
 b-10        92 0 7.221155e-09 300 end
 b-11        92 0 2.924932e-08 300 end
 c-graphite  92 0 0.07291468 300 end
 silicon     92 0 0.01017942 300 end
'fuel coating:
 b-10        95 0 7.221155e-09 300 end
 b-11        95 0 2.924932e-08 300 end
 c-graphite  95 0 0.07291468 300 end
 silicon     95 0 0.01017942 300 end
'1st Fuel Coating:
 c-graphite  101 0 0.056255 300 end
'2nd Fuel coating:
 c-graphite  102 0 0.095714 300 end
'3rd Fuel coating:
 c-graphite  103 0 0.048136 300 end
 si          103 0 0.048136 300 end
'4th Fuel coating:
 c-graphite  104 0 0.093759 300 end
'graphite shell + moderator pebble (region 2):
 c-graphite  96 den=1.59 0.64154 300 end
'c-graphite  96 den=1.77 0.35846 300 end:
 he          89 den=0.0001604 1 300 end
'center graphite matrix:
 b           98 den=1.69 8.2e-07 300 5010 19.9 5011 80.1 end
 c-graphite  98 den=1.69 0.99999918 300 end
end comp
'MODEL A double heterogeneity treatment with coatings explicit and
using cellmix, 30% VF:
read celldata
doublehet fuelmix=82 end
```

```
        gfr=0.02985 91 coatr=0.03588 101 coatr=0.038945 102
coatr=0.041835 103 coatr=0.04645 104 VF=0.3 matrix=98 end grain
        pebble sphtriangp right_bdy=white hpitch=3.64 89 fuelr=2.5
cladr=3.4341 96 end
end celldata
read parameter
           gen=200
           npg=1000
           NSK=10
           FLX=yes
           FDN=yes
           PKI=yes
           FAR=yes
           GAS=yes
           FMP=yes
           MKU=yes
           FMU=yes
           SMU=yes
           NUB=yes
           CFX=yes
end parameter
read geometry
unit 1
com='core at height 117.616 cm'
 zcylinder 18 1 311.793  160  0
  hole 73 0  0  0
  hole 21 288.6  0  0
  hole 21 274.475  89.1823  0
  hole 21 233.482  169.635  0
  hole 21 169.635  233.482  0
  hole 21 89.1823  274.475  0
  hole 21 0  288.6  0
  hole 21 -89.1823  274.475  0
  hole 21 -169.635  233.482  0
  hole 21 -233.482  169.635  0
  hole 21 -274.475  89.1823  0
  hole 21 -274.475  -89.1823  0
  hole 21 -233.482  -169.635  0
  hole 21 -169.635  -233.482  0
  hole 21 -89.1823  -274.475  0
  hole 21 0  -288.6  0
  hole 21 -288.6  0  0
  hole 21 89.1823  -274.475  0
  hole 21 169.635  -233.482  0
  hole 21 233.482  -169.635  0
  hole 21 274.475  -89.1823  0
 zcylinder 17 1 334  160  0
 cuboid 0 1  400  -400  400  -400  160  0
unit 2
 zcylinder 17 1 334  50.83  0
  hole 74 0  0  0
  hole 22 288.6  0  0
  hole 22 274.475  89.1823  0
  hole 22 233.482  169.635  0
```

```
  hole 22 169.635  233.482  0
  hole 22 89.1823  274.475  0
  hole 22 0  288.6  0
  hole 22 -89.1823  274.475  0
  hole 22 -169.635  233.482  0
  hole 22 -233.482  169.635  0
  hole 22 -274.475  89.1823  0
  hole 22 -274.475  -89.1823  0
  hole 22 -233.482  -169.635  0
  hole 22 -169.635  -233.482  0
  hole 22 -89.1823  -274.475  0
  hole 22 0  -288.6  0
  hole 22 -288.6  0  0
  hole 22 89.1823  -274.475  0
  hole 22 169.635  -233.482  0
  hole 22 233.482  -169.635  0
  hole 22 274.475  -89.1823  0
 cuboid 0 1  400  -400  400  -400  50.83  0
unit 3
 zcylinder 12 1 185.75  25.42  0
  hole 75 0  0  0
 zcylinder 16 1 234  25.42  0
 zcylinder 22 1 311.793  25.42  0
  hole 23 288.6  0  0
  hole 23 274.475  89.1823  0
  hole 23 233.482  169.635  0
  hole 23 169.635  233.482  0
  hole 23 89.1823  274.475  0
  hole 23 0  288.6  0
  hole 23 -89.1823  274.475  0
  hole 23 -169.635  233.482  0
  hole 23 -233.482  169.635  0
  hole 23 -274.475  89.1823  0
  hole 23 -274.475  -89.1823  0
  hole 23 -233.482  -169.635  0
  hole 23 -169.635  -233.482  0
  hole 23 -89.1823  -274.475  0
  hole 23 0  -288.6  0
  hole 23 -288.6  0  0
  hole 23 89.1823  -274.475  0
  hole 23 169.635  -233.482  0
  hole 23 233.482  -169.635  0
  hole 23 274.475  -89.1823  0
 zcylinder 17 1 334  25.42  0
 cuboid 0 1  400  -400  400  -400  25.42  0
unit 4
 zcylinder 12 1 185.75  50.83  0
  hole 74 0  0  0
 zcylinder 14 1 214.75  50.83  0
 zcylinder 15 1 234  50.83  0
 zcylinder 22 1 311.793  50.83  0
  hole 56 234  0  15
  hole 22 274.475  89.1823  0
  hole 22 233.482  169.635  0
```

```
  hole 22 169.635  233.482  0
  hole 22 89.1823  274.475  0
  hole 22 0  -288.6  0
  hole 22 -89.1823  274.475  0
  hole 22 -169.635  233.482  0
  hole 22 -233.482  169.635  0
  hole 22 -274.475  89.1823  0
  hole 22 -274.475  -89.1823  0
  hole 22 -233.482  -169.635  0
  hole 22 -169.635  -233.482  0
  hole 22 -89.1823  -274.475  0
  hole 22 0  288.6  0
  hole 22 -288.6  0  0
  hole 22 89.1823  -274.475  0
  hole 22 169.635  -233.482  0
  hole 22 233.482  -169.635  0
  hole 22 274.475  -89.1823  0
 zcylinder 17 1 334  50.83  0
  hole 57 311.8  0  25.4
 cuboid 0 1  400  -400  400  -400  50.83  0
unit 5
 zcylinder 12 1 185.75  25.42  0
  hole 75 0  0  0
 zcylinder 13 1 234  25.42  0
 zcylinder 22 1 311.793  25.42  0
  hole 23 288.6  0  0
  hole 23 274.475  89.1823  0
  hole 23 233.482  169.635  0
  hole 23 169.635  233.482  0
  hole 23 89.1823  274.475  0
  hole 23 0  288.6  0
  hole 23 -89.1823  274.475  0
  hole 23 -169.635  233.482  0
  hole 23 -233.482  169.635  0
  hole 23 -274.475  89.1823  0
  hole 23 -274.475  -89.1823  0
  hole 23 -233.482  -169.635  0
  hole 23 -169.635  -233.482  0
  hole 23 -89.1823  -274.475  0
  hole 23 0  -288.6  0
  hole 23 -288.6  0  0
  hole 23 89.1823  -274.475  0
  hole 23 169.635  -233.482  0
  hole 23 233.482  -169.635  0
  hole 23 274.475  -89.1823  0
 zcylinder 17 1 334  25.42  0
 cuboid 0 1  400  -400  400  -400  25.42  0
unit 6
 zcylinder 10 1 185.75  33.89  0
  hole 76 0  0  0
 zcylinder 11 1 234  33.89  0
 zcylinder 24 1 239.6  33.89  0
 zcylinder 42 1 252.6  33.89  0
  hole 27 246.1  0  0
```

```
  hole 27 144.6538  199.099  0
  hole 27 76.0491  234.0549  0
  hole 27 -76.0491  234.0549  0
  hole 27 -144.6538  199.099  0
  hole 27 -234.0549  76.0491  0
  hole 27 -246.1  0  0
  hole 27 -144.6538  -199.099  0
  hole 27 -76.0491  -234.0549  0
  hole 27 76.0491  -234.0549  0
  hole 27 144.6538  -199.099  0
  hole 27 234.0549  -76.0491  0
  hole 27 -199.099  -144.6538  0
  hole 28 234.0549  76.0491  0
  hole 28 199.099  144.6538  0
  hole 28 0  246.1  0
  hole 28 -199.099  144.6538  0
  hole 28 -234.0549  -76.0491  0
  hole 28 0  -246.1  0
  hole 28 199.099  -144.6538  0
 zcylinder 24 1 284.6  33.89  0
 zcylinder 60 1 292.6  33.89  0
  hole 26 288.6  0  0
  hole 26 274.475  89.1823  0
  hole 26 233.482  169.635  0
  hole 26 169.635  233.482  0
  hole 26 89.1823  274.475  0
  hole 26 0  288.6  0
  hole 26 -89.1823  274.475  0
  hole 26 -169.635  233.482  0
  hole 26 -233.482  169.635  0
  hole 26 -274.475  89.1823  0
  hole 26 -274.475  -89.1823  0
  hole 26 -233.482  -169.635  0
  hole 26 -169.635  -233.482  0
  hole 26 -89.1823  -274.475  0
  hole 26 0  -288.6  0
  hole 26 -288.6  0  0
  hole 26 89.1823  -274.475  0
  hole 26 169.635  -233.482  0
  hole 26 233.482  -169.635  0
  hole 26 274.475  -89.1823  0
 zcylinder 24 1 311.793  33.89  0
 zcylinder 17 1 334  33.89  0
 cuboid 0 1  400  -400  400  -400  33.89  0
unit 7
 zcylinder 9 1 234  47.44  0
  hole 77 0  0  0
 zcylinder 22 1 311.793  47.44  0
  hole 30 246.1  0  0
  hole 30 144.6538  199.099  0
  hole 30 76.0491  234.0549  0
  hole 30 -76.0491  234.0549  0
  hole 30 -144.6538  199.099  0
  hole 30 -234.0549  76.0491  0
```

```
  hole 30 -246.1  0  0
  hole 30 -144.6538  -199.099  0
  hole 30 -76.0491  -234.0549  0
  hole 30 76.0491  -234.0549  0
  hole 30 144.6538  -199.099  0
  hole 30 234.0549  -76.0491  0
  hole 30 -199.099  -144.6538  0
  hole 31 234.0549  76.0491  0
  hole 31 199.099  144.6538  0
  hole 31 0  246.1  0
  hole 31 -199.099  144.6538  0
  hole 31 -234.0549  -76.0491  0
  hole 31 0  -246.1  0
  hole 31 199.099  -144.6538  0
  hole 29 288.6  0  0
  hole 29 274.475  89.1823  0
  hole 29 233.482  169.635  0
  hole 29 169.635  233.482  0
  hole 29 89.1823  274.475  0
  hole 29 0  288.6  0
  hole 29 -89.1823  274.475  0
  hole 29 -169.635  233.482  0
  hole 29 -233.482  169.635  0
  hole 29 -274.475  89.1823  0
  hole 29 -274.475  -89.1823  0
  hole 29 -233.482  -169.635  0
  hole 29 -169.635  -233.482  0
  hole 29 -89.1823  -274.475  0
  hole 29 0  -288.6  0
  hole 29 -288.6  0  0
  hole 29 89.1823  -274.475  0
  hole 29 169.635  -233.482  0
  hole 29 233.482  -169.635  0
  hole 29 274.475  -89.1823  0
 zcylinder 17 1 334  47.44  0
 cuboid 0 1  400  -400  400  -400  47.44  0
unit 8
 zcylinder 8 1 234  22.43  0
  hole 78 0  0  0
 zcylinder 22 1 311.793  22.43  0
  hole 33 246.1  0  0
  hole 33 144.6538  199.099  0
  hole 33 76.0491  234.0549  0
  hole 33 -76.0491  234.0549  0
  hole 33 -144.6538  199.099  0
  hole 33 -234.0549  76.0491  0
  hole 33 -246.1  0  0
  hole 33 -144.6538  -199.099  0
  hole 33 -76.0491  -234.0549  0
  hole 33 76.0491  -234.0549  0
  hole 33 144.6538  -199.099  0
  hole 33 234.0549  -76.0491  0
  hole 33 -199.099  144.6538  0
  hole 34 234.0549  76.0491  0
```

```
  hole 34 199.099  -144.6538  0
  hole 34 0  246.1  0
  hole 34 -199.099  -144.6538  0
  hole 34 -234.0549  -76.0491  0
  hole 34 0  -246.1  0
  hole 34 199.099  144.6538  0
  hole 32 288.6  0  0
  hole 32 274.475  89.1823  0
  hole 32 233.482  169.635  0
  hole 32 169.635  233.482  0
  hole 32 89.1823  274.475  0
  hole 32 0  288.6  0
  hole 32 -89.1823  274.475  0
  hole 32 -169.635  233.482  0
  hole 32 -233.482  169.635  0
  hole 32 -274.475  89.1823  0
  hole 32 -274.475  -89.1823  0
  hole 32 -233.482  -169.635  0
  hole 32 -169.635  -233.482  0
  hole 32 -89.1823  -274.475  0
  hole 32 0  -288.6  0
  hole 32 -288.6  0  0
  hole 32 89.1823  -274.475  0
  hole 32 169.635  -233.482  0
  hole 32 233.482  -169.635  0
  hole 32 274.475  -89.1823  0
 zcylinder 17 1 334  22.43  0
 cuboid 0 1  400  -400  400  -400  22.43  0
unit 9
 zcylinder 83 1 179  10.17  0
  hole 64 0  0  0
 zcylinder 7 1 234  10.17  0
 zcylinder 22 1 311.793  10.17  0
  hole 36 246.1  0  0
  hole 36 144.6538  199.099  0
  hole 36 76.0491  234.0549  0
  hole 36 -76.0491  234.0549  0
  hole 36 -144.6538  199.099  0
  hole 36 -234.0549  76.0491  0
  hole 36 -246.1  0  0
  hole 36 -144.6538  -199.099  0
  hole 36 -76.0491  -234.0549  0
  hole 36 76.0491  -234.0549  0
  hole 36 144.6538  -199.099  0
  hole 36 234.0549  -76.0491  0
  hole 36 -199.099  -144.6538  0
  hole 37 234.0549  76.0491  0
  hole 37 199.099  144.6538  0
  hole 37 0  246.1  0
  hole 37 -199.099  144.6538  0
  hole 37 -234.0549  -76.0491  0
  hole 37 0  -246.1  0
  hole 37 199.099  -144.6538  0
  hole 35 288.6  0  0
```

```
  hole 35 274.475  89.1823  0
  hole 35 233.482  169.635  0
  hole 35 169.635  233.482  0
  hole 35 89.1823  274.475  0
  hole 35 0  288.6  0
  hole 35 -89.1823  274.475  0
  hole 35 -169.635  233.482  0
  hole 35 -233.482  169.635  0
  hole 35 -274.475  89.1823  0
  hole 35 -274.475  -89.1823  0
  hole 35 -233.482  -169.635  0
  hole 35 -169.635  -233.482  0
  hole 35 -89.1823  -274.475  0
  hole 35 0  -288.6  0
  hole 35 -288.6  0  0
  hole 35 89.1823  -274.475  0
  hole 35 169.635  -233.482  0
  hole 35 233.482  -169.635  0
  hole 35 274.475  -89.1823  0
 zcylinder 17 1 334  10.17  0
 cuboid 0 1  400  -400  400  -400  10.17  0
unit 10
 zcylinder 83 1 189  10.17  0
  hole 64 0  0  0
 zcylinder 7 1 234  10.17  0
 zcylinder 22 1 311.793  10.17  0
  hole 36 246.1  0  0
  hole 36 144.6538  199.099  0
  hole 36 76.0491  234.0549  0
  hole 36 -76.0491  234.0549  0
  hole 36 -144.6538  199.099  0
  hole 36 -234.0549  76.0491  0
  hole 36 -246.1  0  0
  hole 36 -144.6538  -199.099  0
  hole 36 -76.0491  -234.0549  0
  hole 36 76.0491  -234.0549  0
  hole 36 144.6538  -199.099  0
  hole 36 234.0549  -76.0491  0
  hole 36 -199.099  -144.6538  0
  hole 37 234.0549  76.0491  0
  hole 37 199.099  144.6538  0
  hole 37 0  246.1  0
  hole 37 -199.099  144.6538  0
  hole 37 -234.0549  -76.0491  0
  hole 37 0  -246.1  0
  hole 37 199.099  -144.6538  0
  hole 35 288.6  0  0
  hole 35 274.475  89.1823  0
  hole 35 233.482  169.635  0
  hole 35 169.635  233.482  0
  hole 35 89.1823  274.475  0
  hole 35 0  288.6  0
  hole 35 -89.1823  274.475  0
  hole 35 -169.635  233.482  0
```

```
  hole 35 -233.482  169.635  0
  hole 35 -274.475  89.1823  0
  hole 35 -274.475  -89.1823  0
  hole 35 -233.482  -169.635  0
  hole 35 -169.635  -233.482  0
  hole 35 -89.1823  -274.475  0
  hole 35 0  -288.6  0
  hole 35 -288.6  0  0
  hole 35 89.1823  -274.475  0
  hole 35 169.635  -233.482  0
  hole 35 233.482  -169.635  0
  hole 35 274.475  -89.1823  0
 zcylinder 17 1 334  10.17  0
 cuboid 0 1  400  -400  400  -400  10.17  0
unit 11
 zcylinder 83 1 199  10.17  0
  hole 64 0  0  0
 zcylinder 7 1 234  10.17  0
 zcylinder 22 1 311.793  10.17  0
  hole 36 246.1  0  0
  hole 36 144.6538  199.099  0
  hole 36 76.0491  234.0549  0
  hole 36 -76.0491  234.0549  0
  hole 36 -144.6538  199.099  0
  hole 36 -234.0549  76.0491  0
  hole 36 -246.1  0  0
  hole 36 -144.6538  -199.099  0
  hole 36 -76.0491  -234.0549  0
  hole 36 76.0491  -234.0549  0
  hole 36 144.6538  -199.099  0
  hole 36 234.0549  -76.0491  0
  hole 36 -199.099  -144.6538  0
  hole 37 234.0549  76.0491  0
  hole 37 199.099  144.6538  0
  hole 37 0  246.1  0
  hole 37 -199.099  144.6538  0
  hole 37 -234.0549  -76.0491  0
  hole 37 0  -246.1  0
  hole 37 199.099  -144.6538  0
  hole 35 288.6  0  0
  hole 35 274.475  89.1823  0
  hole 35 233.482  169.635  0
  hole 35 169.635  233.482  0
  hole 35 89.1823  274.475  0
  hole 35 0  288.6  0
  hole 35 -89.1823  274.475  0
  hole 35 -169.635  233.482  0
  hole 35 -233.482  169.635  0
  hole 35 -274.475  89.1823  0
  hole 35 -274.475  -89.1823  0
  hole 35 -233.482  -169.635  0
  hole 35 -169.635  -233.482  0
  hole 35 -89.1823  -274.475  0
  hole 35 0  -288.6  0
```

```
  hole 35 -288.6  0  0
  hole 35 89.1823  -274.475  0
  hole 35 169.635  -233.482  0
  hole 35 233.482  -169.635  0
  hole 35 274.475  -89.1823  0
 zcylinder 17 1 334  10.17  0
 cuboid 0 1  400  -400  400  -400  10.17  0
unit 12
 zcylinder 83 1 209  10.17  0
  hole 64 0  0  0
 zcylinder 7 1 234  10.17  0
 zcylinder 22 1 311.793  10.17  0
  hole 36 246.1  0  0
  hole 36 144.6538  199.099  0
  hole 36 76.0491  234.0549  0
  hole 36 -76.0491  234.0549  0
  hole 36 -144.6538  199.099  0
  hole 36 -234.0549  76.0491  0
  hole 36 -246.1  0  0
  hole 36 -144.6538  -199.099  0
  hole 36 -76.0491  -234.0549  0
  hole 36 76.0491  -234.0549  0
  hole 36 144.6538  -199.099  0
  hole 36 234.0549  -76.0491  0
  hole 36 -199.099  -144.6538  0
  hole 37 234.0549  76.0491  0
  hole 37 199.099  144.6538  0
  hole 37 0  246.1  0
  hole 37 -199.099  144.6538  0
  hole 37 -234.0549  -76.0491  0
  hole 37 0  -246.1  0
  hole 37 199.099  -144.6538  0
  hole 35 288.6  0  0
  hole 35 274.475  89.1823  0
  hole 35 233.482  169.635  0
  hole 35 169.635  233.482  0
  hole 35 89.1823  274.475  0
  hole 35 0  288.6  0
  hole 35 -89.1823  274.475  0
  hole 35 -169.635  233.482  0
  hole 35 -233.482  169.635  0
  hole 35 -274.475  89.1823  0
  hole 35 -274.475  -89.1823  0
  hole 35 -233.482  -169.635  0
  hole 35 -169.635  -233.482  0
  hole 35 -89.1823  -274.475  0
  hole 35 0  -288.6  0
  hole 35 -288.6  0  0
  hole 35 89.1823  -274.475  0
  hole 35 169.635  -233.482  0
  hole 35 233.482  -169.635  0
  hole 35 274.475  -89.1823  0
 zcylinder 17 1 334  10.17  0
 cuboid 0 1  400  -400  400  -400  10.17  0
```

```
unit 13
 zcylinder 83 1 219  10.17  0
  hole 64 0  0  0
 zcylinder 7 1 234  10.17  0
 zcylinder 22 1 311.793  10.17  0
  hole 36 246.1  0  0
  hole 36 144.6538  199.099  0
  hole 36 76.0491  234.0549  0
  hole 36 -76.0491  234.0549  0
  hole 36 -144.6538  199.099  0
  hole 36 -234.0549  76.0491  0
  hole 36 -246.1  0  0
  hole 36 -144.6538  -199.099  0
  hole 36 -76.0491  -234.0549  0
  hole 36 76.0491  -234.0549  0
  hole 36 144.6538  -199.099  0
  hole 36 234.0549  -76.0491  0
  hole 36 -199.099  -144.6538  0
  hole 37 234.0549  76.0491  0
  hole 37 199.099  144.6538  0
  hole 37 0  246.1  0
  hole 37 -199.099  144.6538  0
  hole 37 -234.0549  -76.0491  0
  hole 37 0  -246.1  0
  hole 37 199.099  -144.6538  0
  hole 35 288.6  0  0
  hole 35 274.475  89.1823  0
  hole 35 233.482  169.635  0
  hole 35 169.635  233.482  0
  hole 35 89.1823  274.475  0
  hole 35 0  288.6  0
  hole 35 -89.1823  274.475  0
  hole 35 -169.635  233.482  0
  hole 35 -233.482  169.635  0
  hole 35 -274.475  89.1823  0
  hole 35 -274.475  -89.1823  0
  hole 35 -233.482  -169.635  0
  hole 35 -169.635  -233.482  0
  hole 35 -89.1823  -274.475  0
  hole 35 0  -288.6  0
  hole 35 -288.6  0  0
  hole 35 89.1823  -274.475  0
  hole 35 169.635  -233.482  0
  hole 35 233.482  -169.635  0
  hole 35 274.475  -89.1823  0
 zcylinder 17 1 334  10.17  0
 cuboid 0 1  400  -400  400  -400  10.17  0
unit 14
 zcylinder 83 1 234  12.11  0
  hole 65 0  0  0
 zcylinder 22 1 311.793  12.11  0
  hole 39 246.1  0  0
  hole 39 144.6538  199.099  0
  hole 39 76.0491  234.0549  0
```

```
  hole 39 -76.0491  234.0549  0
  hole 39 -144.6538  199.099  0
  hole 39 -234.0549  76.0491  0
  hole 39 -246.1  0  0
  hole 39 -144.6538  -199.099  0
  hole 39 -76.0491  -234.0549  0
  hole 39 76.0491  -234.0549  0
  hole 39 144.6538  -199.099  0
  hole 39 234.0549  -76.0491  0
  hole 39 -199.099  -144.6538  0
  hole 40 234.0549  76.0491  0
  hole 40 199.099  144.6538  0
  hole 40 0  246.1  0
  hole 40 -199.099  144.6538  0
  hole 40 -234.0549  -76.0491  0
  hole 40 0  -246.1  0
  hole 40 199.099  -144.6538  0
  hole 38 288.6  0  0
  hole 38 274.475  89.1823  0
  hole 38 233.482  169.635  0
  hole 38 169.635  233.482  0
  hole 38 89.1823  274.475  0
  hole 38 0  288.6  0
  hole 38 -89.1823  274.475  0
  hole 38 -169.635  233.482  0
  hole 38 -233.482  169.635  0
  hole 38 -274.475  89.1823  0
  hole 38 -274.475  -89.1823  0
  hole 38 -233.482  -169.635  0
  hole 38 -169.635  -233.482  0
  hole 38 -89.1823  -274.475  0
  hole 38 0  -288.6  0
  hole 38 -288.6  0  0
  hole 38 89.1823  -274.475  0
  hole 38 169.635  -233.482  0
  hole 38 233.482  -169.635  0
  hole 38 274.475  -89.1823  0
 zcylinder 17 1 334  12.11  0
 cuboid 0 1  400  -400  400  -400  12.11  0
unit 15
 zcylinder 82 1 234  219.286  0
  hole 66 0  0  0
 zcylinder 22 1 311.793  219.286  0
  hole 42 246.1  0  0
  hole 42 144.6538  199.099  0
  hole 42 76.0491  234.0549  0
  hole 42 -76.0491  234.0549  0
  hole 42 -144.6538  199.099  0
  hole 42 -234.0549  76.0491  0
  hole 42 -246.1  0  0
  hole 42 -144.6538  -199.099  0
  hole 42 -76.0491  -234.0549  0
  hole 42 76.0491  -234.0549  0
  hole 42 144.6538  -199.099  0
```

```
  hole 42 234.0549  -76.0491  0
  hole 42 -199.099  -144.6538  0
  hole 43 234.0549  76.0491  0
  hole 43 199.099  144.6538  0
  hole 43 0  246.1  0
  hole 43 -199.099  144.6538  0
  hole 43 -234.0549  -76.0491  0
  hole 43 0  -246.1  0
  hole 43 199.099  -144.6538  0
  hole 41 288.6  0  0
  hole 41 274.475  89.1823  0
  hole 41 233.482  169.635  0
  hole 41 169.635  233.482  0
  hole 41 89.1823  274.475  0
  hole 41 0  288.6  0
  hole 41 -89.1823  274.475  0
  hole 41 -169.635  233.482  0
  hole 41 -233.482  169.635  0
  hole 41 -274.475  89.1823  0
  hole 41 -274.475  -89.1823  0
  hole 41 -233.482  -169.635  0
  hole 41 -169.635  -233.482  0
  hole 41 -89.1823  -274.475  0
  hole 41 0  -288.6  0
  hole 41 -288.6  0  0
  hole 41 89.1823  -274.475  0
  hole 41 169.635  -233.482  0
  hole 41 233.482  -169.635  0
  hole 41 274.475  -89.1823  0
 zcylinder 17 1 334  219.286  0
 cuboid 0 1  400  -400  400  -400  219.286  0
unit 16
 zcylinder 5 1 234  156.22  0
  hole 67 0  0  0
 zcylinder 22 1 311.793  156.22  0
  hole 45 246.1  0  0
  hole 45 144.6538  199.099  0
  hole 45 76.0491  234.0549  0
  hole 45 -76.0491  234.0549  0
  hole 45 -144.6538  199.099  0
  hole 45 -234.0549  76.0491  0
  hole 45 -246.1  0  0
  hole 45 -144.6538  -199.099  0
  hole 45 -76.0491  -234.0549  0
  hole 45 76.0491  -234.0549  0
  hole 45 144.6538  -199.099  0
  hole 45 234.0549  -76.0491  0
  hole 45 -199.099  -144.6538  0
  hole 46 234.0549  76.0491  0
  hole 46 199.099  144.6538  0
  hole 46 0  246.1  0
  hole 46 -199.099  144.6538  0
  hole 46 -234.0549  -76.0491  0
  hole 46 0  -246.1  0
```

```
  hole 46 199.099  -144.6538  0
  hole 44 288.6  0  0
  hole 44 274.475  89.1823  0
  hole 44 233.482  169.635  0
  hole 44 169.635  233.482  0
  hole 44 89.1823  274.475  0
  hole 44 0  288.6  0
  hole 44 -89.1823  274.475  0
  hole 44 -169.635  233.482  0
  hole 44 -233.482  169.635  0
  hole 44 -274.475  89.1823  0
  hole 44 -274.475  -89.1823  0
  hole 44 -233.482  -169.635  0
  hole 44 -169.635  -233.482  0
  hole 44 -89.1823  -274.475  0
  hole 44 0  -288.6  0
  hole 44 -288.6  0  0
  hole 44 89.1823  -274.475  0
  hole 44 169.635  -233.482  0
  hole 44 233.482  -169.635  0
  hole 44 274.475  -89.1823  0
 zcylinder 17 1 334  156.22  0
 cuboid 0 1  400  -400  400  -400  156.22  0
unit 17
 zcylinder 4 1 234  42.36  0
  hole 68 0  0  0
 zcylinder 22 1 311.793  42.36  0
  hole 48 246.1  0  0
  hole 48 144.6538  199.099  0
  hole 48 76.0491  234.0549  0
  hole 48 -76.0491  234.0549  0
  hole 48 -144.6538  199.099  0
  hole 48 -234.0549  76.0491  0
  hole 48 -246.1  0  0
  hole 48 -144.6538  -199.099  0
  hole 48 -76.0491  -234.0549  0
  hole 48 76.0491  -234.0549  0
  hole 48 144.6538  -199.099  0
  hole 48 234.0549  -76.0491  0
  hole 48 -199.099  -144.6538  0
  hole 49 234.0549  76.0491  0
  hole 49 199.099  144.6538  0
  hole 49 0  246.1  0
  hole 49 -199.099  144.6538  0
  hole 49 -234.0549  -76.0491  0
  hole 49 0  -246.1  0
  hole 49 199.099  -144.6538  0
  hole 47 288.6  0  0
  hole 47 274.475  89.1823  0
  hole 47 233.482  169.635  0
  hole 47 169.635  233.482  0
  hole 47 89.1823  274.475  0
  hole 47 0  288.6  0
  hole 47 -89.1823  274.475  0
```

```
  hole 47 -169.635  233.482  0
  hole 47 -233.482  169.635  0
  hole 47 -274.475  89.1823  0
  hole 47 -274.475  -89.1823  0
  hole 47 -233.482  -169.635  0
  hole 47 -169.635  -233.482  0
  hole 47 -89.1823  -274.475  0
  hole 47 0  -288.6  0
  hole 47 -288.6  0  0
  hole 47 89.1823  -274.475  0
  hole 47 169.635  -233.482  0
  hole 47 233.482  -169.635  0
  hole 47 274.475  -89.1823  0
 zcylinder 17 1 334  42.36  0
 cuboid 0 1  400  -400  400  -400  42.36  0
unit 18
 zcylinder 3 1 234  16.944  0
  hole 69 0  0  0
 zcylinder 21 1 239.6  16.944  0
 zcylinder 29 1 252.6  16.944  0
  hole 50 246.1  0  0
  hole 50 144.6538  199.099  0
  hole 50 76.0491  234.0549  0
  hole 50 -76.0491  234.0549  0
  hole 50 -144.6538  199.099  0
  hole 50 -234.0549  76.0491  0
  hole 50 -246.1  0  0
  hole 50 -144.6538  -199.099  0
  hole 50 -76.0491  -234.0549  0
  hole 50 76.0491  -234.0549  0
  hole 50 144.6538  -199.099  0
  hole 50 234.0549  -76.0491  0
  hole 50 -199.099  -144.6538  0
  hole 51 234.0549  76.0491  0
  hole 51 199.099  144.6538  0
  hole 51 0  246.1  0
  hole 51 -199.099  144.6538  0
  hole 51 -234.0549  -76.0491  0
  hole 51 0  -246.1  0
  hole 51 199.099  -144.6538  0
 zcylinder 48 1 284.6  16.944  0
 zcylinder 57 1 292.6  16.944  0
 zcylinder 22 1 311.793  16.944  0
 zcylinder 17 1 334  16.944  0
 cuboid 0 1  400  -400  400  -400  16.944  0
unit 19
 zcylinder 2 1 234  67.2  0
  hole 70 0  0  0
 zcylinder 20 1 239.6  67.2  0
 zcylinder 22 1 311.793  67.2  0
  hole 52 246.1  0  0
  hole 52 144.6538  199.099  0
  hole 52 76.0491  234.0549  0
  hole 52 -76.0491  234.0549  0
```

```
  hole 52 -144.6538  199.099  0
  hole 52 -234.0549  76.0491  0
  hole 52 -246.1  0  0
  hole 52 -144.6538  -199.099  0
  hole 52 -76.0491  -234.0549  0
  hole 52 76.0491  -234.0549  0
  hole 52 144.6538  -199.099  0
  hole 52 234.0549  -76.0491  0
  hole 52 -199.099  -144.6538  0
  hole 53 234.0549  76.0491  0
  hole 53 199.099  144.6538  0
  hole 53 0  246.1  0
  hole 53 -199.099  144.6538  0
  hole 53 -234.0549  -76.0491  0
  hole 53 0  -246.1  0
  hole 53 199.099  -144.6538  0
 zcylinder 17 1 334  67.2  0
 cuboid 0 1  400  -400  400  -400  67.2  0
unit 20
 zcylinder 1 1 234  48.7  0
  hole 71 0  0  0
 zcylinder 19 1 239.6  48.7  0
 zcylinder 17 1 334  48.7  0
  hole 54 246.1  0  0
  hole 54 144.6538  199.099  0
  hole 54 76.0491  234.0549  0
  hole 54 -76.0491  234.0549  0
  hole 54 -144.6538  199.099  0
  hole 54 -234.0549  76.0491  0
  hole 54 -246.1  0  0
  hole 54 -144.6538  -199.099  0
  hole 54 -76.0491  -234.0549  0
  hole 54 76.0491  -234.0549  0
  hole 54 144.6538  -199.099  0
  hole 54 234.0549  -76.0491  0
  hole 54 -199.099  -144.6538  0
  hole 55 234.0549  76.0491  0
  hole 55 199.099  144.6538  0
  hole 55 0  246.1  0
  hole 55 -199.099  144.6538  0
  hole 55 -234.0549  -76.0491  0
  hole 55 0  -246.1  0
  hole 55 199.099  -144.6538  0
 cuboid 0 1  400  -400  400  -400  48.7  0
unit 21
com='20 helium flow channels (unit 1)'
 zcylinder 5 1 4  160  0
unit 22
com='20 helium coolant channels (unit 2,4)'
 zcylinder 5 1 4  50.83  0
unit 23
com='20 helium coolant channels (unit 3,5)'
 zcylinder 5 1 4  25.42  0
unit 26
```

```
com='20 helium coolant channels (unit 6)'
 zcylinder 5 1 3.85  33.89  0
unit 27
com='13 irradition/control rod channels (unit 6)'
 zcylinder 5 1 6.25  33.89  0
unit 28
com='7 absorber ball channels (unit 6)'
 zcylinder 5 1 5.3  33.89  0
unit 29
com='20 helium coolant channels (unit 7)'
 zcylinder 5 1 4  47.44  0
unit 30
com='13 irradition/control rod channels (unit 7)'
 zcylinder 5 1 6.5  47.44  0
unit 31
com='7 absorber ball channels (unit 7)'
 zcylinder 5 1 5.3  47.44  0
unit 32
com='20 helium coolant channels (unit 8)'
 zcylinder 5 1 4  22.43  0
unit 33
com='13 irradition/control rod channels (unit 8)'
 zcylinder 5 1 6.5  22.43  0
unit 34
com='7 absorber ball channels (unit 8)'
 zcylinder 5 1 5.3  22.43  0
unit 35
com='20 helium coolant channels (unit 9-13)'
 zcylinder 5 1 4  10.17  0
unit 36
com='13 irradition/control rod channels (unit 9-13)'
 zcylinder 5 1 6.5  10.17  0
unit 37
com='7 absorber ball channels (unit 9-13)'
 zcylinder 5 1 5.3  10.17  0
unit 38
com='20 helium coolant channels (unit 14)'
 zcylinder 5 1 4  12.11  0
unit 39
com='13 irradition/control rod channels (unit 14)'
 zcylinder 5 1 6.5  12.11  0
unit 40
com='7 absorber ball channels (unit 14)'
 zcylinder 5 1 5.3  12.11  0
unit 41
com='fuel: 20 helium coolant channels (unit 15)'
 zcylinder 5 1 4  219.286  0
unit 42
com='fuel: 13 irradition/control rod channels (unit 15)'
 zcylinder 5 1 6.5  219.286  0
unit 43
com='fuel: 7 absorber ball channels (unit 15)'
 zcylinder 5 1 5.3  219.286  0
unit 44
```

```
com='void: 20 helium coolant channels (unit 16)'
 zcylinder 5 1 4  156.22  0
unit 45
com='void: 13 irradition/control rod channels (unit 16)'
 zcylinder 5 1 6.5  156.22  0
unit 46
com='void: 7 absorber ball channels (unit 16)'
 zcylinder 5 1 5.3  156.22  0
unit 47
com='20 helium coolant channels (unit 17)'
 zcylinder 5 1 4  42.36  0
unit 48
com='13 irradition/control rod channels (unit 17)'
 zcylinder 5 1 6.5  42.36  0
unit 49
com='7 absorber ball channels (unit 17)'
 zcylinder 5 1 5.3  42.36  0
unit 50
com='13 irradition/control rod channels (unit 18)'
 zcylinder 5 1 6.25  16.944  0
unit 51
com='7 absorber ball channels (unit 18)'
 zcylinder 5 1 5.3  16.944  0
unit 52
com='13 irradition/control rod channels (unit 19)'
 zcylinder 5 1 6.25  67.2  0
unit 53
com='7 absorber ball channels (unit 19)'
 zcylinder 5 1 5.3  67.2  0
unit 54
com='13 irradition/control rod channels (unit 20)'
 zcylinder 5 1 6.25  48.7  0
unit 55
com='7 absorber ball channels (unit 20)'
 zcylinder 5 1 5.3  48.7  0
unit 56
com='hot gas duct in region 22, (unit 4)'
 xcylinder 5 1 14.9  75.5  1
unit 57
com='hot gas duct in region 17, (unit 4)'
 xcylinder 5 1 14.9  20.5  1
unit 58
com='graphite center (unit 4)'
 zcylinder 1 1 144  30  0
unit 59
com='graphite center (unit 3)'
 zcylinder 1 1 144  15  0
unit 60
com='graphite block (unit 1)'
 zcylinder 1 1 144  70  0
unit 61
com='graphite column (unit 6)'
 zcylinder 1 1 144  20  0
unit 62
```

```
com='graphite column (unit 7)'
 zcylinder 1 1 144  28  0
unit 63
com='graphite column (unit 8)'
 zcylinder 1 1 144  13.236  0
unit 64
com='graphite column (unit 9 and 10)'
 zcylinder 1 1 144  10.17  0
unit 65
com='graphite column (unit 11-14)'
 zcylinder 1 1 144  12.11  0
unit 66
com='graphite column (unit 15)'
 zcylinder 1 1 144  219.286  0
unit 67
com='graphite column (unit 16)'
 zcylinder 1 1 144  156.22  0
unit 68
com='graphite columnn (unit 17)'
 zcylinder 1 1 144  42.36  0
unit 69
com='graphite column (unit 18)'
 zcylinder 1 1 144  16.944  0
unit 70
com='graphite column (unit 19)'
 zcylinder 1 1 144  67.2  0
unit 71
com='graphite column (unit 20)'
 zcylinder 1 1 144  48.7  0
unit 72
 zcylinder 18 1 144  70  0
unit 73
com='graphite column (unit 1)'
 zcylinder 1 1 144  160  0
unit 74
com='graphite column (unit 2,4)'
 zcylinder 1 1 144  50.83  0
unit 75
com='graphite column (unit 3,5)'
 zcylinder 1 1 144  25.42  0
unit 76
com='graphite column (unit 6)'
 zcylinder 1 1 144  33.89  0
unit 77
com='graphite column (unit 7)'
 zcylinder 1 1 144  47.44  0
unit 78
com='graphite column (unit 8)'
 zcylinder 1 1 144  22.43  0
end geometry
read array
ara=1 nux=1 nuy=1 nuz=20  gbl=1
fill 1 2 3 4 5 6 7 8 9 10 11 12 13 14 15 16 17 18 19 20
end fill
```

```
end array
end data
end
```

VITA

Megan L. Pritchard graduated from Texas A&M University in August 2006 with a Bachelor of Science degree in nuclear engineering and a minor in mathematics and physics. She entered the nuclear engineering program at Texas A&M University in September 2006, and received her Master of Science degree in December 2007. Future contact may be made by email at mego1221@gmail.com or by mail forwarded through the Department of Nuclear Engineering, c/o Dr. Pavel V. Tsvetkov, Texas A&M University, College Station, TX 77843-3133.